Hypocapnia, Autonomic Signatures, and Gamma-Band Reconfiguration During Wim Hof Breathing Method and Cold Immersion:

A comparative study between naive and Level 2 experts

Rodrigo Montenegro[1 2]

Cedric Cannard[3 4]

Alexandre Batissou[2]

Alice Guyon[5]

Renaud Evrard[2]

John A. Chavez[6]

*Corresponding Author: rmontenegro11@gmail.com

[1] Sleep Consciousness Institute, London, UK.

[2] Interpsy Laboratory, Nancy, France.

[3] Institute of Noetic Sciences, California, USA.

[4] Centre de Recherche Cerveau et Cognition (CerCo), CNRS, France.

[5] Centre de Recherche en Psychologie et Neurosciences (CRPN), UMR 7770 Aix Marseille Université-CNRS. 3, place Victor-Hugo 13003 Marseille, France

[6] DMT Quest.

I. Abstract

Background: The Wim Hof Breathing Method (WHBM), which involves controlled hyperventilation interleaved with breath retention, has been proposed to modulate interoception and autonomic tone; however, neural signatures in trained versus naïve practitioners remain incompletely characterised.

Methods: Seventeen adults (10 Level-2 WHM experts; 7 novices) completed eyes-closed baseline rest, a standardised WHBM bout (~10–12 min; three rounds of nasal power breaths with a low-lung-volume retention and a recovery inhalation), and post-WHM rest; experts also underwent brief eyes-closed cold-water immersion. A 64-channel EEG dataset was acquired. Spectral power, source-level beamforming, and multivariate functional connectivity were compared across phases using cluster-based permutation testing. End-tidal CO_2, SpO_2, heart rate, respiratory rate and autonomous activity were monitored.

Results: Compared to baseline, WHBM yielded distinct patterns. Experts: scalp—frontopolar delta, left-posterior low-beta, strong posterior gamma; source—left superior temporal delta, left lateral occipital alpha suppression, right precuneus beta, left precuneus/right paracentral high-gamma; connectivity—theta in sensorimotor–salience hubs and gamma linking posterior DMN to ACC/lateral PFC; physiology—deeper hypocapnia (~2.54% $EtCO_2$), steadier RR (~10.1/min), higher pulse (~76.4 bpm). Novices: scalp—posterior alpha/beta and frontopolar gamma; source—right temporal-pole delta, right parahippocampal alpha, right fusiform beta, left pericalcarine gamma; connectivity—beta DMN–visual and posterior-temporal gamma; physiology—shallower hypocapnia (~3.48%), higher RR (~11.96/min), lower pulse (~69.9 bpm).

Conclusions: WHBM acutely induces a physiologically aroused yet internally directed cortical state, marked by gamma enhancement and integration across interoceptive–salience–DMN

networks, with clear sympathetic activation. Expertise is associated with more organised, posterior-dominant dynamics.

II. Introduction:

The Wim Hof Breathing Method (WHBM) and cold immersion therapy have received increased attention from the scientific community over the past few years. The WHBM is composed of two main components: 1) a cyclic breathing practice and 2) a graded exposure to cold.

The cyclic breathing practice is organised into sub-phases. The first sub-phase is a controlled hyperventilation methodology that consists of ~30–40 deep, fast breaths at a steady pace (about 3–4 s per breath), followed by full inhalations (from the diaphragm into the chest) through the mouth, combined with a "relaxed/passive" (not forced) exhalation. A condition that raises ventilation, typically producing hypocapnia (i.e., a state of low carbon dioxide levels in the blood, below 35 mmHg)/ and respiratory alkalosis (hypocapnia but also causing blood pH to rise above normal), and a transient surge in sympathetic nervous system activity surge, triggering heightened alertness, increased heart rate (HR), and other fight-or-flight responses. The second sub-phase involves a low-lung-volume retention (apnea) performed after a relaxed exhale following the last breath of the first phase, leading to hypoxia (i.e., the tissues receive insufficient oxygen to meet their metabolic needs). The breath is held at low lung volume until a clear urge to breathe returns (varying by individual capacity and round). Some practitioners add a brief, optional "body squeeze" (isometric tensing of trunk near the end of the hold) to accentuate interoceptive focus and autonomic arousal. The 3rd sub-phase is a recovery breath. This phase involves a single, deep inhalation to achieve full lung capacity, followed by a 10– to 15–second hold. Some perform this with a gentle glottic (brief closure of the vocal cords) or diaphragmatic (intentionally tightening

and holding the diaphragm in a fixed position) "lock," creating a short, Valsalva-like pressurisation (i.e., increase in intrathoracic pressure and stabilisation of the torso) before releasing and beginning the next cycle. Under this guidance, each sub-phase round can last ~3–3.5 min.

In the guided WHBM available online for beginners (Hof, 2019), which was used on our study, power breaths last ≈1:30 per round, with the last breath being a deep inhalation followed by a relaxed exhalation leading directly into apnea, while the retention/apnea rounds last about ≈1:00–1:30 with the breath being held at low lung volume until a clear urge to breathe, finalized by a recovery breath lasting 15 s and one full inhalation to total lung capacity which starts the next sub-phase or round.

Beneath the technicality of the WHBM, the practice can be seen as a deliberate method to shift positive bodily states through a cyclic breathing practice paired with graded cold exposure, which together target autonomic, interoceptive awareness, and immune control (see Acute Autonomic–Immune Signature section). This framing emphasises WHBM's specific components—the hyperventilation-breath-retention hypoxic cycles, the thermal stimulus (which includes cold exposure as an integral part of the method, the disciplined practice context emphasised by WHBM, with the assertion that their combinations recruit mechanisms spanning sympathetic outflow, anti-inflammatory signalling, and top-down regulation of internal sensation.

Mechanistic Background for WHBM

Controlled breathing, such as the one in WHBM, has been used for centuries to shift bodily and mental states in practices such as pranayama and qì gōng. Contemporary work shows that voluntary breath control can alter autonomic activity and brain dynamics via medullary respiratory rhythm generators such as the preBötzinger complex (preBötC), the medullary kernel for

inspiratory rhythm generation. However, although many studies have shown that respiratory rhythms influence a variety of behavioural effects in cognitive, emotional, and perceptual areas, a complete framework to clarify these effects remains to be fully developed. Herrero et al. (2018) intracranial Electroencephalogram (EEG) recording in humans indicated that the breathing cycle phase-locks neuronal activity across widespread cortical and limbic sites, with the gamma-band envelope (≈40–150 Hz) further demonstrating coherence increases during volitionally paced breathing in a frontotemporal-insular network and during attention to breath in the anterior cingulate, premotor, insula, and hippocampus. Findings that link respiration to interoceptive and attentional control, highlighting the involvement of higher brain circuits beyond brainstem reflexes. Contemplating this, Zelano et al. (2016) found that nasal respiration entrains delta/theta power in piriform cortex (PC), associated with olfactory detection and discrimination, amygdala, and hippocampus, strengthening theta–beta cross-frequency coupling in PC to improve behavior (faster fear discrimination; better recognition memory) specifically during inhalation (effects that largely vanish with mouth breathing, underscoring a nasal/olfactory pathway for respiration–brain coupling). At the same time, a recent review of the literature synthesised findings into a gradient model of respiratory-modulated brain oscillations (RMBOs). Braendholt et al. (2023) study supports the idea that airflow-driven rhythms and brainstem pattern generators propagate to locus coeruleus (LC), a widespread cortical and subcortical hub with noradrenergic projections involved in the regulation of neural excitability, as well as thalamic and olfactory circuits, modulating neural gain and cross-frequency coupling to facilitate predictive coding (e.i, precision-weighted prediction errors) across sensory, interoceptive, and cognitive systems. The study complements other similar findings, as reported by Zelano et al. (2016) and others (discussed below), suggesting that airflow-driven rhythms in the nasal cavity trigger mechanoreceptors connected to the olfactory bulb, translate these rhythms into infraslow neural oscillations (i.e., < 0.5 Hz), and suggest they

further propagate to higher-order brain areas modulating faster oscillations across a wide range of frequency bands. These include Delta, Theta, Alpha, Beta, and Gamma, implying that the influence of respiratory rhythms is not limited to a single frequency band. A systematic review by Goheen et al. (2023) equally found similar results showing that between spontaneous, slow and hyperventilated breathing conditions there were 16 regions in the brain modulated by respiration including frontal [medial and lateral prefrontal cortex (PFC), orbitofrontal PFC, superior frontal gyrus], temporal [superior temporal gyrus (STG), parietal (somatosensory cortex (SSC), and primary motor cortex (PMC)], occipital [occipital cortex (OC) and supramarginal gyrus (SMG)], midline [anterior cingulate cortex (ACC), medial cingulate cortex (MCC), and posterior cingulate cortex (PCC)/precuneus and cuneus], insular [anterior (aINS), medial (mINS), and posterior (pINS)], cerebellar areas and subcortical areas (thalamus, caudate, and putamen).

A systematic review by Goheen et al. (2023) equally found similar results, not only showing that different frequencies could modulate all areas of the brain but equally that between spontaneous, slow and hyperventilated breathing conditions there were 16 regions in the brain modulated by respiration including frontal [medial and lateral prefrontal cortex (PFC), orbitofrontal PFC, superior frontal gyrus], temporal [superior temporal gyrus (STG), parietal (somatosensory cortex (SSC), and primary motor cortex (PMC)], occipital [occipital cortex (OC) and supramarginal gyrus (SMG)], midline [anterior cingulate cortex (ACC), medial cingulate cortex (MCC), and posterior cingulate cortex (PCC)/precuneus and cuneus], insular [anterior (aINS), medial (mINS), and posterior (pINS)], cerebellar areas and subcortical areas (thalamus, caudate, and putamen). Kluger and Gross (2021) also found that breathing effects were shown in areas such as the posterior cingulate cortex (PCC), precuneus, and cuneus due to the bidirectional interplay between the respiratory control network (RCN) and resting-state networks like the Default Mode Network (DMN), again showing modulation across various frequencies. Kluger and

Gross (2021) also found that breathing affects areas such as the posterior cingulate cortex (PCC), precuneus, and cuneus through bidirectional interplays between the respiratory control network (RCN) and resting-state networks, including the Default Mode Network (DMN), again showing modulation across various frequencies.

Furthermore, meta-analytic evidence indicates that structured breathwork reduces perceived stress and improves stress-related (medium effect size), anxiety, and depressive symptoms in randomised studies, with small-to-moderate effects, and that slow breathing increases heart-rate-variability (HRV) indices of vagal control (Fincham et al., 2023; Laborde et al., 2022). Together, these findings suggest that the WHBM could produce robust systemic effects, but neural endpoints have been sparsely measured, and studies using concurrent EEG and electrodermal activity are lacking.

Accordingly, our study set out to (i) quantify WHBM's neural and autonomic effects (EEG, EDA/GSR, capnography/SpO_2), (ii) compare naïve practitioners of the WHBM with no prior or only minimal WHBM exposure (operationally: 0 years of practice; see Table 1**)** with Level-2 (L2) experienced practitioners (operationally: ~6 years of practice, range 4–7 years). (Kox et al., 2014)

Acute Autonomic–Immune Signature of WHBM Breathing

Across controlled studies, WHBM's most reproducible physiological signature is a fast, sympathetic surge during the breathing bouts, rising epinephrine, that is followed by an anti-inflammatory tilt which increases IL-10, reduces TNF-α/IL-6/IL-8 and which seems at its strongest when breathing is paired with cold exposure (Almahayni & Hammond, 2024; Zwaag et al., 2020). Kox et al. (2014) found that TNF-α, IL-6, and IL-8 were 53%, 57%, and 51% lower, respectively,

and IL-10 was ~194% higher compared to controls, while IL-10 correlated negatively with pro-inflammatory cytokines.

Although cold alone, without breathing, can affect Monocyte Chemoattractant Protein-1 (MCP-1)—a pro-inflammatory cytokine that plays a key role in recruiting monocytes and memory T cells—cold alone without breathing only modestly shifts cytokines. However, when cold exposure was combined with breathing exercises, the anti-inflammatory effects were significantly enhanced. Indeed, a clinical trial by Zwaag et al. (2022) suggests that the combination of cold exposure training and breathing exercises significantly enhances anti-inflammatory effects during experimental human endotoxemia—a controlled experimental model used to study systemic inflammation and the immune response in humans.

Furthermore, Zwaag et al. (2022) suggest that the effects of the training are independent of the training length and can be elicited with or without prolonged breath retention. In the same study, the authors show that prolonged breath retention sustains catecholamine (epinephrine) elevations longer than breathing exercise without retention.

Across nine papers (eight trials) identified by a recent systematic review by Almahayni and Hammond (2024), convergent findings of the WHBM include a robust epinephrine rise during WHBM and during experimental endotoxemia, WHBM was associated with earlier/higher IL-10 and lower TNF-α/IL-6/IL-8, as well as lactate/pyruvate elevations that track with IL-10 and reproduce anti-inflammatory effects in vitro.

Notwithstanding these convergences, the evidence comes from heterogeneous cohorts—healthy volunteers, athletes, a polar-expedition field sample, and a patient RCT in axial spondyloarthritis—tested under non-standardised doses and mixed component sets (full WHBM vs breathing-only), with high risk of bias in several trials (Almahayni & Hammond, 2024). This

heterogeneity, plus the scarcity of event-locked, sub-phase–resolved measures, limits mechanistic inference.

Behavioural and Mood Effects of WHBM

Psychologically, WHBM studies to date report encouraging but heterogeneous outcomes. Higher optimism and expectancy, which covary with epinephrine and IL-10 in endotoxemia paradigms (van Middendorp et al., 2016) and subjective benefits such as improved SF-36 physical/mental (PCS/MCS) scores in one cohort—alongside null findings on EQ-5D and occasional adverse sensations (e.g., 'deafness,' 'heaviness') during breathing sessions (Buijze et al., 2019). One study reported that three-quarters of participants experienced positive effects, including increased energy, reduced fatigue, improved breathing, and enhanced perceived performance during physical activities, particularly during the repeated-sprint test (Citherlet et al., 2021). Another study reported that depressive symptoms decreased significantly over an 8-week field study, as indicated by lower scores on the Beck Depression Inventory (BDI-II) in the intervention group compared with the control group (Petraskova Touskova et al., 2022). A randomised clinical trial in high-stress women compared WHBM breathing plus cold to slow breathing plus warm showers and found improvements in mood and stress across groups (Blades et al., 2024). However, Buijze et al. (2019), in another trial, found no significant changes in the Hospital Anxiety and Depression Scale (HADS) scores for either anxiety or depression within the intervention or control groups during the 8-week intervention period.

WHBM Neurophysiology to Date: Evidence and Gaps

Neural readouts equally mirror this gap. Coupled with the above scarcity, WHBM neurophysiology has not been appraised beyond a single-case fMRI study during cold exposure. Muzik et al. (2018), using an oscillating cold-challenge fMRI paradigm and complementary PET/CT, show that practising the WHBM during cooling robustly increases BOLD signal in the periaqueductal grey (PAG)—a key node for descending antinociception and often associated with stress-induced analgesia—while producing phase-opposed reductions in bilateral insula (left anterior, right mid-insula), consistent with damped interoceptive salience under stress, considering the insular cortex is central to interoception as it integrates bottom-up sensory signals with top-down cognitive and motivational information. In other words, phase-opposed reductions, when the PAG showed increased activity during cooling (associated with stress-induced analgesia), the insula displayed decreased activity, suggesting a shift in focus away from sensory processing of cold stimuli.

Muzik et al. (2018) also reported that cold exposure was associated with activity in the Pontine Respiratory Group (PRG)—a network in the pons that regulates respiratory depth and rate. An activation that aligns with the WHBM's emphasis on controlled breathing and which primes the autonomic system to support thermoregulation. Furthermore, in the pons, the study indicated that the participant showed a BOLD increase near nuclei implicated in respiratory and autonomic regulation (parabrachial complex/locus coeruleus territory), suggesting engagement of brainstem arousal circuits during WHBM-assisted cold defence.

A Priori Hypotheses and Multimodal Predictions

To isolate the mechanism and test generalizability, we therefore examine healthy participants under a standardised guided protocol, stratified by experience (naïve vs Level 2 (L2) WHBM

practitioners). This design minimises differences within previous studies such variances in breathing protocols (e.g., retention variants), training levels, clinical and environmental confounds (Almahayni & Hammond, 2024), while allowing us to test whether the canonical sympathetic activation patterns (indexed by EDA/GSR with $EtCO_2$/SpO_2 context) extend to healthy novices—our first hypothesis—and whether expertise consolidates responses into reproducible neural signatures.

Given our goal to identify the neurophysiological signatures of the WHBMB, we analysed WHBM—specifically, basic breathing—as an integrated protocol rather than isolating sub-phases, treating Phase 2 (WHBM breathing, Table 4) as a single integrated intervention. This choice reflects the mechanistic synergy and current evidence that combined components yield the clearest immune-autonomic signatures and provide the strongest immunomodulatory effects when working together, arguing for a whole-protocol lens rather than reduction to micro-epoch. Furthermore, whole-phase comparisons tell us whether the intervention produces meaningful changes in integrated systems—namely cardio-respiratory coupling, autonomic balance, and cortical arousal. Finally, this choice reflects the fact that WHBM is taught and practised as a round-based sequence with specific pacing and cues. Hence, the methodology preserves the natural ecological validity while avoiding analytic over-segmentation. Consistent with this integrated framing and to keep the protocol focused, we excluded other WHBM "pillar" activities (e.g., push-ups, stretching, yoga poses) from the broader WHBM training curriculum.

Considering that hyperventilation-induced hypocapnia reduces CBF, classically evoking a slow-wave build-up Delta that is generally frontally dominant and is mechanistically associated with vasoconstriction and reduced perfusion (Acharya & Acharya, 2021; Son et al., 2012), our predictions suggest that we will see enhanced Delta activity during WHBM.

We predict WHBM will exhibit phase-locked alpha reductions during Phase 2 (breathing), with maximal reductions over posterior sources on sensor and source-localised maps. Alpha power increases in task-irrelevant cortices to suppress processing (visual alpha blocks visual input; auditory alpha dampens sounds) and decreases in task-relevant networks to release them from inhibition. Hypothetically, we should observe lower alpha in the sensorimotor cortex and the salience/insula, as these circuits are responsible for processing respiratory effort and internal signals. Considering that Muzik et al. (2018) highlight insular activation, which is part of the salience network and involved in interoception, self-reflection, and integrating sensory and cognitive information, we should see Alpha modulation over the salience/insula areas.

Furthermore, in WHBM, we should see Beta oscillations equally associated with motor tasks, with movement-related beta decrease (MRBD) occurring during movement execution and post-movement beta rebound (PMBR) following movement cessation as reported in classic Beta Event-Related Desynchronization (ERD)/ Event-Related Synchronisation (ERS) patterns (Barone & Rossiter, 2021).

WHBM should also produce intense interoceptive focus and respiratory effort, which can increase gamma activity, consistent with fast-band integration of somatosensory, salience/insula, and control hubs.

Blades et al. (2024) assessed the WHBM, indicating a parasympathetic tone in the slow-paced breathing condition, without specifying the exact physiological measures used in this analysis. Considering the initial demonstration by Kox et al. (2014) of the activity of the sympathetic nervous system using plasma epinephrine levels and cardiorespiratory parameters indicative of sympathetic activation, we considered using Galvanic Skin Response (GSR) and Electrodermal Activity (EDA) to provide indirect, but generally reliable, measures of sympathetic nervous system activity. GSR/EDA allows noninvasive sympathetic sudomotor readouts that

reflect eccrine sweat gland drive from sympathetic outflow, allowing measures of sympathetic activation during WHBM. This exploration aligns with Locus-Coeruleus-Norepinephrine (LC-NE) function and classical theories of the autonomous nervous system (ANS), which suggest that phasic and tonic modes of LC activity are associated with different arousal and behavioural states, correlating with changes in EDA as a measure of autonomic engagement (Aston-Jones & Cohen, 2005). Given prior reports that WHBM breathing elevates plasma epinephrine and that the locus coeruleus (LC) coordinates central noradrenergic arousal and sympathetic outflow, we hypothesised that WHBM would increase phasic EDA (SCR frequency, amplitude, area) during the breathing bouts—indexing transient sympathetic bursts that co-occur with the epinephrine surge. Indeed, induced hyperventilation modulates electrodermal responses in laboratory paradigms (see discussion). In WHBM, sudomotor nerve bursting would provide a quantitative proxy for the central arousal dynamics of the LC–NE, which should be more phasic during WHBM and express more tonic levels in baseline and rest phases. Furthermore, considering results from the study by Zwaag et al. (2022), which suggest that epinephrine levels during WHBM breathing are independent of training length, we hypothesise that there will be relatively low phasic differences between naïve and expert WHBM level 2 (L2) participants. If deliberate hyperventilation/retention cycles recruit the preBötC and LC pathways to up-modulate arousal, this should be expressed peripherally as increased skin conductance responses (SCRs) frequency and larger SCR amplitude/area during the breathing phase, with partial normalisation at rest.

Measuring capnographic data—such as carbon dioxide (CO_2) levels and hypocapnia—is crucial in an EEG study of WHBM practitioners because the breathing techniques inherent to WHBM can significantly alter respiratory physiology. We do not expect our capnographic/blood-gas profiles to deviate from those reported in prior WHBM studies summarised in the literature review by Almahayni and Hammond (2024, p. 14).

Finally, although the study by Muzik et al. (2018) of peripheral imaging indicated indicated that cold-activated brown adipose tissue (BAT) was small and metabolically unremarkable, whereas both glucose uptake (FDG SUV) and sympathetic innervation (HED retention index) were selectively elevated in intercostal muscles during cold exposure, implicating respiratory work as a principal heat source that warms pulmonary blood, we decided to do an exploratory research to test if BAT thermogenesis would be triggered during WHBM, and would further reflect sympathetic nervous system activation considering temperature changes we reported in similar breathing techniques (see review in Benson et al., 1982; Kozhevnikov et al., 2013).

III. Materials and Methods:

Study Design:

Participants performed the standardized beginner guided Wim Hof breathing (Hof, 2019) used in our study: each round comprised ~90 s of paced "power" breaths, a relaxed exhale into low-lung-volume retention for ~60–90 s, and a ~15 s recovery inhalation to total lung capacity that initiated the next round; to minimize EEG artefacts, breathing was instructed through the nose rather than the mouth.

During a single visit, participants first completed a quiet baseline 64-channel EEG recording in the same room where the intervention was conducted. The researchers present in the room refrained from speaking but did not suppress incidental and occasional ambient sounds, ensuring that the background noise matched subsequent phases. The WHBM intervention then followed the standardised beginner audio guidance by Wim Hof (Hof, 2019), delivered through speakers. This audio is a Wim Hof basic protocol (not the power breathing). In our protocol, the guidance was

played only during Phase 2, while Phases 1 and 3 were performed with eyes closed without audio. Each round reproduced the canonical three sub-phases already described the Introduction—~30–40 paced "power breaths" (controlled hyperventilation) with relaxed/passive exhalations; a low-lung-volume breath-hold after a relaxed exhale (without the optional gentle "body squeeze" near the end of the hold); and a single full-inhalation recovery breath held for 10–15 s before release—completed for three consecutive rounds of ≈3–3.5 min each (total ≈10–12 min), followed by a quiet post-breath rest (Figure 1). It should be noted that this report focuses on neurophysiology (EEG/physiology) and its behavioural correlates. While exploratory psychometric indices of the WHBM subjective experiences were collected through the psychedelic-like experience (HRS) scale (our washout period), considering reports of phenomenological similarities in the experiences, these were not analysed here due to a prospectively reassessed scope of the study (see discussion). However, they will be reported subsequently.

This sequence mirrors commonly used WHBM/WHBM parameters in the literature. It preserves the physiological features (hypocapnia/respiratory alkalosis during power breaths and hypoxia during apnoea) that have been associated with sympathetic activation and subsequent recovery. Naïve and L2 participants followed the sequence in equal measure, adhering closely to Wim Hof’s guidance.

Importantly, unlike typical WHBM instructions, all breathing was performed through the nose rather than the mouth to reduce mouth-opening episodes during Phase 2, thereby limiting EEG motion and electromyographic artefacts.

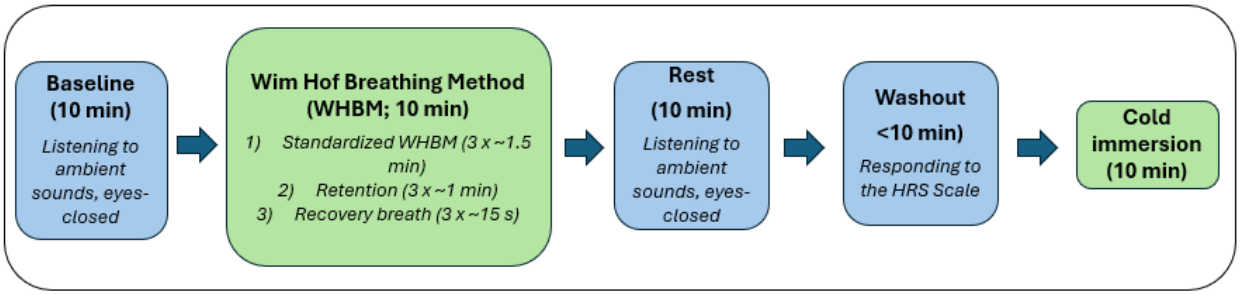

Figure 1

Study flow and task phases

It should be noted that the cold immersion phase was performed with eyes closed within temperatures that were marginally within a set of temperatures (Table 1) that were normally used during WHBM training and in studies during cold training, and was performed without pre breathing normally recommended to activate physiological responses, energise the body, and optimise the oxygen-carbon dioxide ratio in the blood. This methodology was designed to avoid any physiological confounders that might be carried over between the different phases.

Participants:

Seventeen adults participated in the study, comprising 10 experts (L2) and 7 novices. Participants were recruited through the Wim Hof Centre in France, with the advertisement approved by IRB #SCI-DMT-Q-01. Exclusion criteria were: (1) schizophrenia, dissociative disorder, or any other psychiatric disorder; (2) insufficient proficiency in English (language of testing); (3) age < 18 years; (4) Heart Disease, (5) chronic pain and/or chronic use of analgesics; and (5) current use of medications that affect the autonomic nervous system, including psychotropic drugs (e.g., antidepressants).

Due to the difficulty in estimating the effect, incidence and variability, a formal sample size calculation was not feasible. A convenience sample was used, and no a priori power analysis was conducted. The final sample comprised ten experts and seven novices. All participants provided written informed consent in accordance with procedures approved by the institutional review board (IRB).

Participant consent was obtained electronically via Adobe PDF (e-signature), with signed forms stored in a secure online repository. Files were de-identified, encrypted, and password-protected, with access restricted to authorised study personnel; the linkage key between the ID and the identifiable information was kept separately, with restricted access, in an encrypted file.

We employed an a priori age-stratified recruitment scheme, targeting equal numbers in three age bands—26–34, 35–44, and 45–54—within each experience stratum (naïve vs. L2). This balance was achieved except for the naïve 45–54 band, where EEG technical failures and the fixed data-collection window prevented rescheduling, resulting in a shortfall that we note in the descriptives and consider when interpreting between-group comparisons.

L2 participants were older on average than naïve (L2: M = 40.8 years, SD = 8.2, range = 29–51; Naïve: M = 36.7, SD = 5.7, range = 30–47). L2 reported 5.85 ± 1.11 years of WHBM practice (range = 4–7), whereas naïve participants had no prior practice (Table 1). Of the 17 participants, nine were female and eight were male (Table 2). Females were older on average than males (41.9 ± 8.4 vs 36.0 ± 4.7 years; ranges 29–51 and 30–45, respectively). Years of WHBM practice (with naïve coded as 0 years) averaged 2.94 ± 2.90 years for females and 4.00 ± 3.38 years for males (both ranges 0–7; medians 4.0 and 5.5 years, respectively). The number of previous WHBM attempts was recorded for the naïve group (M = 2.43, SD = 2.64, range = 0–7) and was not applicable for the L2 group. Sex distribution was balanced across groups (L2: 5 females/5 males; Naïve: 4 females/3 males; overall: 9 females/8 males), as shown in Table 3.

Only the L2 group underwent cold immersion (water temperature: M = 0.99 °C, SD = 0.64, range = 0.00–1.80 °C), while naïve participants were not exposed (temperature missing by design, as shown in Table 1). The immersion tub was packed with ice and maintained at ~0 °C by replenishing ice as needed. Immersion lasted 10 min, barring intolerance.

	Participant Type	N	Missing	Mean	Median	SD	Min.	Max.
Age	L2	10	0	40.800	39.50	8.217	29	51
	Naïve	7	0	36.714	36	5.648	30	47
Years of Practice	L2	10	0	5.850	5.75	1.107	4.00	7.00
	Naïve	7	0	0.000	0.00	0.000	0.00	0.00
Celsius (Cold Exposure)	L2	10	0	0.994	1.15	0.638	0.00	1.80
	Naïve	0	7	NaN	NaN	NaN	NaN	NaN
Number of Attempts	L2	0	10	NaN	NaN	NaN	NaN	NaN
	Naïve	7	0	2.429	2	2.637	0	7

Table 1

Participant characteristics by group — Age, WHBM experience, cold-immersion temperature, and practice attempts.

	SEX	N	Missing	Mean	Median	SD	Minimum	Maximum
AGE	F	9	0	41.89	41	8.42	29	51
	M	8	0	36.00	36.00	4.69	30	45
YEARS OF PRACTICE	F	9	0	2.94	4.00	2.90	0.00	7.00
	M	8	0	4.00	5.50	3.38	0.00	7.00

Table 2

Participant characteristics by sex — age, and WHBM years of practice

Participant Type	SEX	Counts	% of Total	Cumulative %
L2	F	5	29.4%	29.4%
	M	5	29.4%	58.8%
Naïve	F	4	23.5%	82.4%

Participant Type	**SEX**	**Counts**	**% of Total**	**Cumulative %**
	M	3	17.6%	100.0%

Table 3

Frequency of Participant Types

Data Collection

64-channel EEG signals were acquired using a 6-channel unipolar EEG DC-coupled amplifier with 24-bit resolution at a 512 Hz sampling rate. Manufacturer-specified input noise was <1.0 μVrms, with input impedance $>10^{12}$ Ω and CMRR >90 dB. Data was streamed via a bi-directional glass-fibre link (FUSBI) to the host computer. Electrodes were positioned according to the international 10–20 system using active Ag/AgCl sensors and 3 different headcaps to accommodate different head sizes (report headcap sizes), with ground at AFz and reference at FCz during acquisition. Impedances were maintained below 20 kΩ.

Autonomic activity was recorded using the Shimmer3 platform (Shimmer Sensing, Dublin, Ireland) equipped with the GSR+ module for continuous electrodermal activity (EDA) monitoring. Ag/AgCl electrodes (8 mm diameter) were placed on the distal phalanges of the index and middle fingers of the non-dominant (left) hand, following manufacturer guidelines. Data was sampled at 256 Hz and digitally stored for offline analysis. Skin conductance was expressed in microsiemens (μS) after low-pass filtering at 5 Hz and visual inspection for artefacts. Both tonic (skin conductance level; SCL) and phasic components SCRs were extracted using continuous decomposition analysis, yielding indices such as SCR frequency, amplitude, and area under the curve. EDA measures were time-locked to the EEG recording and breathing phases to assess the dynamics of sympathetic activation.

Ventilatory and oxygenation indices were monitored using a Creative PC-900B handheld capnograph/oximeter (NDIR capnography). Adult nasal sampling lines were connected through a manufacturer-specified filter/water trap that locks to the device with a 45° twist. The trap protects the IR cell from moisture and occlusion. The PC-900B displays/records $EtCO_2$, respiratory rate, SpO_2, and pulse rate, and provides trend views and pump control.

Skin/ambient thermal context was logged with calibrated iButtonLink DS1921H 1-Wire temperature loggers. Each sensor was equipped with an ISO/IEC 17025-accredited calibration certificate, providing NIST traceability, and reported "as found/as left" results at multiple set points. The certificate reported point calibrations within the physiological range (≈28.5 °C, 36 °C, 40 °C) with an expanded uncertainty of approximately ±0.057 °C (k = 2), and the manufacturer's maximum error tolerance was noted for reference. Calibration status and decision rules followed the lab's risk analysis procedure. Cutaneous temperature was logged at three trunk sites chosen a priori to differentiate localised thermogenesis from generalised vasomotor effects: (i) the supraclavicular fossa, overlying a principal human brown-adipose-tissue (BAT) depot, to probe BAT-linked heat production; (ii) the mid-sternal/upper chest as a core-proximal trunk reference that is less BAT-dense; and (iii) the upper thoracic paraspinal region (approx. T1–T4) to index trunk skin under typical clothing/insulation and posture-related convection. Sensors were secured to clean, dry skin with hypoallergenic adhesive and a light occlusive dressing to reduce airflow artefacts. Devices were programmed to a fixed logging interval and synchronised to session timestamps; raw series were exported and phase-segmented (Baseline, WHBM, Rest). For each site ("Gauge 1/2/3"), we computed the within-participant ΔT as the phase mean minus the baseline mean.

Together, this instrumentation—high-dynamic-range, time-synchronised EDA, handheld $EtCO_2/SpO_2$, calibrated temperature logging, and standardised phenomenology enabled a multimodal capture of the WHBM breathing phases with event timing and artefact control suitable for neurophysiological analyses.

Data Processing

EEG data were processed using EEGLAB v2025 (Scott Makeig et al., 2004), MATLAB v2025a (The MathWorks, Inc.). Data were downsampled to 512 Hz when necessary (two files had a higher sampling rate than the rest), high-pass filtered at 1 Hz to remove low-frequency DC drifts, and notch filtered at 50 Hz to remove power line noise (both using EEGLAB's default zero-phase, non-causal FIR filters). EEG channels with excessive noise or poor correlation with their neighbours were identified and removed using EEGLAB's multivariate correlation and noise-based methods (minimum correlation threshold = 0.65; maximum line noise threshold = 100; maximum tolerance = 50% of the file; RANDSAC samples = 200 for increased robustness). Artefact Subspace Reconstruction (ASR) as referred by Chang et al. (2018) was then applied with a conservative cutoff of 80 to reconstruct very large transient artefacts, thereby increasing the accuracy of independent component analysis (ICA) (Makeig et al., 1995; S. Makeig et al., 2004); while preserving relevant brain oscillations with large amplitude that the algorithm can incorrectly reconstruct. Bad channels were interpolated using spherical splines (Perrin et al., 1989), and the data were rereferenced to the common average (using the modified method to avoid potential data rank issues (Kim et al., 2023). ICA was performed to separate EEG sources using the Picard algorithm (Ablin et al., 2018), accounting for data rank (Kim et al., 2023). Artifactual components were classified using ICLabel (Pion-Tonachini et al., 2019) and extracted: ocular components with at least 90% confidence and muscular components with at least 95% confidence. Cleaned datasets were saved for subsequent analysis. On average across the group, 0.4 out of 64 EEG channels (SD = 0.6) were flagged as abnormal and interpolated, and 1.6 independent components (SD = 1.6) were flagged and extracted.

For computing spectral measures, continuous EEG data were downsampled to 256 Hz to reduce computational load and segmented by condition block. Scalp power spectral density (PSD) was computed across frequencies 1-95 Hz using a 2-s Hamming window, 50% overlap, and

Welch's method. Source reconstruction was conducted using the v1 version of the ROIconnect EEGLAB plugin (Pellegrini et al., 2023), which applies the Linearly Constrained Minimum Variance (LCMV) beamformer to project sensor-level data into source space —a method superior to alternatives such as eLORETA. A standard boundary element method (BEM) head model and a 68-region Talairach atlas were used to define cortical regions of interest (ROIs).

The resulting source time series for each region were orthogonalized using symmetric orthogonalization to minimize spatial leakage, and PSDs were computed using the multitaper method. All PSDs were normalized to decibels (dB) prior to statistical analysis. Functional connectivity (FC) was estimated using the default multivariate interaction measure (MIM), computed from a time-reversed multivariate autoregressive (MVAR) model. The default ROIconnect modelling (order 20 at a 100 Hz sampling rate) yields a 200-ms history window but limits the frequency resolution to 50 Hz. To address this, we modified the algorithm to calculate FC using a 200 Hz sampling rate and a model order of 40, while maintaining a 200 ms interaction window and extending the frequency range to 100 Hz. This configuration enables the detection of both fast, local interactions and slightly delayed dynamics, without compromising sensitivity to rapid activity.

For EDA, the analysis was made using the AcqKnowledge software. Tonic skin conductance level (SCL) was evaluated from the mean voltage of all dots in a given period. Spontaneous skin conductance responses (SCRs) were detected using AcqKnowledge software, which was properly adjusted to measure the time, amplitude, and area of the responses. For each phase (Baseline, WHBM, Rest), spontaneous SCRs were automatically detected on the phasic channel; artefactual segments were excluded on visual inspection. We extracted the SCR frequency (counts per phase divided by phase duration), amplitude (trough-to-onset to peak, ΔμS), and area (integral in μS·s from onset to offset). Tonic SCL was computed as the mean conductance across the phase after

excluding SCR transients. Traces were visually inspected, and motion/artefact segments were excluded prior to detection.

The capnograph/oximeter device stored a time-stamped trend record ($EtCO_2$, RR; SpO_2/Pulse Rate) logging measurements at 4-s intervals. Three hundred two lines were obtained for each participant (151 for the 10-minute baseline, 151 for the 10-minute experimental phase). Trends were exported from the instrument and compiled into Excel spreadsheets for analysis. Before analysis, we screened the Excel logs for device status messages and technical artefacts. Samples coincident with instrument errors or line issues (e.g., Apnea, Occlusion, Line Off, or Pump Off), abrupt pump flow disruptions, or visible capnogram failure (where available) were excluded, as recommended by the manufacturer for accurate trend interpretation. Entries with impossible physiologic values (e.g., $EtCO_2 < 0$ mmHg) were also discarded. When spurious or missing points occurred within a phase, they were not interpolated; instead, per-phase summaries were computed on the remaining valid samples. Two participants were excluded because the data were not recorded correctly by the capnograph (Naïve participant n. 3 and L2 participant n. 10). Otherwise, only two lines during the experiment show corrupted data. Otherwise, only two lines out of 302 for participant 17 were corrupted (8 seconds) during the experiment; therefore, they have been removed from the spreadsheet and didn't show any significant impact on the overall study results. Further analysis shows that the corrupted data.

For the capnograph/oximeter data, only six naïve (n=6, 12 pooled observations across phases) and nine experienced L2 practitioners (n=9; 18 pooled observations) were recorded with full capnography and oximetry variables—end-tidal CO_2 ($EtCO_2$), respiratory rate (RR), oxygen saturation (SpO_2), and pulse.

Cutaneous temperature was recorded with calibrated wire loggers. Devices were initialised, time-synchronised, and downloaded with ExactLog Software Setup v3.5.8; raw logs were exported

to Excel (.xlsx) for phase segmentation (Baseline, WHBM, Rest). Samples within each phase were averaged per site, and we computed ΔT = phase mean − Baseline mean for each of the three a priori locations (supraclavicular BAT depot, mid-sternal reference, upper thoracic paraspinal).

Statistics:

For EEG, non-parametric mass-univariate paired t-tests were used between conditions, employing a 10,000-iteration permutation procedure to estimate the null distribution (H0; Maris & Oostenveld, 2007). Type 1 error controlled using robust spatiotemporal cluster-based correction (Pernet et al., 2015). The significance level was set at $\alpha = 0.05$. EEG data were analyzed across four main conditions: 1) baseline resting state, 2) WHBM, 3) post-WHBM resting state, and 4) cold exposure (experts only) to assess spectral power and FC at both the scalp and source level. For functional connectivity (FC) statistical analyses, to reduce computational cost and large amounts of statistical tests, we averaged the data for each main frequency band: delta (1-3 Hz), theta (307 Hz), alpha (8-13 Hz), beta (13-30 Hz), low-gamma (30-45 Hz), mid-gamma (55-70 Hz), and high-gamma (70-95 Hz). Then, we used Fieldtrip's statcondfieldtrip() function to perform the permutations paired t-tests (10,000 iterations), alpha = 0.05, and cluster-based corrections for family-wise error (FWE).

The EDA data were analysed using Prism. For each outcome (frequency, amplitude, area), we conducted a one-way repeated-measures ANOVA for the full sample and a two-way mixed ANOVA (Phase within-subjects × Group between-subjects) followed by post-hoc comparisons: Baseline vs. WHBM and WHBM vs. Rest, using paired t-tests. Normality of the paired differences was assessed using the Shapiro–Wilk test; when this assumption was violated, a Wilcoxon signed-

rank test was used as a robustness check. The analysis was conducted on the entire population (N = 17), and participants were then segregated into two groups: naive (N = 7) and expert (N = 10).

The capnography/oximetry data were analysed using paired comparisons within participants (N = 15). For each variable, we computed participant-level means per phase (Baseline and WHBM) and analysed difference scores (WHBM − Baseline). Normality of paired differences was evaluated using the Shapiro–Wilk test; when the assumption was met, we applied paired-samples Student's t-tests. When normality was borderline/violated ($EtCO_2$), we used the Wilcoxon signed-rank test.

For the comparison between groups, distributional assumptions were assessed using the Shapiro–Wilk test (normality) and the Levene test (homogeneity of variance). When assumptions were met, we used independent-samples Student t-tests. For variables violating normality and/or homoscedasticity ($EtCO_2$: W $p = .003$, Levene $p = .013$; SpO_2: W $p = .017$), we reported Welch's t alongside a non-parametric Mann–Whitney U test as a robustness check. Two-sided $\alpha=.05$. Effect sizes were Cohen's d for parametric tests and rank-biserial r for Mann–Whitney, with $|d|>0.80$ or $|r|>0.30$ interpreted as large. In figures/tables, statistical markers are: * $p < 0.05$, ** $p < 0.01$, † $p < 0.10$ (trend). Boxplots were used to visualise distribution overlap and differences in dispersion between groups. Choice of variables follows standard WHBM physiology readouts and prior literature on ventilatory/oximetry responses.

We tested the effect of the WHBM breathing epoch on capnography/oximetry endpoints—end-tidal CO_2 ($EtCO_2$), respiratory rate (RR), oxygen saturation (SpO_2), and pulse—using paired comparisons within participants (N=15). For each variable, we computed participant-level means per phase (Baseline, WHBM) and analysed difference scores (WHBM − Baseline). Normality of paired differences was evaluated using the Shapiro–Wilk test; when the assumption was met, we

applied paired-samples Student's t-tests. When normality was borderline/violated ($EtCO_2$), we used the Wilcoxon signed-rank test.

IV. Results:

1. EEG Scalp Analysis: WHBM vs Baseline

Considering the whole group (Naïve and L2 practitioners combined), the scalp spectral analysis comparing WHBM to baseline revealed widespread increases in parietal and posterior high-frequency activity (Figure 5A). Significant widespread increases were observed in the beta frequency range (11–26 Hz; peaking in bilateral occipitoparietal regions; see Figure 5.B) and the gamma frequency band (29.5–95 Hz, peaking in the left posterior region at 92.5 Hz; see Figure 5.C). Compared to the Rest condition following WHBM (See Figure S1 in Supplementary Data), WHBM elicited additional increases in the delta frequency band (1–5 Hz; peaking over centroparietal regions), the mid-to-high beta frequency band (peaking over parietal areas), and in the gamma frequency band (peaking over the right temporoparietal electrodes).

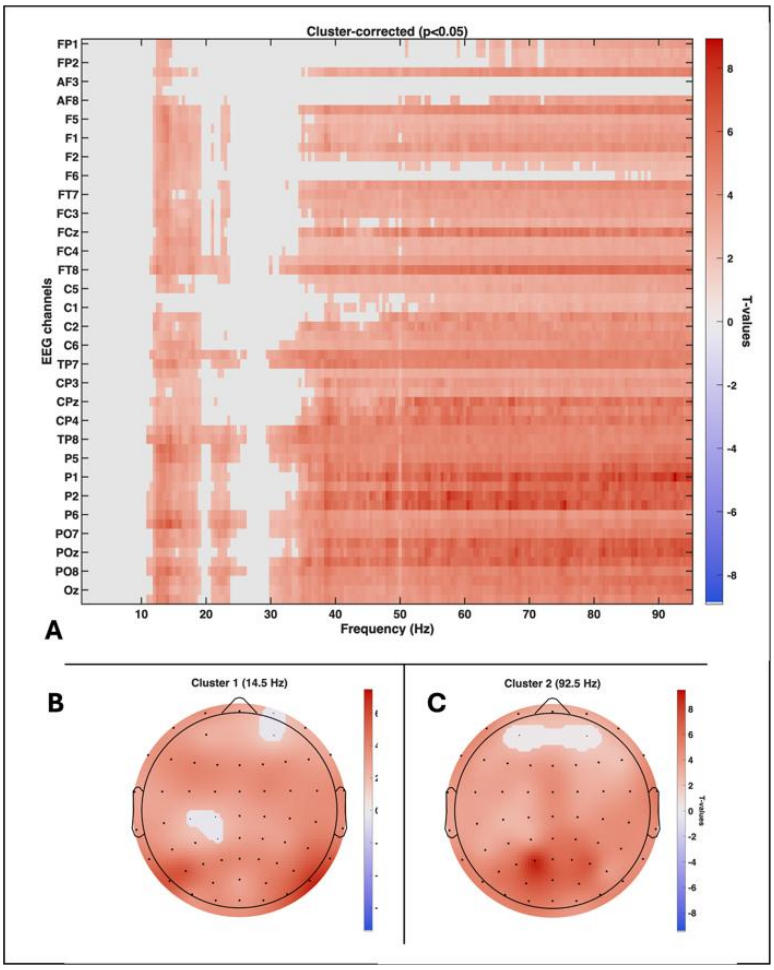

Figure 2. Comparing WHBMB vs Baseline on the whole group (N = 17). **A.** Mass-univariate result (10,000 permutations t-test with spatiotemporal cluster correction at alpha = 0.05), showing the two significant spatiotemporal clusters (11-26 Hz and 29.5 to 95 Hz), reflecting widespread increases in EEG spectral power in these frequencies during WHBMB relative to baseline. X-axis: Frequencies. Y-axis: EEG electrodes. **B.** Scalp topography at the peak frequency of cluster 1 (at 14.5 Hz at electrode P8; t-value = 6.7). **C.** Scalp topography at the peak frequency of cluster 2 (92.5 Hz at electrode P1; t-value = 8.9). **Note:** Red colours show positive t-values (i.e., increases) and blue colours show negative t-values (decreases).

When considering Experts only (n = 10), we observed three significant clusters (Figure 6.A), showing widespread increases in the delta frequency band (1–1.5 Hz; Figure 6.B), low-beta frequency band (12.5-18.5 Hz peaking in the left posterior areas; Figure 6.C), and gamma frequency band (31–95 Hz; peaking over central posterior sites; Figure 6.D). Compared to the Rest condition following the WHBM task (see Figure S2 in Supplementary data), experts demonstrated low-frequency frontal increases, posterior alpha suppression, and strong gamma enhancement over central-parietal electrodes.

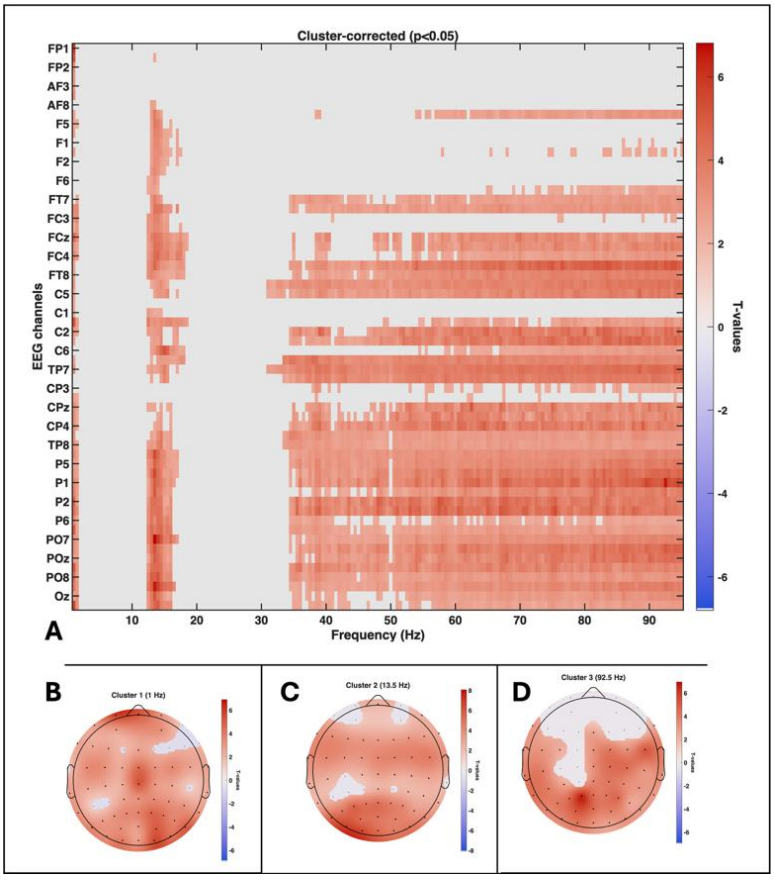

Figure 3. Comparing WHBMB vs Baseline on the group of L2 practitioners (N = 10). **A.** Mass-univariate result (10,000 permutations t-test with spatiotemporal cluster correction at alpha = 0.05), showing the three significant spatiotemporal clusters (1-1.5 Hz, 12.5-18.5 Hz, 31-95 Hz),

615 reflecting widespread increases in EEG spectral power in these frequencies during WHBMB
616 relative to baseline. X-axis: Frequencies. Y-axis: EEG electrodes. **B.** Scalp topography at the
617 peak frequency of cluster 1 (at 1 Hz at electrode FP1; t-value = 5.9). **C.** Scalp topography at the
618 peak frequency of cluster 2 (13.5 Hz at electrode PO7; t-value = 6.8). **D.** Scalp topography at the
619 peak frequency of cluster 3 (92.5 Hz at electrode P1; t-value = 6.6). **Note:** Red colours show
620 positive t-values (i.e., increases) and blue colours show negative t-values (decreases).
621
622 Naives, in contrast, showed broader and less topographically specific changes (Figure 7.A).
623 WHBM vs. baseline revealed moderate increases in posterior alpha/beta (Figure 7 B) and very
624 strong gamma increases at frontopolar electrodes (AF8; Figure 7C). Compared to Rest following
625 the WHBM task (see Figure S3 in Supplementary data), novices displayed smaller delta increases,
626 slight alpha enhancements over the left posterior cortex, and beta increases in the right temporal-
627 parietal area.
628

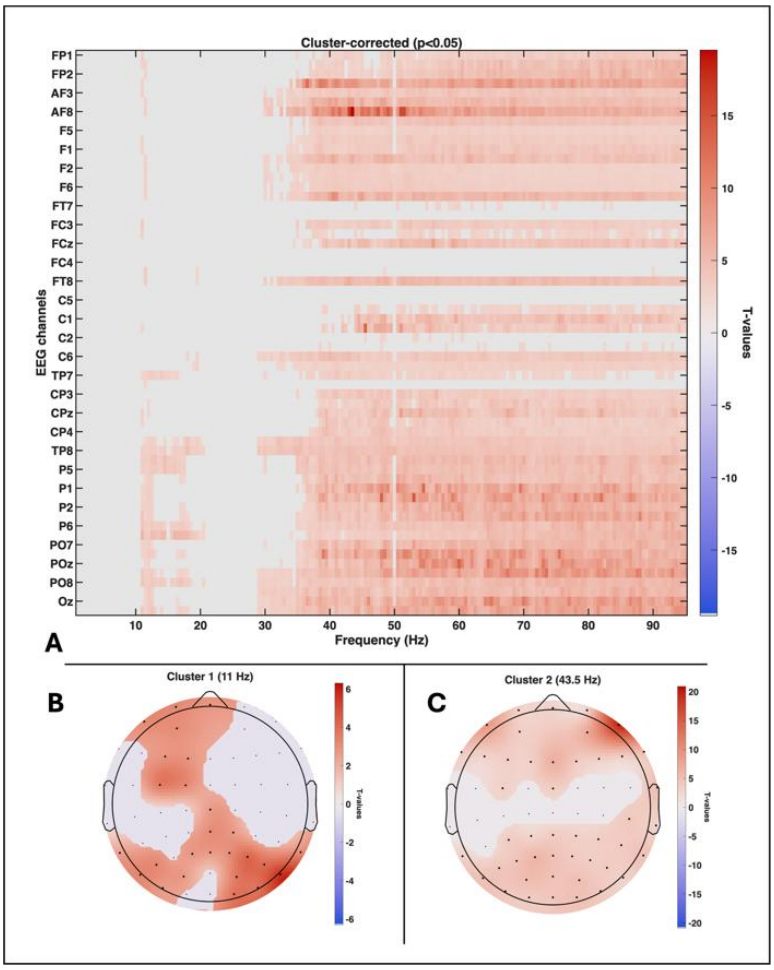

Figure 4. Comparing WHBMB vs Baseline in the group of Novices (N = 7). **A.** Mass-univariate result (10,000 permutations t-test with spatiotemporal cluster correction at alpha = 0.05), showing two significant spatiotemporal clusters (11-20.5 Hz and 29-95 Hz), reflecting widespread increases in EEG spectral power in these frequencies during WHBMB relative to baseline. X-axis: Frequencies. Y-axis: EEG electrodes. **B.** Scalp topography at the peak frequency of cluster 1 (at 11 Hz at electrode P8; t-value = 5.7). **C.** Scalp topography at the peak frequency of cluster 2 (43.5 Hz at electrode AF8; t-value = 19.5). **Note:** Red colours show positive t-values (i.e., increases) and blue colours show negative t-values (decreases).

2. EEG Scalp Analysis: Cold Immersion versus Rest

Relative to the Rest condition preceding the immersion in cold water, we observed a widespread spectral power increase in the gamma frequency range (27–95 Hz; see Figure 8.A), peaking over electrode PO7 in the left posterior regions at 66 Hz (t-value = 9.7; Figure 8.B).

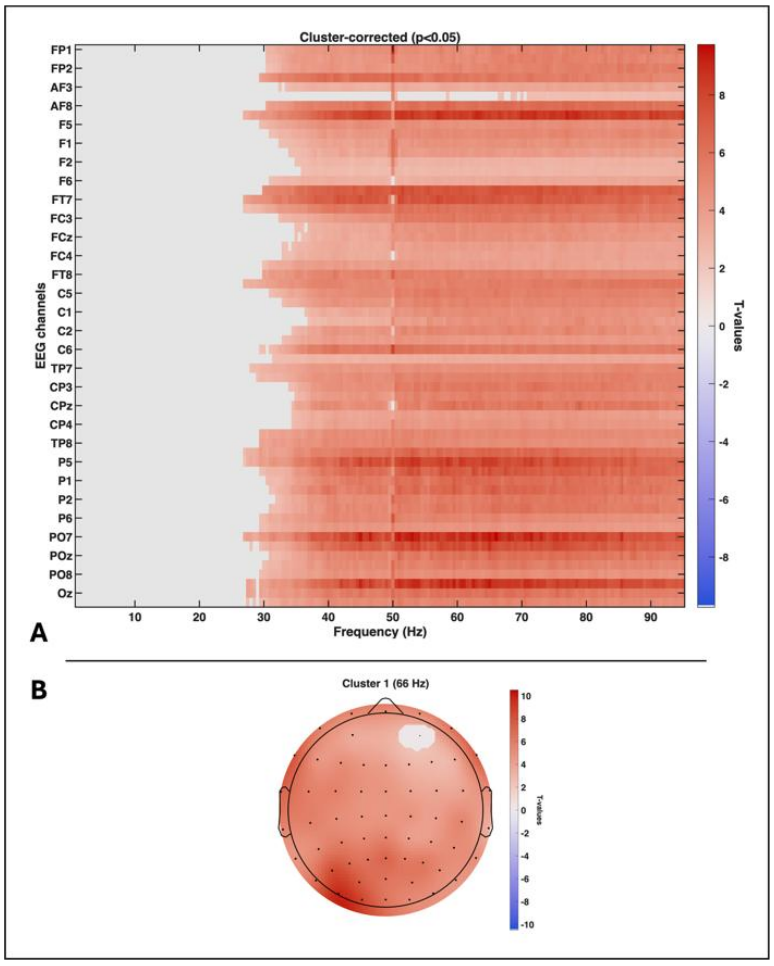

Figure 5. Comparing Cold immersion vs Rest in the group of L2 practitioners (N = 10). **A.** Mass-univariate result (10,000 permutations t-test with spatiotemporal cluster correction at alpha = 0.05), showing one significant spatiotemporal cluster (27 Hz and 95 Hz), reflecting widespread increases in EEG spectral power in these frequencies during Cold immersion relative to Rest. X-axis: Frequencies. Y-axis: EEG electrodes. **B.** Scalp topography at the peak frequency of the

cluster (at 66 Hz at electrode PO7; *t-value = 9.7*). **Note:** Red colours show positive t-values (i.e., increases) and blue colours show negative t-values (decreases).

3. EEG source spectral analysis: WHBM vs Baseline

Considering the whole group (Naives and L2 practicioners combined), source-level spectral power analysis revealed five major significant clusters (see Figure 9), depicting spectral increases in the 1-2 Hz range (peaking in the left middle temporal gyrus; t-value = 5.5; Figure 9.B), the 11-16.5 Hz range (peaking in the left lateral occipital area at 12 Hz; t-value = 4.2; Figure 9.C), the 21.5-26 Hz (peaking in the same area at 24.5 Hz; t-value = 3.6; Figure 9.D), the 29.5-49 Hz range (peaking in the right cuneus at 40.5 Hz; t-value = 4.5; Figure 9.E), and the 51-95 Hz range (peaking in the left precuneus at 79.5 Hz; t-value = 5.5; Figure 9.F).

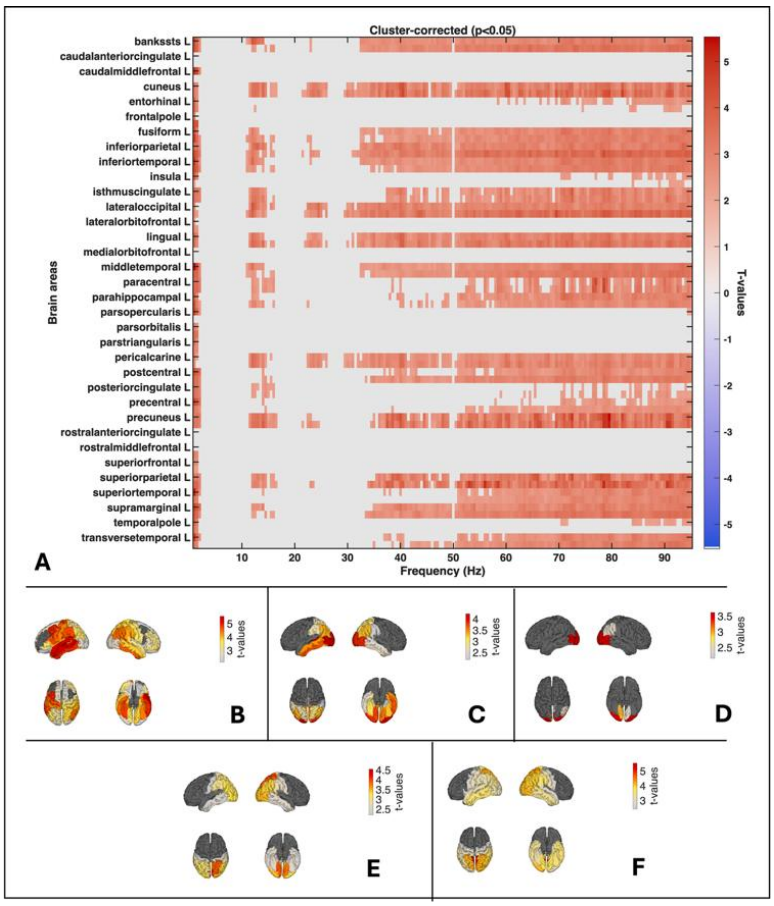

664

665 **Figure 6.** Comparing source spectral power between the WHBMB and Baseline conditions for
666 the whole group (Naives and L2 practitioners combined; N = 17). A. Mass-univariate result
667 (10,000 permutations t-test with spatiotemporal cluster correction at alpha = 0.05), showing five
668 significant spatiotemporal clusters (1-2 Hz, 11-16.5 Hz, 21.5-26 Hz, 29.5-49 Hz, and 51-95 Hz),
669 reflecting widespread increases in spectral power in these frequencies during WHBMB relative
670 to baseline. X-axis: Frequencies. Y-axis: Brain areas. B. Corrected cortical surface t-map
671 showing the peak of cluster 1 at 1 Hz in the left middle temporal area. C. Corrected cortical
672 surface t-map showing the peak of cluster 2 at 12 Hz in the left lateral occipital area. D.
673 Corrected cortical surface t-map showing the peak of cluster 3 at 24.5 Hz in the left lateral
674 occipital area. E. Corrected cortical surface t-map showing the peak of cluster 4 at 40.5 Hz in the
675 right cuneus. F. Corrected cortical surface t-map showing the peak of cluster 5 at 79.5 Hz in the

left precuneus. Note: Red colours show positive t-values (i.e., increases) and blue colours show negative t-values (decreases).

When considering only the L2 practitioners, we observed six significant clusters (Figure 7): increased power in the delta band peaking in the left superior temporal area (t-value = 4; Figure 7.B), decreased power in the alpha band peaking at 9.5 Hz in the left lateral occipital area (t-value = 4.5; Figure 7.C), increased power in the beta band peaking right precuneus at 14 Hz (t-value = 3.6; Figure 7.D), increased power in the 38-40.5 Hz range peaking at 40.5 Hz in the right cuneus (t-value = 3.3; Figure 10.E), increased power in the 66-68 Hz range peaking in the left precuneus at 66.5 Hz (t-value = 2.9; Figure 7.F), and increased power in the 70-95 Hz range peaking in the right paracentral area at 78.5 Hz (t-value = 4.8; Figure 7.G). Compared to rest, experts continued to exhibit widespread posterior gamma increases and focused beta enhancements in right occipital regions, reinforcing the interpretation of a regulated, internally focused brain state with increased precision in sensory integration and body awareness (see Figure S5 in Supplementary Data).

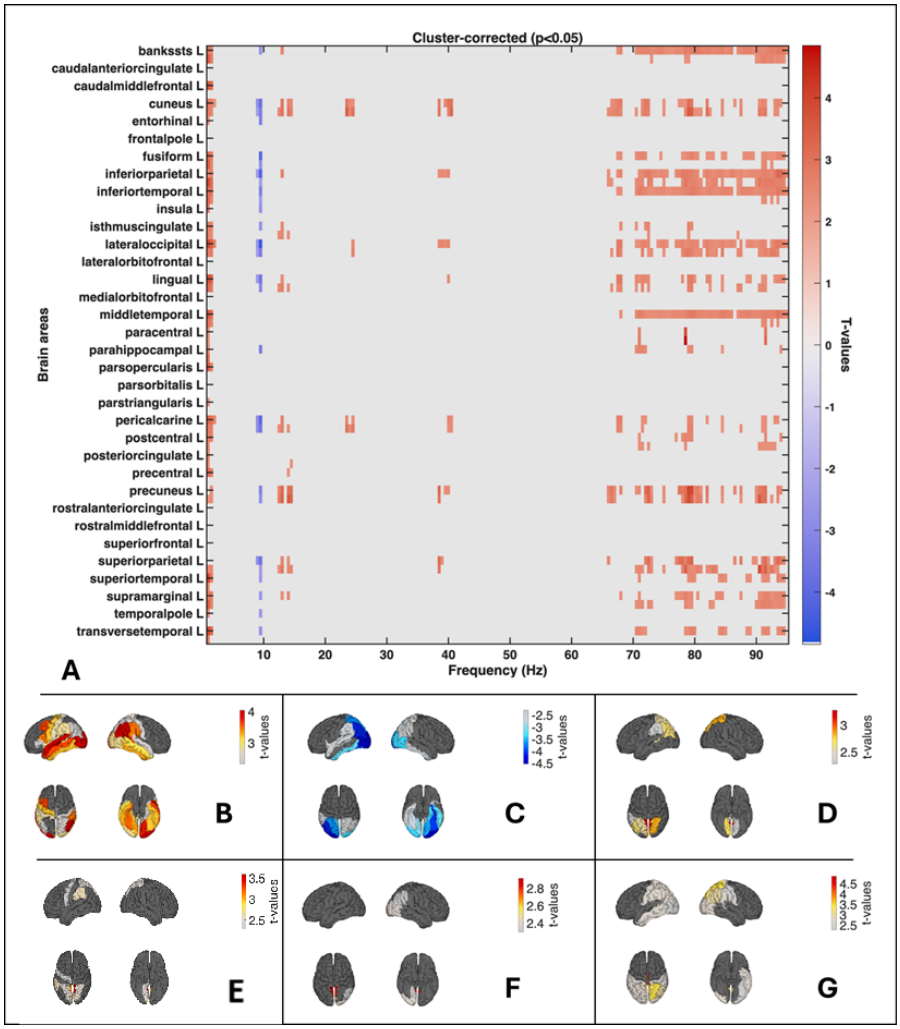

692

693 **Figure 7.** Comparing source spectral power between the WHBMB and Baseline conditions for
694 the L2 practitioners group. **A.** Mass-univariate result (10,000 permutations t-test with
695 spatiotemporal cluster correction at alpha = 0.05), showing six significant spatiotemporal clusters
696 (1-2 Hz, 9-9.5 Hz, 12.5-24.5 Hz, 23.5-24.5 Hz, 66-68 Hz, and 70-95 Hz), reflecting widespread
697 increases in spectral power in these frequencies during WHBMB relative to baseline. X-axis:
698 Frequencies. Y-axis: Brain areas. **B.** Corrected cortical surface t-map showing the peak of cluster
699 1 at 1 Hz in the left superior temporal area. **C.** Corrected cortical surface t-map showing the
700 peak of cluster 2 at 9.5 Hz in the left lateral occipital area. **D.** Corrected cortical surface t-map
701 showing the peak of cluster 3 at 14 Hz in the right precuneus. **E.** Corrected cortical surface t-

map showing the peak of cluster 5 at 23.5 Hz in the left and right cuneus. **F.** Corrected cortical surface t-map showing the peak of cluster 5 at 66.5 Hz in the left precuneus. **G.** Corrected cortical surface t-map showing the peak of cluster 6 at 78.5 Hz in the right paracentral area. **Note**: Red colours show positive t-values (i.e., increases) and blue colours show negative t-values (decreases).

When considering Naives only, we observed four significant clusters (Figure 8): increased power in the delta band peaking at 1.5 Hz in the right temporal pole (t-value = 6; Figure 8.B), increased power in the alpha band peaking at 11 Hz in the right parahippocampal area (t-value = 3.8; Figure 8.C), increased power in the 16.5-32 Hz peaking in the right fusiform area at 25.5 Hz (t-value = 4.5; Figure 8.D), and increased power in the 33-49 Hz range peaking at 41 Hz in the left pericalcarine area (t-value = 8.3; Figure 11.E). Compared to rest (see Figure S12-13 in Supplementary Data), novices showed a posterior-dominant profile with increased gamma in pericalcarine cortex and alpha/beta activity in medial visual and associative areas, suggesting early recruitment of sensory-integration and DMN hubs, albeit without the frontal and regulatory engagement seen in experts and novices. Source spectral analysis for cluster-corrected effects was sparse.

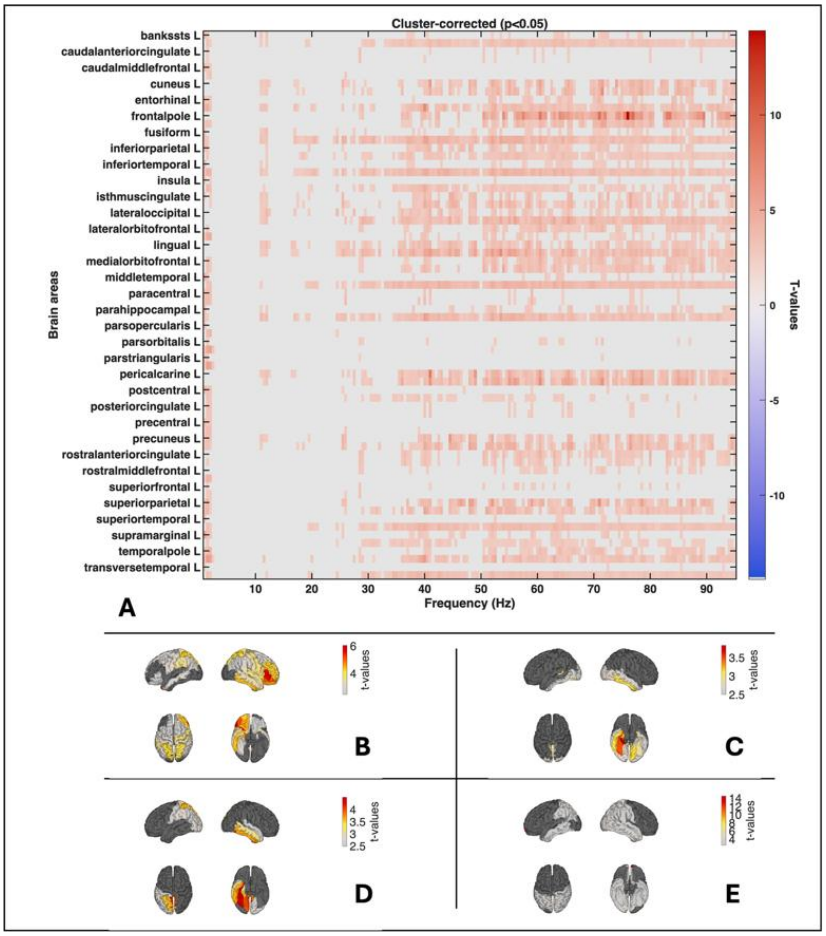

720

721 **Figure 8.** Comparing source spectral power between the WHBMB and Baseline conditions for
722 the Naives group. **A.** Mass-univariate result (10,000 permutations t-test with spatiotemporal
723 cluster correction at alpha = 0.05), showing four significant spatiotemporal clusters (1-2 Hz, 11-
724 12.5 Hz, 16.5-32 Hz, 33-49.5 Hz), reflecting widespread increases in spectral power in these
725 frequencies during WHBMB relative to baseline. X-axis: Frequencies. Y-axis: Brain areas. **B.**
726 Corrected cortical surface t-map showing the peak of cluster 1 at 1.5 Hz in the right temporal
727 pole. **C.** Corrected cortical surface t-map showing the peak of cluster 2 at 11 Hz in the right
728 parahippocampal area. **D.** Corrected cortical surface t-map showing the peak of cluster 3 at 25.5
729 Hz in the right fusiform area. **E.** Corrected cortical surface t-map showing the peak of cluster 4

at 41 Hz in the pericalcarine. **Note**: Red colours show positive t-values (i.e., increases) and blue colours show negative t-values (decreases).

4. EEG spectral analysis in brain areas: Cold immersion versus Rest

After source reconstruction, when comparing the Cold Immersion and Rest conditions within the L2 practitioners group, two significant clusters were identified (Figure 9). The first cluster showed increased power between 1 and 10.5 Hz, with a peak effect in the left inferior temporal region at 1 Hz (t-value = 6.2; Figure 9.B). The second cluster extended from 12.5 to 95 Hz, peaking at 39.5 Hz in the same left inferior temporal region (t-value = 9; Figure 9.C), reflecting a broadband enhancement of both low- and high-frequency activity during cold immersion relative to rest.

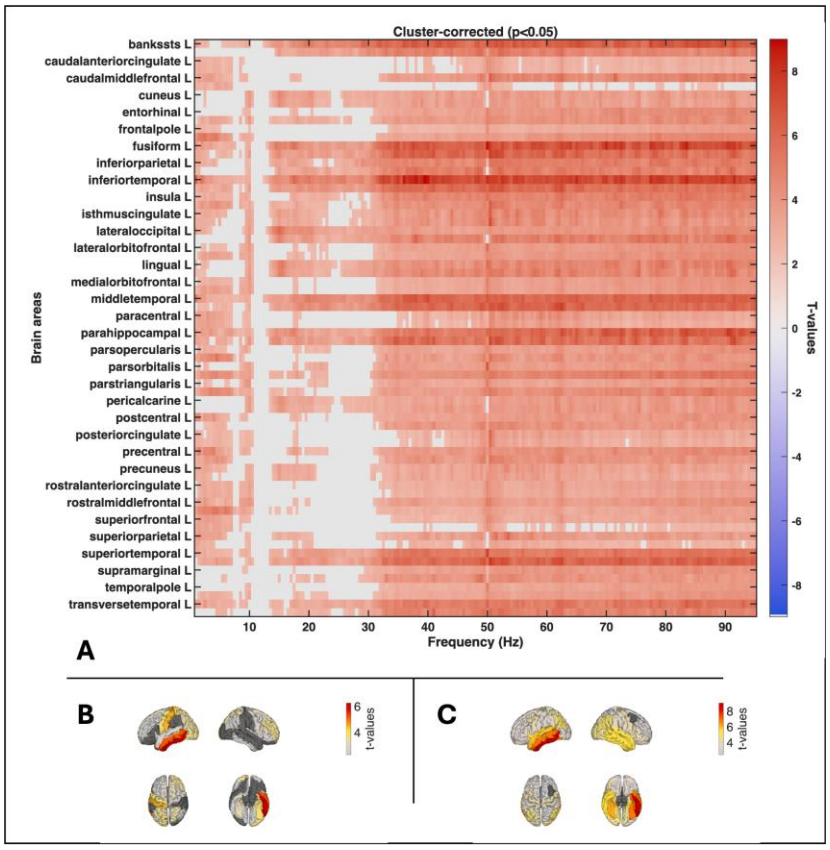

743

744 **Figure 9.** Comparing source spectral power between the Cold immersion and the Rest condition
745 that preceded it (L2 practitioners only). **A.** Mass-univariate result (10,000 permutations t-test
746 with spatiotemporal cluster correction at alpha = 0.05), showing two significant spatiotemporal
747 clusters (1-10.5 Hz and 12.5-95 Hz), reflecting widespread increases in spectral power in these
748 frequencies during Cold immersion relative to Rest. X-axis: Frequencies. Y-axis: Brain areas. **B.**
749 Corrected cortical surface t-map showing the peak of cluster 1 at 1 Hz in the left inferior
750 temporal area. **C.** Corrected cortical surface t-map showing the significant areas of cluster 2 at
751 39.5 Hz in the same area. **Note**: Red colours show positive t-values (i.e., increases) and blue
752 colours show negative t-values (decreases).

753

754 **5. EEG functional connectivity (FC) analysis: WHBM vs Baseline**

Considering the whole group (Naives and L2 practitioners combined), we observed differences in FC in the theta (3-7 Hz), mid-gamma (55-70 Hz), and high-gamma (70-95 Hz) frequency bands. In the theta band (Figure 10.A), the most prominent hubs included the postcentral and precentral gyri, which exhibited widespread increased synchrony with prefrontal areas (rostral and caudal middle frontal, superior frontal, frontal poles), limbic structures (anterior and posterior cingulate, insula), and temporal regions (temporal poles, fusiform, superior and transverse temporal gyri, entorhinal cortex). In the mid-gamma band (Figure 10.B), FC during WHBM relative to baseline showed widespread increases, particularly among posterior midline and limbic regions. Top effects included strengthened connectivity between the posterior cingulate cortex (PCC) and bilateral pericalcarine and cuneus cortices, suggesting heightened integration between default mode and early visual areas. The isthmus of the cingulate gyrus emerged as a key hub, showing increased coupling with the precuneus, superior temporal, supramarginal, and lateral orbitofrontal cortices. Several high t-value connections also involved the paracentral lobule, entorhinal cortex, and parahippocampal regions, indicating enhanced crosstalk between sensorimotor, mnemonic, and viscerosensory systems. In high gamma (Figure 10C), 1,994 significant region pairs showed enhanced coupling during WHBM relative to the baseline. The most prominent effects involved the postcentral and precentral gyri acting as major hubs of increased synchrony with prefrontal cortices (superior frontal, rostral and caudal middle frontal, frontal poles), limbic structures (insula, anterior and posterior cingulate), and temporal regions (temporal poles, fusiform, superior temporal gyrus).

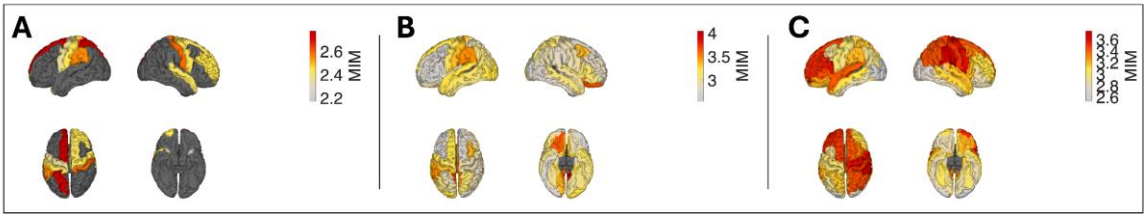

Figure 10. Cortical surface t-maps of functional connectivity (FC) between brain areas, comparing WHBM versus Baseline (Naives and L2 practitioners combined), obtained using 10,000 permutations statistics and spatiotemporal cluster correction for family-wise error (FWE), at $\alpha = 0.05$. **A.** FC differences in the theta frequency band (3-7 Hz). **B.** FC differences in the mid-gamma frequency band (55-70 Hz). **C.** FC differences in the high-gamma frequency band (70-95 Hz).

When considering only the L2 practitioners group, significant FC differences were observed in the same frequency bands: theta (3-7 Hz), mid-gamma (55-70 Hz), and high-gamma (70-95 Hz). In the theta band (Figure 11A), expert practitioners exhibited enhanced functional connectivity centred on the postcentral gyri, indicating stronger integration within somatosensory and sensorimotor systems. The right superior temporal gyrus was strongly linked to left precentral and postcentral cortices, reflecting cross-hemispheric coordination between auditory and motor-sensory areas. Additional connections with parietal, frontal, and posterior cingulate regions suggest broader engagement of parietal-somatosensory, top-down control, and self-referential networks. Mid-gamma FC (Figure 11.B) was centred on postcentral, posterior cingulate, and superior parietal areas. High-gamma FC (Figure 11.C) was increased between posterior midline structures (particularly the posterior and isthmus cingulate cortices) and frontal control regions, including caudal middle frontal and anterior cingulate cortices. Additional strong connections emerged

between the precuneus, paracentral, and frontal pole areas, as well as between lateral frontal (e.g., pars opercularis, pars triangularis) and posterior somatosensory or occipital cortices.

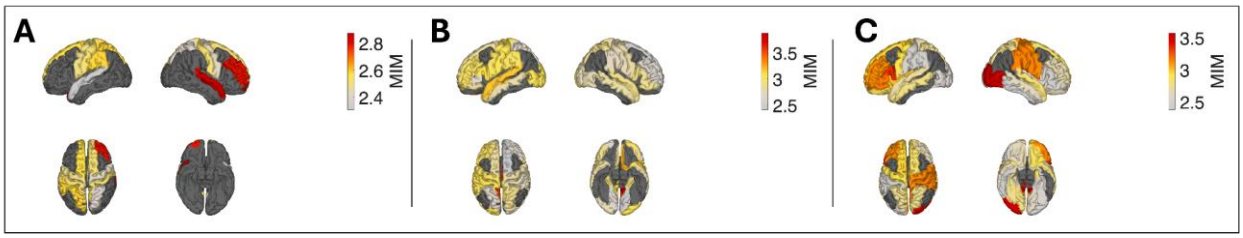

Figure 11. Cortical surface t-maps of functional connectivity (FC) between brain areas, comparing WHBM versus Baseline (L2 practitioners only), obtained using 10,000 permutations statistics and spatiotemporal cluster correction for family-wise error (FWE), at $\alpha = 0.05$. **A.** FC differences in the theta frequency band (3-7 Hz). **B.** FC differences in the mid-gamma frequency band (55-70 Hz). **C.** FC differences in the high-gamma frequency band (70-95 Hz).

When considering the Naive group, significant FC increases were found in the beta (13–30 Hz), mid-gamma (55–70 Hz), and high-gamma (70–95 Hz) ranges (Figure 12). In the beta band (Figure 12A), enhanced connectivity is linked to posterior midline regions—particularly the precuneus and isthmus cingulate—with lateral occipital and parahippocampal cortices, indicating stronger integration within posterior default-mode and visual-associative networks. In the mid-gamma range (Figure 12 B), connectivity was strongest between the right superior and transverse temporal regions and the left occipital areas (lingual and lateral occipital cortices), with additional bilateral couplings among the parahippocampal, fusiform, entorhinal, and temporal cortices, reflecting the engagement of medial temporal and high-level visual systems. In the high-gamma band (Figure 12, C), increased connectivity emerged between right superior and transverse temporal areas and bilateral occipitotemporal regions, including lingual, lateral occipital, and

fusiform cortices. Additional links involving medial temporal, posterior cingulate, and midline sensorimotor regions (paracentral, cuneus) suggest integrated activation across perceptual, mnemonic, and sensorimotor networks.

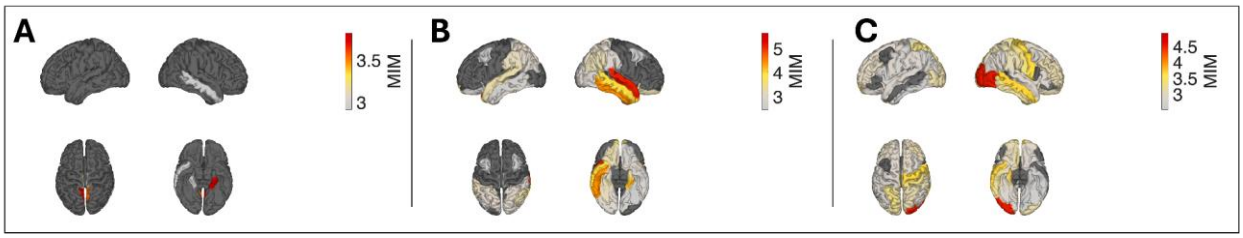

Figure 12. Cortical surface t-maps of functional connectivity (FC) between brain areas, comparing WHBM versus Baseline (Naive group), obtained using 10,000 permutations statistics and spatiotemporal cluster correction for family-wise error (FWE), at $\alpha = 0.05$. **A.** FC differences in the beta frequency band (13-30 Hz). **B.** FC differences in the mid-gamma frequency band (55-70 Hz). **C.** FC differences in the high-gamma frequency band (70-95 Hz).

6. EEG functional connectivity (FC) analysis: WHBM vs Baseline

During cold immersion, L2 practitioners showed widespread alpha-band (8-13 Hz) FC increases (151 region pairs; Figure 13.A), reflecting strong engagement of posterior sensory and parietal networks. Prominent links between somatosensory and visual areas (postcentral, occipital, cuneus, fusiform) indicated enhanced visual-somatosensory integration. Additional connections involving the supramarginal, inferior parietal, insular, and orbitofrontal regions suggested coordinated activity across multisensory, interoceptive, and affective networks, while links between the posterior cingulate and precuneus pointed to maintained self-referential awareness during cold exposure. We observed marked increases in low gamma-band (30–45 Hz) connectivity

across 1,700 region pairs (Figure 13.B), representing the strongest effects observed across all frequencies (peak t = 10.44). Dominant hubs included the right postcentral gyrus, lingual gyri, inferior parietal lobules, insula, and visual-associative regions such as the pericalcarine and precuneus. In the mid-gamma band (55–70 Hz), FC also increased relative to rest, spanning 2,112 region pairs (Figure 13.C). The strongest effects occurred between visual areas (pericalcarine, lateral occipital, lingual) and frontal or opercular regions (pars opercularis, pars orbitalis, caudal middle frontal). Additional increases were observed between temporal poles and occipital or limbic structures. During cold immersion, L2 practitioners exhibited significantly increased high gamma-band (70–95 Hz) connectivity relative to rest, encompassing 1,932 region pairs (Figure 13.D). The dominant pattern involved strong posterior–frontal coupling, particularly between the right lateral occipital cortex and caudal middle frontal, precentral, paracentral, and posterior cingulate regions. Additional widespread increases were observed across right occipitoparietal and temporal areas, including frontoparietal, cingulo-opercular, and dorsal attention network regions such as the rostral middle frontal, superior parietal, anterior cingulate, and insula.

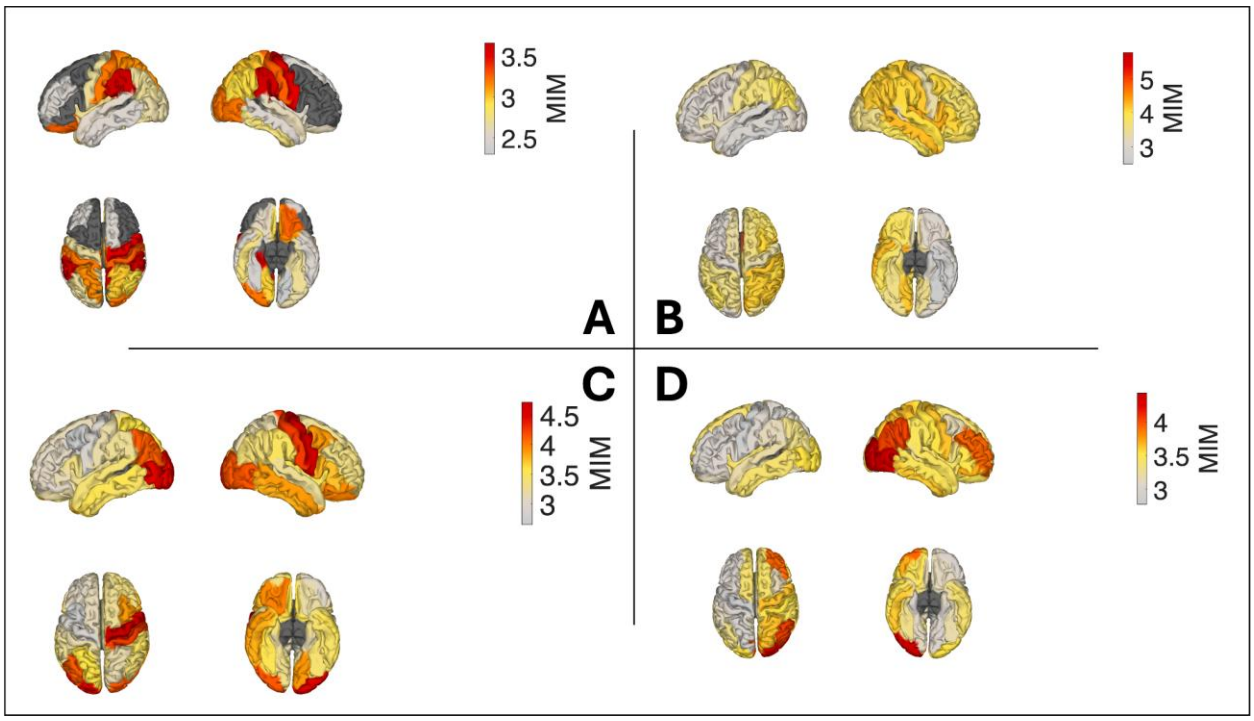

Figure 13. Cortical surface t-maps of functional connectivity (FC) between brain areas, comparing WHBM versus Baseline (Naive group), obtained using 10,000 permutations statistics and spatiotemporal cluster correction for family-wise error (FWE), at $\alpha = 0.05$. **A.** FC differences in the alpha frequency band (8-13 Hz). **B.** FC differences in the low-gamma frequency band (30-45 Hz). **C.** FC differences in the mid-gamma frequency band (55-70 Hz). **D.** FC differences in the high-gamma frequency band (70-95 Hz).

7. GSR Data

In the full sample (N = 17), WHBM produced clear sympathetic activation across all SCR metrics (Figure 14). Frequency rose sharply from Baseline to WHBM (***$p < 0.001$) and then declined during Rest, remaining significantly lower than WHBM (+++$p < 0.001$). Amplitude likewise increased from Baseline to WHBM (**$p < 0.01$) and decreased during Rest relative to

WHBM (++p < 0.01). Area (µS·s) showed the same pattern, with larger responses during WHBM than Baseline (**p < 0.01) and a reduction at Rest compared with WHBM (++p < 0.01). Bars in the lower panels display group means ± SD, while the upper "connected line" plots show that these effects were evident in most participants.

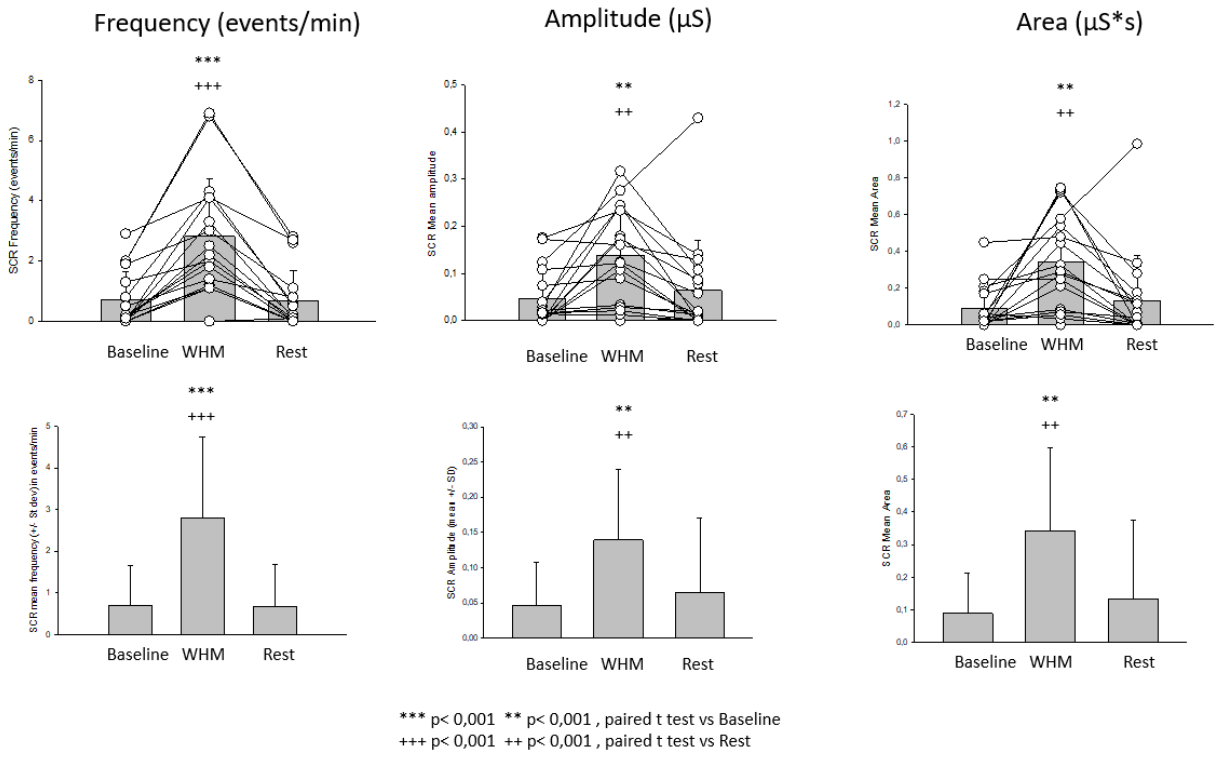

Figure 14

Electrodermal activity across phases of the Wim Hof Method

(Spontaneous SCR frequency (events·min⁻¹), amplitude (µS), and area (µS·s)).

Data are summarised as mean + SD (N=17). Each dot on top represents a single participant.

Naive (n = 7) and experienced (n = 10) practitioners showed the same phase-dependent pattern across all GSR metrics (Figure 15). Within each group, SCR frequency, amplitude, and

area increased from Baseline to WHBM and decreased from WHBM to Rest (paired comparisons within group; p-values as annotated). Critically, these changes did not differ reliably between groups: there were no significant between-group differences at any phase for any metric, and no evidence that the phase-related pattern was modulated by experience (all $p > 0.05$).

Within-group a priori contrasts showed: frequency increased from Baseline to WHBM (naïve $p < .05$; experienced $p < .001$) and decreased from WHBM to Rest (naïve $p < .05$; experienced $p < .001$); amplitude increased from Baseline to WHBM in both groups ($p < .05$) but the WHBM to Rest decrease was significant only in the experienced group ($p < .05$); area increased from Baseline to WHBM in both groups ($p < .05$) and decreased from WHBM to Rest only in the experienced group ($p < .01$). Collectively, these results indicate a robust phasic sympathetic activation during WHBM in both cohorts with stronger WHBM to Rest reversals for amplitude and area among experienced practitioners.

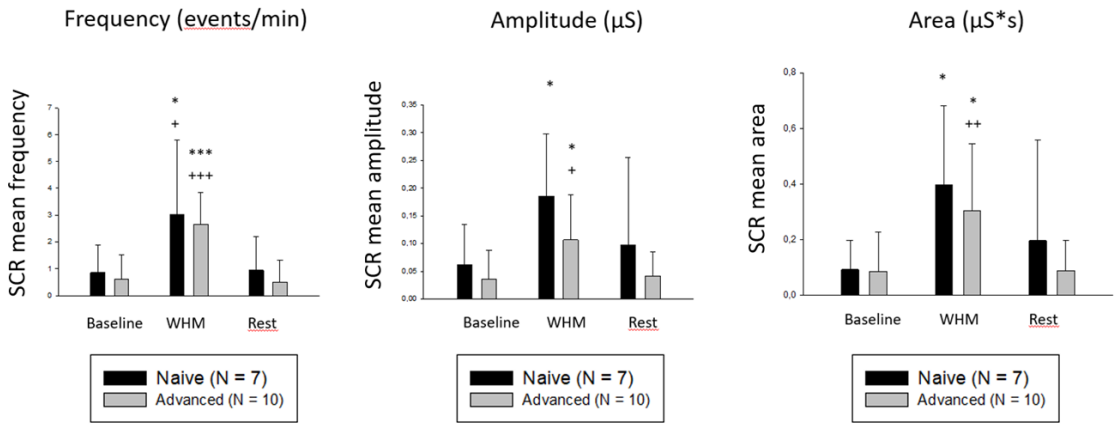

*** p< 0,001 * p< 0,05 , paired t test vs. Baseline
+++ p<0,001, ++p<0,01, +p<0,05 paired t test vs. Rest
Mean +/- Standard dev
No significant difference between naive and Experienced

Figure 15

Frequency, Amplitude and Area across

(Group bars depict mean ± SD)

8. Capnography Results

Overall, for the whole group (n=15), WHBM breathing produced the expected physiological shift: $EtCO_2$ fell markedly from 5.73% (SD = 0.539; range = 4.44–6.62) at Baseline to 2.92% (SD = 0.782; 1.87–4.63) during the Experimental phase, consistent with pronounced hypocapnia (Table 4).

	N	Mean	Median	SD	Minimum	Maximum
SpO2_Mn. Baseline	15	97.61	98.07	1.582	94.32	99.00
SpO2_Mn. WHBM	15	96.21	96.47	1.726	93.43	98.89
EtCO2_Mn. Baseline	15	5.73	5.78	0.539	4.44	6.62
EtCO2_Mn. WHBM	15	2.92	2.72	0.782	1.87	4.63
Pulse_Mn. Baseline	15	65.86	64.86	6.936	57.28	77.28
Pulse_Mn. WHBM	15	73.78	73.10	7.812	59.31	88.87

	N	Mean	Median	SD	Minimum	Maximum
Respiratory rate_Mn. Baseline	15	10.60	11.03	4.205	5.28	18.49
Respiratory rate_Mn. WHBM	15	10.53	10.11	0.887	9.71	12.54

Table 4

Within Subject Baseline vs WHBM Descriptives

Boxplots (Figure 16) show the expected WHBM physiological signature: $EtCO_2$ shifts from a Baseline centre near ~5.7% to clearly lower values during WHBM (median ≈2.7–2.8%, IQR ~2.4–3.2%, a few higher outliers ≤~4.6%), indicating marked hypocapnia. SpO_2 shows a modest decline (97.61%→96.21%; Baseline median ≈98.1% with a few ~94–95% outliers vs WHBM median ≈96.5–96.7% spanning ~93–99%). Pulse rises (65.86→73.78 bpm; Baseline median ≈64–65 to ≈73 bpm) with a broader upper tail to ~89 bpm, consistent with sympathetic activation. Respiratory rate (RR) maintains a similar central tendency (10.60 vs 10.53 $br \cdot min^{-1}$). Still, its dispersion decreases from SD 4.205 and a range of 5.28–18.49 to SD 0.887 and 9.71–12.54, reflecting convergence to a paced rhythm with intervening apneas.

Overall, the plots depict a coordinated shift—lower $EtCO_2$, slightly lower SpO_2, higher pulse, and stabilised RR variability—characteristic of controlled hyperventilation followed by low-volume breath retentions in the WHBM phase.

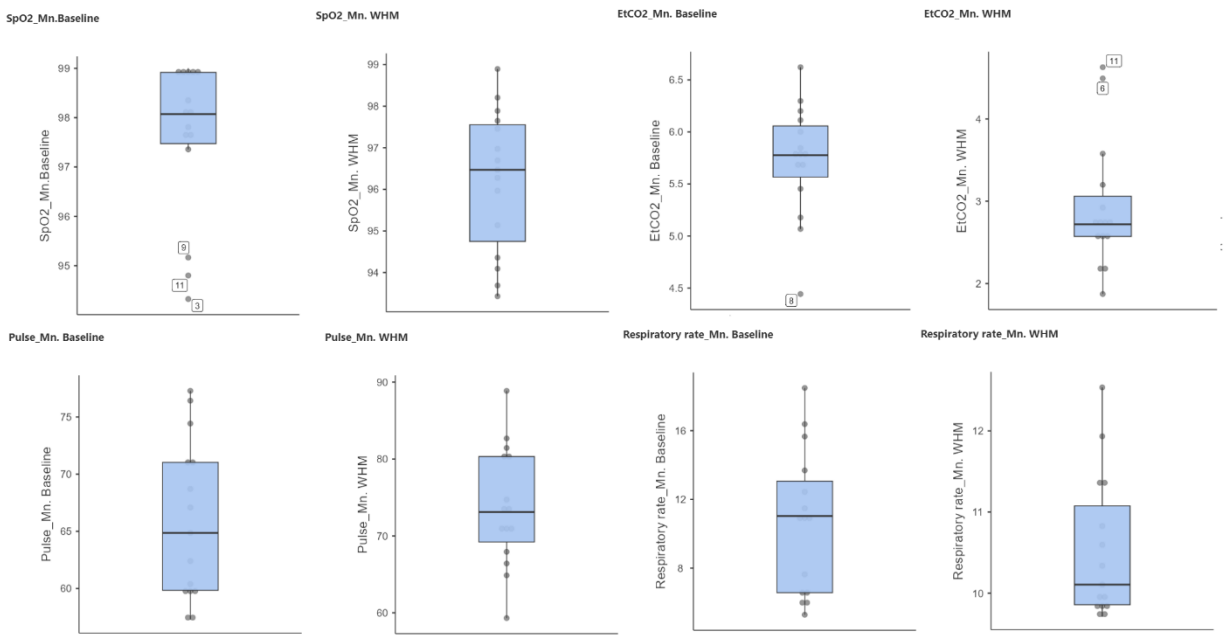

Figure 16

Boxplots show per-participant means during Baseline (left in each pair) and WHBM (right). WHBM produced the canonical shift: $EtCO_2$ ↓ (Wilcoxon W=120, p<.001), SpO_2 ↓ slightly (paired t(14)=2.58, p=.022), Pulse ↑ (paired t(14)=−6.90, p<.001). At the same time, the Respiratory rate maintained a similar central tendency (t(14) = 0.07, p = .942), but with markedly reduced dispersion during WHBM, consistent with paced breathing and retention. Dots denote individual participants; boxes = IQR with median line; whiskers = 1.5×IQR; isolated points indicate outliers.

Comparing naïve and L2 groups show the canonical WHBM pattern (Table 6). $EtCO_2$ drops sharply in L2 (5.81→2.54%) and in Naïve (5.60→3.48%), with medians mirroring the means (L2: 5.78→2.60; Naïve: 5.79→3.25). SpO_2 shows a modest decline in both groups (L2: 97.6→96.0%; Naïve: 97.6→96.5%). Pulse rises in both (L2: 67.5→76.4 bpm; Naïve: 63.4→69.9 bpm).

Respiratory rate (RR) converges toward ~10–11 br·min^{-1}: it increases in L2 (9.20→10.1) but decreases in Naïve (12.7→11.2), consistent with paced breathing/retention.

During WHBM, RR variance collapses (L2 SD 3.81→0.405; Naïve SD 4.19→1.01) and extremes narrow (e.g., L2 max 16.4→10.8; Naïve max 18.5→12.5), indicating a more uniform cadence. $EtCO_2$ variability is stable/slightly lower in L2 (SD 0.442→0.401) and a bit higher in Naïve (0.684→0.906), while SpO_2 spreads slightly in both (L2 SD 1.75→1.92; Naïve 1.46→1.51). Pulse shows wider spread in Naïve under WHBM (SD 5.14→7.22) and is similar in L2 (7.76→7.64). Phase minima and maxima move as expected (e.g., L2 $EtCO_2$ min 5.07→1.87; Naïve 4.44→2.55), reinforcing strong hypocapnia, mild desaturation, sympathetic acceleration, and standardised RR during the WHBM epoch.

Variable	Baseline	Experimental	Test	p-value	Effect-size
$EtCO_2$ (%)	5.73 ± 0.54	2.92 ± 0.78	W = 120	<0.001***	r = 1.00
Respiratory rate (/min)	10.60 ± 4.20	10.53 ± 0.89	t = 0.07	0.942	d = 0.02
SpO_2 (%)	97.61 ± 1.58	96.21 ± 1.73	t = 2.58	0.022*	d = 0.67
Pulse (bpm)	65.86 ± 6.94	73.78 ± 7.81	t = -6.90	<0.001***	d = -1.78

Table 5

Comparison between phase: baseline VS experimental

(* p < 0.05, *** p < 0.001)

Variable	L2 (N=18)	Naive (N=12)	Test	p-value	Effect-size
$EtCO_2$ (%)	4.18 ± 1.73	4.54 ± 1.35	t = -0.64	0.525	d = -0.23
Respiratory rate (/min)	9.64 ± 2.66	11.96 ± 3.01	t = -2.22	0.035*	d = -0.83
SpO_2 (%)	96.82 ± 1.96	97.05 ± 1.53	t = -0.35	0.730	d = -0.13
Pulse (bpm)	71.92 ± 8.68	66.67 ± 6.88	t = 1.76	0.090	d = 0.66

Table 6:

Comparison between groups: L2 vs Naïve

(* p < 0.05, *** p < 0.001)

959

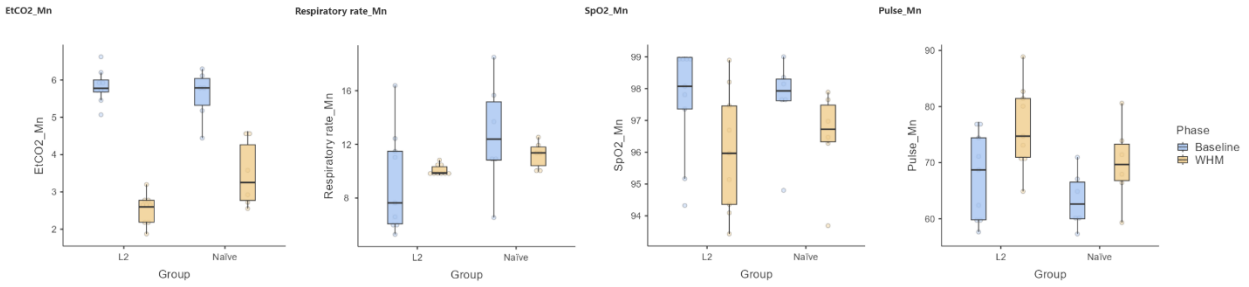

Figure 17

Comparison Across Phases Between Groups

Boxplots show per-participant means for L2 vs Naïve at Baseline (blue) and WHBM (gold). Both groups exhibit the WHBM shift—$EtCO_2$ ↓, SpO_2 slight ↓, Pulse ↑, and RR converging to a narrower range. Across phases, naïve displays higher RR than L2 (independent t-test, p = .035, d = 0.83), while $EtCO_2$ and SpO_2 show no reliable group separation; pulse is higher in L2 with a trend only (p = .090). Dots are individuals; boxes = IQR with median; whiskers = 1.5× IQR.

Across phases, both groups show the canonical WHBM shift (↓$EtCO_2$, ↓SpO_2, ↑pulse, stabilised RR), but the experienced (L2) cohort displays a lower $EtCO_2$ and higher Pulse in L2 (not statistically significant). At Baseline, $EtCO_2$ is comparable (L2 ≈5.8% vs naïve ≈5.6%); during WHBM, L2 falls lower (≈2.5% vs ≈3.5%), indicating more pronounced ventilatory "washout." Respiratory rate is consistently lower in L2 (Baseline ≈9.2 vs 12.7 br·min^{-1}; WHBM ≈10.1 vs 11.2), and the pooled between-group test confirms higher RR in naïve ($t(28)=-2.22$, $p=.035$, $d=-0.83$). Pulse runs higher in L2 at both phases (Baseline ≈67.5 vs 63.4 bpm; WHBM ≈76.4 vs 69.9 bpm), with a trend toward a group difference (p=.090). SpO_2 decreases modestly in both groups, with no meaningful between-group separation.

Dispersion patterns echo the boxplots: during WHBM, RR variability collapses in both groups (tighter boxes/whiskers), consistent with paced breathing and retentions; $EtCO_2$ and pulse

show wider spread in L2 (e.g., $EtCO_2$ spans ~1.9–6.6% and pulse ~58–89 bpm in L2 vs ~2.6–6.3% and ~57–81 bpm in naïve), suggesting greater individual range in depth of hypocapnia and sympathetic engagement among experienced practitioners. Overall, the figures support lower RR and deeper $EtCO_2$ reductions in L2, similar oxygenation, and higher pulse activity, with formal tests indicating a robust group effect on RR and only trends/overlap for the other endpoints.

9. Temperature Results

Across the analyzable recordings, most phase-wise temperature changes were small (≈ ±0.1–0.6 °C) with mixed directionality across participants and gauges; a single extreme at Gauge 3 in participant WHBM14 (−1.875 °C) was observed. These magnitudes are comparable to typical cutaneous variability and to the practical limits of agreement for skin sensors, making it difficult to distinguish them from experimental noise in this sample. Operational constraints (limited number of instrumented sets; intermittent read-out/software issues on one device) further reduced power. Given (i) effect sizes largely within measurement uncertainty, (ii) heterogeneous signs across participants/sites, and (iii) an isolated outlier that cannot justify inference, we do not report inferential statistics for temperature in the main results, treating these data as an exploratory context for future autonomic findings.

Discussion:

V. EEG Discussion

1. General EEG Discussion:

During the WHBM taskepoch, scalp and source power, and functional connectivity analyses converge on a clearrobust, frequency-specific shift reconfiguration in cortical activity relative to baseline. At the scalp level, the whole group shows a parietal/posterior surge in high-frequency power (the Alpha/Beta frequency range (11–26 Hz) and the Gamma frequency band (3029.5–95 Hz; peaks at P8, Beta and P1, in Gamma), consistent with increased cortical excitation during the breathing/retention cycles (Fig. 1–2).

Beta rhythms (~13–30 Hz) increase when the brain maintains an ongoing sensorimotor or cognitive "set" (the "status quo" hypothesis), which supports the maintenance of the current sensorimotor or cognitive state and strengthens top-down control across distributed networks (Engel & Fries, 2010). In motor/respiratory contexts, beta rhythms support sustained control and predictive timing loops between motor/pre-motor regions and sensory areas—exactly what paced, guided breathing demands. In other words, as hypothesised, after breathing movements are completed, beta power rebounds (synchronisation), potentially signalling a return to the resting state or stabilisation of the sensorimotor system (Spitzer & Haegens, 2017). This rebound may help reset the system and prepare it for subsequent actions or sensory inputs. This finding suggests that WHBM phase 2 cycles, which rhythmically alternate between active breathing and low lung volume maintenance, should normally result in a decrease in beta, but are instead dominated by a rebound in PMBR, which outweighs the movement-related decrease in Beta. Although scalp-to-cortex mapping is variable, Beta peaks at P8 commonly overlap the inferior/superior lateral occipital cortex and the angular gyrus, a region that participates in higher-order visual association and visuospatial monitoring. This activity may be associated with a top-down "regulatory" mechanism in which top-down influences from the beta band reinforce control over sensory processing, as in selective attention tasks, particularly when they require increased control (Bastos,

Vezoli, et al., 2015). This activity could help further suppress irrelevant visual processing and keep a steady internal set towards the auditory cueing and interoceptive focus. The co-occurring Gamma, which peaks at the P1 site, is indeed compatible with this possibility.

Reviews spanning non-human primates and humans place BA5/BA7 in the posterior parietal cortex—also called the superior parietal lobule (SPL)—where P1 is located, is a convergence zone for proprioceptive, tactile, and visual signals used to update limb/body state and guide action (Passarelli et al., 2021). Indeed, large-sample resting-state mapping identifies multiple SPL subregions with differentiated links to somatosensory, visual and frontoparietal control networks (Alahmadi, 2021), which is exactly the architecture expected for integrating proprioception with attention and action planning during WHBM. And across the cortex, Gamma is associated with feedforward or precision activity, integrating somatosensory and salient input attention, which increases with perceived intensity and attentional gain, consistent with high-precision bottom-up signalling and prediction errors from lower to higher hierarchical levels in the brain (Bastos, Litvak, et al., 2015; Fiebelkorn et al., 2018; Liu et al., 2015). Because SPL integrates proprioception to update body state, gamma bursts at P1/SPL during WHBM plausibly represent phase-locked, precision-weighted proprioceptive/interoceptive updates (e.g., at transitions into/out of breath holds) riding on top of slower feedback control. Beta in posterior association cortex (our P8 locus) may reflect top-down feedback that stabilises the current set of paced breathing, interoceptive focus, and auditory guidance, and selectively gates visual/sensory channels. At the same time, SPL gamma carries high-fidelity, breath-phase–dependent somatosensory/interoceptive updates up the hierarchy on the Beta scaffold.

The anterior gamma in novices (AF8 peak) is one of the clearest group contrasts (Fig. 6), and it is a particularly interesting finding to compare with L2. This novice anterior Gamma (~43.5 Hz) at AF8 is consistent with greater executive and more “intellectual” engagement in following

instructions, keeping time, and regulating breathing. Although the mapping is probabilistic, AF8 generally sits over the right anterior–lateral prefrontal cortex (frontopolar/DLPFC border), so this peak in Gamma plausibly indexes working memory, prospective timing, and top-down attention (Burgess et al., 2007; Lundqvist et al., 2018; Volle et al., 2011), which the novices needed more than L2. This area is also engaged in encoding relative uncertainty in the choice and tracking alternative actions (Hogeveen et al., 2022). While the condition may reflect how novices repeatedly decide "keep holding or breathe now," often under uncertainty of their capability considering their level of practices, and is as such consistent with right frontopolar recruitment, the activity may equally reflect a more sustain need to reflect on cognition and experience typical of metacognitive perception associated with this brain area (Baird et al., 2013). Considering that Gamma activity is recruited equally across PFC areas, this finding supports the idea that gamma bursts (~50–120 Hz) are related to event memorization, with a ramp-up particularly pronounced at informative sites, where spiking carries specific object information needed for the forthcoming decision.

The novice peak Cluster 1 (11 to 20.5 Hz), with a peak effect over P8 at 11 Hz ($t = 5.7$), as shown in Figure 4, is also noteworthy as a difference between L2 and novices. Alpha over parieto-occipital cortex implements functional inhibition of task-irrelevant input—"gating by inhibition"—and increases with internally directed attention. Naïve participant shows an increase in Alpha over the P8 around the secondary visual cortex or inferior occipital gyrus (BA 19), which may indicate that they have an increased focus of internal attention, allowing the suppression of external sensory input to prioritise internal cognitive processes such as focusing on breathing or hold—the main function of increase alpha (Foxe & Snyder, 2011). In contrast, experts show less reliance on shifting their expertise from coarse suppression (alpha) to efficient precision signalling (gamma), and possibly an increase in interoceptive focus.

Indeed, expert practitioners exhibit a more structured version of the overall profile above. Scalp spectra show frontopolar delta increases, Alpha/Beta increase with a Beta peak increase in the secondary visual cortex (PO7), and sustained temporo-parietal and posterior high-gamma (up to 95 Hz) during WHBM versus baseline, with a continued peak effect at P1 (Fig. 3–4).

The more specific Beta increased over PO7 may be seen to be associated with top-down stabilisation and gating mechanisms in the visual cortex to maintain *more* specifically internally driven tasks, enabling the maintenance and manipulation of task-relevant information in working memory and decision-making processes beyond the Alpha gating mechanism mentioned above (Spitzer & Haegens, 2017).

The overall increase in Alpha-Beta in the expert group also indicates an increase in the top-down influence that are reflected by these distinct frequencies when analyzed together when compared to just alpha or beta top-down influences, considering that Alpha might mediate suppression of irrelevant background while beta might facilitate bottom-up communication of attended stimuli and more so, that infragranular layers, responsible for outputting information from the brainstem and thalamus sending feedback projections, show predominantly alpha-beta-band synchronization (Michalareas et al., 2016). In L2, the rise of alpha–beta power may indicates enhanced top-down influence because feedback from higher association areas is preferentially expressed in the alpha–beta range (notably via infragranular projections), the joint increase of these bands—together with theta organization of frontoparietal sampling and posterior gamma precision signals—suggest that experts exert sharper gating, more stable internal set control, and more precise interoceptive routing during WHBM than novices.

The Gamma peak at 92.5 Hz in the experts, seen in P1 over the superior parietal lobule (SPL/BA7), is, this time, restricted to the tempoparietal and occipital cortices. This notable increase suggests an intensification of high-precision task-locked sensory activation reported in

the ~80-200 Hz range across studies (Miller et al., 2014) and reflects feedforward processing across hierarchies, riding on Beta feedback (see FC discussion). These are equally consistent with movement control and coordination (e.g., linked with the cerebellum) and somatosensorial amplification seen in Gamma oscillation in the 60-90 Hz range, primarily associated with the motor cortex, specifically the primary motor cortex (M1), the somatosensory drive in the somatosensory cortex (S1) and the parietal cortex (e.g., sensory processing and attention), as well as in subcortical areas (Alahmadi, 2021; Cheyne & Ferrari, 2013)—all areas with increased Gamma activity as reported in our findings. It should be noted that scalp high-Gamma can, in principle, pick up myogenic/oculographic transients, however, our Gamma topography with a posterior midline, P1 and clustering across subjects favours a neural origin. As such, the WHBM-evoked P1 (SPL/BA7) high-Gamma peak likely indexes precision-weighted proprioceptive/interoceptive updates during the breath-phase, consistent with feedforward Gamma in dorsal parietal circuits that integrate body-state signals for goal-directed control.

During WHBM vs baseline, experts show an overall increase in Delta activity, with frontopolar delta (1–1.5 Hz) peaking at FP1 ($t = 5.9$; Fig. 3–4). As mentioned, hyperventilation has been associated with increasing delta. Busek and Kemlink (2005), analysing the short initial parts of each respiratory sequence, also indicated that Delta waves (0.1 Hz) were increased in anterior temporal regions during inspiration, while intracranial recordings by Zelano et al. (2016) also indicated that the inspiratory phase was associated with increased power in the delta frequency range (0.5-4 Hz). Son et al. (2012) further indicated that Delta changes occurred within a 10-second frame and suggested that hyperventilation-induced reduction in PCO_2 was the leading mechanism altering neuronal excitability and contributing to the EEG changes. While Son et al. (2012) equally suggested that it was the magnitude of PCO_2 reduction, rather than its absolute value that played a key role in inducing EEG changes, we did not see the referred Delta changes

in the naïve group, even though both groups experienced a marked drop in PCO_2 levels during WHBM, indicative of hypocapnia, with a more pronounced hypocapnia for L2 (see capnography discussion below).

As such, the frontopolar/medial-frontal delta peak in L2 could be considered a slow control and monitoring signal during internal, tonic attention, which sustains interoceptive set-maintenance rather than being fully explained by hyperventilation-induced EEG changes. Reviews and experiments have indeed linked delta to internally directed control, sensory interference suppression, and mindset maintenance, specifically reported in prefrontal–parietal systems (Angioletti & Balconi, 2022). Although this notion fits the experts' larger FP1 Delta during paced breathing/retention, our data didn't show any increase in FC in areas such as the lateral prefrontal cortex (LPFC) and inferior parietal lobule (IPL), which play critical roles for respectively facilitating synchronization with other brain regions and supporting the integration of information (Pagnotta et al., 2024). The lack may be attributed to L2 practitioners' increased expertise and to a somewhat automated flow and neural efficiency.

On the other hand, Delta oscillations align with the rhythmic fluctuations in speech, particularly with prosodic features—such when emphasis is placed on certain words to help convey meaning, emotion, and structure—leading to an auditory cortical delta-entrainment specifically seen in superior temporal gyrus (STG) that is considered a marker of how the brain parses and encodes speech (Keitel et al., 2017). This reality may have been particularly true for L2 practitioners—being habituated to self-paced WHBM cycles— and who had to entrain more strongly to the external WHBMB audio guidance to override their intrinsic tempo. Considering that we found a Delta cluster (1-2 Hz) increase in the left superior temporal gyrus (STG) peaking at 1 Hz (t=4.0), which would correspond to the processing of the sound speaker place in the right

side, speech-prosody–locked delta entrainment could have inflated the frontopolar slow-band signal and should be considered a potential confound in interpreting the L2 delta effects.

2. Source Spectral Power Analysis Discussion:

Excluding the Delta Cluster 1 (Figure 8), the source clusters largely recapitulate the scalp pattern for the whole group. Although the left Delta does not appear in the scalp patterns for the whole group, this delta activity (1 to 2 Hz) peak in in the L middle temporal (MTG), associated with language processing periodicity (1.8 Hz to 2.6Hz), being more particularly involved in language processing, semantic memory and deduction reasoning and is functionally coupled with the STG (Rimmele et al., 2021; Xu et al., 2015). Considering that the delta phase organises parsing and prediction of upcoming syllables/phrases, a left MTG delta generator would have been expected across the whole sample, independent of expertise, as shown by source power localisation.

Source reconstructions located fast-band increases with peak effects in the right cuneus (peak at 40.5 Hz; t = 4.5) and left precuneus (peak at 79.5 Hz; t = 5.5) areas that express functional connectivity and are associated with involved in distinct but interconnected functions. Most specifically, the precuneus integrates multimodal information. Being a functionally heterogeneous area, the precuneus is known to relate to sensorimotor functions and bodily awareness, connecting to the SPL, above-mentioned—a condition consistent with the precuneus's role in sensorimotor functions and general gamma wave functions previously referred to (Yamaguchi & Jitsuishi, 2024).

In the experts, Cluster 2 (Figure 7, C) shows a narrow, low-alpha suppression in the left lateral occipital cortex (9–9.5 Hz; peak t = −4.5), which differs from the whole-group pattern. As

noted, Alpha amplitude implements gating by inhibition in sensory cortices, with decreases reflecting heightened excitability. In other words, in experts, the low-alpha ERD (9–9.5 Hz) at the left lateral occipital indicates focal disinhibition. We may hypothesise that while our novices increase Alpha to control sensory input and prioritise internal cognition, by contrast, the experts rely on practice to disinhibit the system without the need for increased control, given their levels of practice. Mechanistically, low-Alpha ERD may reflect a targeted release of inhibition increasing local cortical excitation, as shown by Foxe and Snyder (2011), thereby releasing perceptual Gamma-coded precision updates and possibly intensifying interoception. Experts equally show a focal Alpha-band enhancement over medial posterior cortex—right precuneus (Fig. 7, D, Cluster 3: 12.5–13 Hz; peak 13 Hz, t=3.3)—a dissociation which we similarly interpret as practice-dependent up-regulation of an "integrative" posterior alpha that stabilises internally oriented attention and bodily self-monitoring together with the concomitant lateral-occipital low-Alpha ERD, which disinhibits extrastriate regions to permit Gamma-coded precision updates.

Experts exhibit a Beta–Gamma multiplex within medial SPL (precuneus) with a narrow low-beta enhancement in right precuneus (Cluster 4, D: 14–14.5 Hz; peak 14 Hz, t=3.6, figure 7) and a mid/high-gamma increase in left precuneus (Cluster 5, F: 66–68 Hz; peak 66.5 Hz, t=2.9, figure 7). We interpret the right-precuneus Beta as a predictive, set-maintenance signal that provides top-down feedback to posterior sensory cortices, while the left-precuneus Gamma reflects precision-weighted feedforward updates of interoceptive/proprioceptive state during breath–hold transitions. This division of labour accords with hierarchical communication accounts in which beta carries feedback predictions and gamma carries feedforward prediction-error/precision signals (Michalareas et al., 2016), with the precuneus acting as a posterior integrative hub for bodily awareness.

Paracentral, which is formed by extensions of the primary motor cortex (BA 4) and posterior primary somatosensory cortex (BA 1, 2 and 3) where high-Gamma activity (70.5–95 Hz; peak 78.5 Hz, right, t=4.8, Figure 7) is in line with classic MEG findings that 60–90 Hz Gamma tracking local spiking during voluntary movement and somatosensory reafference; in WHBM it most plausibly reflects respiratory motor control (diaphragm/intercostal and glottal co-contraction) and phase-transition feedback at the end of the exhale/hold and recovery breaths as seen in interference trials when a dominant movement onset response must be suppressed in favor of an alternate one (Gaetz et al., 2013).

3. FC:

Frequency-resolved statistical dependencies between activity in distinct cortical regions, or FC. During WHBM, Theta-band (4–7 Hz) FC was anchored in the postcentral/precentral gyri and strengthened links with the prefrontal, anterior cingulate, insula, and temporal cortices (Figure 10). Mechanistically, this is the signature of a sensorimotor–salience control loop operating under an interoceptive focus: sensorimotor hubs (S1/M1) provide phase-structured input about breath mechanics while the insula/ACC (salience–control) integrate bodily signals—specifically here breathing—to set behavioural priorities allowing the prefrontal regions implement top-down guidance and the temporal cortex tracks the guidance (Eisma et al., 2021; Menon, 2025)

The Theta band is the canonical carrier for long-range coordination in such control networks (frontal-midline/ACC Theta), and it often organises faster, local precision signals Gamma via cross-frequency coupling—exactly the division of labour we see when Theta-anchored networks co-exist with posterior Gamma during WHBM (Kluger & Gross, 2021).

In mid-gamma (55–70 Hz), FC (Figure 10) increases, as reported in the results, consistent with tighter posterior integration and interoceptive–affective crosstalk during practice. Fries' review argues that inter-areal communication is gated by frequency-specific synchronization, with Gamma (30–90 Hz) especially suited for rapid, precise information transfer (Fries, 2015)—a condition that allow Gamma waves to create sequences of excitation and inhibition, sensitive to short temporal windows as one the seen in breathing further allowing for a rhythmic synchronization that enhances connectivity and ensures precise and selective communication between neuronal groups. The Gamma activity in the PCC, as reported in the results, is consistent with the PCC being a highly connected hub for internally directed cognition and self-related DMN processing, and with it generally showing increased activity during internally focused tasks (Leech & Sharp, 2014).

In the gamma range, WHBM drives rapid synchronisation among posterior midline hubs, including the isthmus and prefrontal nodes, including the orbitofrontal cortex (OFC) on the ventrolateral frontal surface (Figure 10). The lOFC is a multisensory and value/affect integrator, likely participates in reappraisal and valuation of bodily sensations (e.g., breath-hold comfort/urge, effort), enabling the reappraisal and valuation of bodily sensations and associating sensory stimuli with their expected reward value, playing a key role in affective learning and emotions (Rolls, 2019). Together with the Gamma activity of the isthmus, part of the corpus callosum, which facilitates inter-hemispheric communication and synchronisation of neural activity, essential for cognitive processes such as perception, attention, and memory (Zaehle & Herrmann, 2011), the pattern fits a state of heightened bodily awareness and emotional valence (Yang et al., 2020), considering previous positive emotional findinds.

As noted in the results, several high t-value connections also involved the paracentral lobule, entorhinal cortex, and parahippocampal regions. The entorhinal–hippocampal Gamma route is

known to coordinate information flow, with Gamma participating in the encoding and retrieval, and the parahippocampal cortex is specifically associated with context associations and, as such, higher-level cognition, binding relevant information with fast Gamma oscillations around the 60-80 Hz (Aminoff et al., 2013; Griffiths et al., 2019).

Relative to baseline, WHBM produced 1,994 strengthened edges in the high-Gamma band (70-95 Hz, Figure 10), with postcentral and precentral gyri emerging as major hubs that synchronise with prefrontal poles and middle frontal cortex, insula and cingulate (ACC/PCC), as well as the temporal poles, fusiform and STG. In a communication-through-coherence framework, Gamma-band synchrony is the canonical carrier for rapid, precision-rich inter-areal exchange, and synchronisation depending on the attended stimuli—a bottom-up activity—controlled by Alpha/Beta—top-down—feedback mediation (Bastos, Vezoli, et al., 2015; Fries, 2015; Michalareas et al., 2016). Hence, widespread Gamma coupling is expected when bottom-up somatosensory and interoceptive updates must be globally integrated during practice.

Convergent Gamma links between the insula and ACC fit the salience network's role in integrating interoceptive and affective signals and in prioritising behaviorally relevant input, while strengthened coupling with the PCC and the precuneus, along with posterior-midline hubs, support internally directed cognition, bodily/self-context, and large-scale integration (Craig, 2009). The Gamma activity of the precuneus can also be seen to act as a functional integrator, given its multimodal, body-self-related, and rich cortical/subcortical connectivity (Cavanna & Trimble, 2006). Furthermore, the limbic activation showing connectivity between the insula, the PCC, and the temporal poles suggests that the above-referred heightened interoceptive signalling indicates some form of emotional salience that could lead to regulation, considering that these hubs are central to emotion generation and processing.

It should be noted that the overall pattern—posterior-midline, sensorimotor, salience, and prefrontal systems coupled at fast timescales—is equally compatible with the noted effect of the cold-immersion phase in experts and prior meditation work reporting parieto-occipital high-gamma increases and gamma-sensitive signatures of enhanced moment-to-moment awareness.

Connectivity in experts strengthens within theta over somatosensory and parietal circuits (Figure 10) and, critically, in mid- and high-gamma between posterior DMN nodes (precuneus/PCC) and frontal executive/salience hubs (caudal middle frontal, ACC), indicating refined top-down modulation during the practice (Figure 11), see subsequent discussion.

While gamma-band coordination plays a key role in carrying any biased sensory stream, considering its role in the rhythmic interplay in frontoparietal networks, and the timing of attentional sampling when selection is engaged, these effects are known to be enhanced by theta rhythms in the frontoparietal network, which organises alternating attentional states and enhances performance control (Cavanagh & Frank, 2014; Fiebelkorn et al., 2018). This is indeed specifically demonstrated by L2 (Experts), who established enhanced theta-band FC predominantly centred around somatosensory and parietal regions (Figure 11), in areas seen to increase Theta during improve performance during challenging tasks (Kenville et al., 2025), with strong links between the postcentral gyri and prefrontal, cingulate, insular, and temporal regions, demonstrating an improved interoceptive awareness, consistent attention, and bodily consciousness developed through ongoing WHBM practice.

Finally, respiration itself entrains distributed cortical rhythms—including those in the ACC, premotor, insula, and limbic areas—providing a physiological driver for the observed theta-synchronous integration during paced WHBM breathing (Herrero et al., 2018; Zelano et al., 2016). This Theta activity is another interesting difference to compare with novices, who do not show increased Theta-FC integration. A condition likely set because the Theta network needs stable

rhythmic scaffolding and practice-dependent coordination**,** showing increased Theta during alternating states that promote either increased sensory sampling or motor shifting, providing an increased clocking mechanism to sort conflicts (Fiebelkorn & Kastner, 2019), both of which novices lack.

In trained practitioners, mid-Gamma synchrony (55-70 Hz, Figure 11) forms a coherent bridge from posterior midline hubs (precuneus/PCC) to associative visual cortices and onward to frontoparietal and limbic controllers. Interpreted within the frequency-specific communication theory (as referred to above), this pattern further suggests the referred promotion of precision-rich posterior updates that are rapidly integrated and broadcast to control hubs for set maintenance and interoceptive regulation including the two large-scale intrinsic networks (e.g., the PCC, part of the DMN) identified as part of the unified allostatic–interoceptive system (Kleckner et al., 2017). These two systems integrate interoception (the representation of internal bodily sensations) and allostasis (the predictive regulation of the body's energy needs to maintain stability). By contrast, novice-only mid-Gamma FC (Figure 12) suggest a more posterior-temporal-centric activity with heavier engagement of STG, suggesting an instruction-locked speech analysis (Zion Golumbic et al., 2013), fusiform/occipito-temporal, which supports high-level visual codes as well as lexical processing (Palejwala et al., 2020), and medial temporal structures (parahippocampal/entorhinal) supporting semantic/contextual processing—i.e., a sensory–semantic rather than a more integrated embodiment relying on Gamma emphasis. In other words, both groups exhibit mid-Gamma-synchronous integration. Still, experts preferentially recruit the posterior DMN and the frontal control loop for embodied regulation, whereas novices lean on auditory–visual–mnemonic Gamma to parse instructions and construct meaning, with weaker executive coupling.

Beyond mirroring the whole-group pattern and mid-gamma activity, experts show a tightly organised fast-band bridge (70-95 Hz) linking posterior midline hubs (PCC/precuneus) with lateral

PFC and dorsal ACC, as well as pericentral and posterior visual nodes (Figure 11). This layout fits what intracranial and MEG work report for cognitive control at high temporal precision which demonstrate coordination of high high Gamma activity (60–140 Hz) between ACC and lateral PFC during adaptive behavior, with high Gamma power coupling strongest around feedback and adjustments (Rothé et al., 2011)—direct evidence that these two control areas synchronise in the high Gamma band when maintaining and updating an internal set. Furthermore, rapid variations in body states, such as breathing, are also known to entrain 30-80 Hz gamma activity (McGinley et al., 2015).

The high gamma-band FC activity in the posterior DMN linking frontal executive regions, the ACC, caudal middle frontal cortex, is a typical dynamic fast integration between the DMN and other networks, such as the frontoparietal and salience networks, which involve regions like the ACC and the middle frontal cortex and are essential for cognitive control and network switching during attention demanding tasks (Menon, 2023).

In novices, the selective Beta-band FC between precuneus and the isthmus cingulate and the lateral occipital and parahippocampal cortices most plausibly reflects a reliance on posterior feedback set-maintenance to stabilise an internally oriented state and gate sensory–mnemonic channels—a control mode consistent with Beta's role in top-down predictions and endogenous content re-activation (Spitzer & Haegens, 2017) if compared to the shift to the Theta-anchored long-range coordination and Gamma-based precision integration of the experts.

The results across scalp, source, and functional connectivity analyses generally support the hypotheses proposed for each condition. During baseline, EEG activity reflects a relatively relaxed, resting-state profile, with some engagement of auditory and associative regions, particularly in novices, consistent with passive sound exposure and minimal task demands. In contrast, the WHBM condition induces widespread neural changes, including elevated gamma

power and connectivity, especially over posterior and sensorimotor regions, along with enhanced theta-band integration among interoceptive, salience, and default mode networks. These effects are most structured in experts, reflecting a physiologically active yet internally directed state marked by cortical excitation and sensory-mnemonic integration during deep breathing and breath retention.

4. Cold Immersion EEG:

Immersion performed equally with eyes closed, produced a single posterior high-frequency cluster (27–95 Hz), peaking at PO7 at ~66 Hz, with no delta/alpha/beta clusters surviving correction (Figure 5). This pattern fits a shift from general visual "gating" (alpha–beta feedback) to heightened sensory monitoring, with gamma carrying precision-weighted, feed-forward updates from somatosensory/visual association areas as cold afferents dominate the stream. Converging evidence shows (i) occipito-parietal gamma rises (35-45 Hz and 60-110 Hz) during open-monitoring meditation such as eyes-closed Vipassana and indexes enhanced sensory awareness and perceptual clarity (Braboszcz et al., 2017; Cahn et al., 2010), and (ii) gamma in somatosensory/parietal cortex scales with stimulus intensity and conscious perception, serving feature binding/stimulus representation and nociceptive/thermal processing with a higher frequency (∼55 Hz) for tonic Pain-induced gamma-band oscillations (GBOs) at the sensorimotor cortex (Li et al., 2023; Zis et al., 2022). The above findings align with ours in showing that gamma rhythms are associated with stimulus representation and moment-to-moment conscious awareness of the cold-immersion effect on the skin, indicating a heightened awareness of present-moment sensory experience during cold immersion in experts.

In experts, cold immersion vs. pre-immersion rest yielded two corrected source clusters that co-localised in left inferior temporal (IT) cortex—a low-frequency increase (1–10.5 Hz; peak 1 Hz) and a fast-band increase (12.5–95 Hz; peak 39.5 Hz) (Figure 9). Functionally, the ventral inferior temporal cortex serves as a high-level representational hub that supports object/scene categorisation, as well as conceptual/semantic coding, beyond immediate sensation. It is also engaged by top-down imagery in the absence of visual input (Conway, 2018). Studies also suggest that this area of the brain carries representations linked to perceptual and conceptual mental spaces, suggesting that the inferior temporal cortex supports hierarchical information structures that mirror behavioural judgments of categories (Grill-Spector & Weiner, 2014). As such, the inferior temporal cortex is equally associated with the representation of the body, specifically with the upper and lower limbs and trunk (Orlov et al., 2010). We therefore read the left-lateral IT Delta/Gamma "tandem" as a hierarchical integration reflecting a Delta autonomically driven set-maintenance during cold stress reported during autonomic challenges and sudden increases in arousal and attention in response to external stimuli (Rho et al., 2023), while Gamma in ventral temporal cortex indexes top-down, content-rich reinstatement that helps interpret and regulate the ongoing interoceptive state.

Considering the out-of-normal scope, cold immersion, which was done without pre-breathing activation (see study design), making it possibly a generally more challenging, the above findings suggest that the expert cold immersion likely engages a delta paced allostatic scaffold (sympathetic challenge; central–autonomic coupling) that gates Gamma expressed, IT representations—the perceptual–conceptual "mental space" for "cold/ice/immersion"—to stabilize interpretation and regulation of the bodily state.

5. FC Cold Immersion:

No significant region pairing was observed in the Delta (1-3 Hz) and Theta bands (3-7 Hz) for cold immersion. This lack of Theta may be seen as an exteroceptive challenge that shifts the cortex into a desynchronized state, suppressing slow Theta rhythms and boosting fast activity. Indeed, noradrenergic and cholinergic arousal—robustly engaged by cold stress—is likely to reduce theta synchrony (Reimer et al., 2016) and further explain the shift towards higher-frequency oscillations, such as Gamma, as a function of Norepinephrine ignition (Mather et al., 2016).

However, during cold immersion, expert practitioners exhibited a relatively widespread increase in alpha-band functional connectivity across 151 significant brain region pairs, reflecting strong engagement of posterior sensory and parietal networks (Figure 13.A). The most prominent connections linked somatosensory regions (e.g., the postcentral gyrus) with visual processing areas, including the lateral occipital cortex, pericalcarine cortex, cuneus, and fusiform gyrus, suggesting heightened integration of visual-somatosensory pathways. Consistent involvement of the supramarginal and inferior parietal lobules—hubs of the dorsal attention and multisensory integration networks—paired with visual and cingulate cortices indicates a possible sustained interoceptive and exteroceptive monitoring during extreme cold exposure.

Mechanistically, the Alpha-band FC during cold immersion with eyes closed and a strong exteroceptive load from cold afferents implements top-down, feedback-style control that gates sensory excitability and coordinates long-range integration, regulating sensory information processing based on cognitive relevance (Sadaghiani et al., 2012). This sensory regulation is notably evident through connections between the temporal poles, transverse temporal regions, and orbitofrontal cortices, further suggesting a coupling between limbic-affective and perceptual systems.

The insula, a central node for interoception and autonomic awareness, was frequently connected to visual areas. More specifically, the dominance of posterior alpha connectivity—typically associated with internal attention and sensory gating—may reflect a regulated state of sensory control during physiological stress. Indeed, dominance of posterior Alpha is typically associated with internal attention and sensory gating playing a critical role in regulating cortical excitability and information flow, particularly in tasks requiring internal focus or protection of information from external interference (Wang et al., 2016).

The default mode network also appeared to be engaged through connections between the PCC and precuneus, as well as the lateral occipital cortex, suggesting that self-referential awareness was maintained, considering that increased connectivity between the DMN and precuneus often highly an internally driven cognition, which may include an awareness that aims to integrate internally and externally driven information through the PCC (Utevsky et al., 2014). Considering Alpha coordinates long-range, top-down control and gates excitability in the sensory cortex ("gating-by-inhibition"), the elevated PCC, precuneus, and the lateral occipital cortex Alpha-FC signals reflect that assumption.

There was also no significant connectivity in the Beta range (13-30 Hz). This lack may reflect a shift in the network away from beta's "set-maintenance/feedback" approach to rely instead on alpha for broad top-down gating and gamma. The 30–45 Hz low-Gamma FC result with the 1,700 significant edges (Figure 13.B), the mid-Gamma (55-70 Hz) increased FC across 2,112 significant brain areas (Figure 13.C), and the high-gamma-band (70–95 Hz) connectivity relative to rest, encompassing 1,932 region pairs (Figure 16.D), all express long-range cortico-cortical synchronization considering Gamma supports rapid inter-areal communication, and more specifically within the areas of increased FC have been associated with selective attention, sensorimotor tasks and multisensory processing (Hipp et al., 2011; Siegel et al., 2012). Certainly,

the mid-Gamma FC increased in hubs such as S1, SMG, the insula, and the occipito-parietal cortex is consistent with the prior acknowledged mechanisms supporting multisensory information with Gamma indexing precision-rich sensory exchange across multimodal binding (Gregoriou et al., 2009).

Consistent with the absence of Beta-band coupling, the 55–70 Hz range is where Gamma express the most inter-areal integration, tying early and associative visual cortex (pericalcarine/V1, lingual/V2–V3, lateral occipital) to inferior-frontal opercular cortices part of the pars opercularis BA 44 and pars orbitalis BA 47, as well as the caudal middle frontal part of the DLPFC with a frequency signature of top-down hyper selection and appraisal. The activity of the lateral occipital cortex has been associated with tactile discrimination through the sense of touch and, more distinctively, with haptic sensations and vividness of perception, and as such would correspond to the salient perception of very cold water during immersion, specifically when vision is unavailable (Dijkstra et al., 2017; Lucan et al., 2010). On the other hand, the pars orbitalis (BA 47), a subdivision of the ventrolateral prefrontal cortex (VLPFC), may plausibility be a component associated with an affective appraisal of the cold sensation, considering this area is more specifically associated with processing non-reward and aversive stimuli (Rolls, 2019). Weighing up the above, the activity of the caudal middle frontal cortex can be seen as an activity possibility leading to increased response inhibition of motor function and attentional control, bearing in mind the intensity of cold and contemplating this area has been associated with contextual rules of attention contributing to task-specific control (Friedman & Robbins, 2022).

The FC across 1,932 total significant brain areas in the High-Gamma (70-95 Hz), notably within the dorsal attention network nodes, more specifically the rostral middle frontal, superior parietal, ACC, and insula are networks that relay interoceptive awareness of body internal states, which correspond to activities in a PET study by Muzik et al. (2018) during cold-immersion. The

cortical activation seen in the High-Gamma band suggest a cortical configuration that may be a counterpart of what Muzik et al. (2018) reported in their multimodal case study of Wim Hof under cold stress showing an engagement of the Periaqueductal Gray (PAG)—a descending pain and aversive-control hub—during cold and a pons activation consistent with PAG nucleus and futher LC activity where where excitatory inputs are required to drive LC noradrenaline (NA) neuron activity (Barcomb et al., 2022)and insular involvement supporting interoceptive focus, particularly in the context of stress, pain, and thermoregulation. Although our EEG source and FC pipeline cannot resolve brainstem nuclei directly, and as such cannot provide a direct demonstration of its coupling, much less of the sub-division of the PAG, including the ventrolateral PAG (vlPAG) and the Lateral PAG (lPAG), the topography of expert high-Gamma connectivity during cold immersion involve networks that are known to have functional connectivity with the PAG such as the ACC and the insula also connecting with the cingulo-opercular, and dorsal attention network (Kong et al., 2010; Muzik et al., 2018).

The overall increased FC during cold immersion reflects findings by Yankouskaya et al. (2023) of 5-minute head-only immersion with increased large-scale interaction between large-scale networks at a water temperature of approximately 19.93°C ± 0.13°C, compared to our 0.99°C, SD = 0.64, range = 0.00–1.80 °C (Table 1).

II. EDA/GSR Discussion:

Building on evidence that the respiratory central pattern generator (i.e., preBötC) sends efferent to the LC and onward to thalamic and cortical targets—thereby coupling breathing rhythm to global noradrenergic arousal and cortical excitability (Braendholt et al., 2023)—we included electrodermal activity (EDA/GSR) as a peripheral, high-temporal-resolution readout of the

predicted autonomic consequences of WHBM breathing. Sympathetic sudomotor fibres are regulated by the autonomic nervous system through cholinergic and adrenergic pathways (Vittrant et al., 2024), which drive EDA, making their phasic skin-conductance responses (SCRs) a selective index of transient sympathetic bursts rather than mixed autonomic tone.

As indicated in the results, we index the phasic (event-related) component of electrodermal activity with three standard measures. SCR frequency (events·min^{-1}) counts the number of discrete skin-conductance responses per minute and reflects transient sympathetic discharges, in contrast to the slowly drifting tonic skin-conductance level (SCL). SCR amplitude is the onset-to-peak height of each response in micro-Siemens (μS); we report the mean amplitude within each phase. SCR area is the time-integral of an SCR (units μS·s), capturing both height and duration and therefore distinguishing equally tall but longer versus shorter-lasting bursts. Applied to our WHBM protocol, all three metrics increased from Baseline to WHBM and then declined during the post-breathing Rest period; this phase-dependent pattern was evident in both naïve and Level-2 practitioners with no reliable between-group differences, although the WHBM versus Rest reversal for amplitude and area was more pronounced in the experienced group (Figures 14–15).

Our results further support lab checks of the WHBM breathing reported by Blades et al. (2024) showing increased sympathetic activity as well as findings by Muzik et al. (2018) which indicated activity in loci associated with the PAG–insula–pontine-LC region, which aligns with a model in which targeted breathing recruits central arousal systems. These findings suggest that the WHBM engages both autonomic brainstem regions and higher-order cortical areas, allowing for enhanced control over autonomic functions, not only during cold exposure, but equally during the WHBM. Considering that the LC-NE activation can influence the vagus nerve, which regulates the cholinergic anti-inflammatory response through the α7-nicotinic acetylcholine (ACh) receptor (α7-AChR)-dependent pathway, this activation could be another theoretical mechanism by which

the WHBM reduces inflammation through acetylcholine-mediated suppression of cytokine release (Samuels & Szabadi, 2008; Simon et al., 2023).

III. Capnograph Discussion:

The Capnograph results suggest that prior experience with breathing techniques selectively modulates physiological responses during the WHBM session, chiefly at the level of ventilatory regulation. A significant group difference in respiratory rate (RR; $p = .035$, $d = -0.83$, L2 < naïve) indicates that naïve participants breathed faster on average (M = 11.96 vs. 9.64 breaths/min), which plausibly reflects less precise voluntary control or greater anticipatory arousal. In contrast, experienced practitioners maintained a more controlled cadence. End-tidal CO_2 ($EtCO_2$) did not differ significantly between groups (parametric $p = 0.525$; non-parametric $p = 0.545$), indicating broadly comparable CO_2 washout when averaged across phases, despite greater dispersion among the experienced group—consistent with individualised tolerance to hypocapnia. SpO_2 likewise showed no reliable group separation ($p = .730$; both ≈97%). Pulse showed a non-significant trend toward higher values in the experienced cohort ($p = .090$; 71.92 vs 66.67 bpm), suggesting a potentially more dynamic cardiovascular engagement that warrants confirmation with larger samples. Overall, experience appears to shape breathing cadence without producing large between-group differences in gas exchange or oxygenation at the group level. See Tables 5–6 and Figures 16–17.

Repeated-measures analyses compared per-phase means (Baseline vs WHBM) across 151 timepoints per phase (n = 15). Descriptively, SpO_2 fell modestly (97.61% → 96.21%), $EtCO_2$ dropped markedly (5.73% → 2.92%), pulse rose substantially (65.86 → 73.78 bpm), and mean RR was stable (10.60 → 10.53 breaths·min^{-1}) with a pronounced reduction in dispersion during

WHBM (SD 4.20 → 0.89), reflecting convergence to a paced rhythm interleaved with breath retentions. Inferential tests confirmed: SpO_2 decreased (paired $t(14) = 2.58$, $p = .022$, $d = 0.67$), $EtCO_2$ decreased strongly (Wilcoxon $W = 120$, $p < .001$, $r = 1.00$), pulse increased (paired $t(14) = -6.90$, $p < .001$, $d = -1.78$), while RR showed no mean change ($t(14) = 0.07$, $p = .942$, $d = 0.02$). Boxplots illustrate robust hypocapnia, mild desaturation, heart-rate increase, and narrowed RR variability during WHBM. See Table 4 and Figure 16.

The Experimental phase produced acute physiological alterations consistent with controlled hyperventilation interleaved with retentions: pronounced hypocapnia ($EtCO_2$ reduction), modest desaturation (SpO_2), and tachycardia, without a net shift in average RR—likely because breath-holds offset periods of rapid, low-volume breathing. The pattern is compatible with transient respiratory alkalosis (and associated cerebral vasoconstrictive and autonomic effects), though blood gases were not directly sampled here; thus, mechanistic inferences about pH remain provisional. Despite the modest sample ($n = 15$), effect sizes were large for $EtCO_2$ and pulse. The small SpO_2 drop suggests safety in healthy participants but raises caution for vulnerable populations. Limitations include sample size and the absence of direct arterial/venous blood gas measures, which could clarify interactions between ventilation, CO_2, and cardiovascular responses.

The observed signature—$EtCO_2$ reduced to a median of ~2.7–2.8% (≈20.5–22.8 mmHg), a small SpO_2 decline (~1–2%), an increased heart rate, and markedly narrowed respiratory-rate dispersion—aligns with prior WHBM reports of acute hypocapnia during hyperventilation cycles, modest desaturation consistent with breath retentions, and variable effects on mean RR due to compensatory apneas. Our data replicate this acute profile (Tables 4–6; Figures 16–17) but do not address longer-term inflammatory outcomes, which require targeted designs.

Our findings are consistent with several studies. In a controlled crossover study using an authentic WHBM breathing bout before exercise, end-tidal CO_2 fell to 19 ± 3 mmHg (WHBM) and

17 ± 3 mmHg (voluntary hyperventilation) at the end of the last hyperventilation, indicating marked hypocapnia and respiratory alkalosis (estimated arterial pH +0.17 to +0.18) (Citherlet et al., 2021). A closely related high-ventilation breathwork in a recent experimental report showed deliberate hyperventilation reducing $EtCO_2$ to <20 mmHg and linked the drop to altered states of consciousness—corroborating the magnitude seen with WHBM-style ventilation (Havenith et al., 2025). Kox et al. (2014) reported that during WHBM-style cycles, the respiratory rate (RR) alternates between rapid breathing (~20 breaths per minute) and zero during voluntary breath holds. Our data show a mean RR that remains unchanged from Baseline to WHBM (10.60 → 10.53 $br \cdot min^{-1}$), but with collapsed variances (SD 4.205 → 0.887) that is consistent with a paced rhythm interleaved with retentions—exactly the mechanism visible in Kox's minute-scale trace. Finally, qualitatively, our capnography/oximetry reproduces Zwaag's physiology (Zwaag et al., 2022)—CO_2 washout with expected alkalosis, transient O_2 dips linked to retentions, and increased heart rate. Differences in sampling strategy (Zwaag's arterial, time-locked draws vs. our phase-averaged capnography/SpO_2) explain why their O_2 nadirs appear larger, while our $EtCO_2$ trajectory and pulse increase align with the same underlying mechanism.

It is interesting to note that high-amplitude rhythmic slowing (HIHARS) delta waves are thought to be associated mechanistically with hypocapnic cerebral vasoconstriction and subsequent cerebral ischemic hypoxia (Acharya & Acharya, 2021). However, in novices, scalp-level delta did not survive correction when WHBM was averaged over entire cycles, although source analysis revealed a 1–2 Hz cluster, consistent with brief hypocapnia/alkalosis-related slowing that is less temporally consistent than in L2. This may be due to the modest SpO_2 reductions, possibly without frank ischemic hypoxia or phase averaging that dilutes the effects of brief hyperventilation.

Limitations and Future Studies

WHBM Phase-2 was analysed as a single block "because WHBM is taught and practised round-by-round," but this necessarily sacrifices mechanistic specificity regarding hyperventilation vs. breath-hold vs. recovery. Treating the WHBM breathing epoch as an *integrated* intervention maximises ecological validity, but it also "time-smears" sub-phase effects (power breaths vs. low-lung-volume retention vs. recovery) and necessarily compresses several distinct drivers, and may therefore. A condition that precludes breath-cycle–locked analyses of fast transients (e.g., delta bursts at inspiration or gamma transients at the hold/release transitions). As a result, we cannot disentangle which sub-phase most strongly drives the observed spectral and connectivity signatures, nor can we quantify phase-specific hysteresis or carry-over into Rest. To accurately interpret EEG data, it's essential to differentiate between neural activity stemming from WHBM and activity resulting from physiological changes due to altered CO_2 levels. Accordingly, future studies should adopt a *phase-fitting* protocol that time-locks high-density EEG to nasal airflow and capnography ($EtCO_2$/flow) to compute a continuous respiratory phase (Hilbert transform of the airflow/capnogram), bins cycles into inspiration, low-lung-volume hold, expiration and release, and fit it to circular–linear General Linea Modelling time–frequency power and source-space connectivity with instantaneous $EtCO_2$/SpO_2 covariates. A condition that would thereby dissociate respiration-phase entrainment from hypocapnia/alkalosis effects and explicitly test the inspiration-locked frequency shifts and the cycle-dependent cortical excitability. In other words, future work should time-lock EEG, EDA, and capnography to individual cycles to model the WHBM sub-phases explicitly.

Given the breadth of the dataset (scalp power, source reconstructions, functional connectivity, and physiology), we have centred the main discussion on the two contrasts with the

highest interpretability and mechanistic leverage: the Baseline vs. WHBM—the primary within-subject manipulation that isolates the neural consequences of the breathing/retention protocol and Naïve vs. Expert—the key between-subject factor that tests training-dependent organisation of those effects. Focusing on the analysis of the WHBM versus Baseline delivers a clean, first-order signature of "the intervention," but it limits mechanistic considerations. Indeed, treating Rest primarily as a corroborative context, rather than a formal condition, may have limited what could have been said about (i) the persistence versus transience of the WHBM effects, such as understanding how spectral and connectivity changes endure after active breathing stops and normalise. We interpret Rest findings descriptively and reserve claims about persistence or "state resetting" for future work that explicitly maps the recovery trajectory rather than comparing single Rest blocks.

We instructed participants to breathe through their noses (to reduce artefacts) and delivered audio guidance only during Phase 2. Both decisions can alter respiration–brain coupling (e.g., nasal afferents; speech-prosody entrainment) and may differentially affect naïve vs L2 participants. Considering studies such as the one by Heck et al. (2016), which indicate a variation between nasal and mouth breathing, we need to limit the generalisation of our findings to the canonical, mouth-ventilated, self-paced WHBM.

Capnography/SpO_2 were sampled every 4 s and analysed as per-phase means (151 samples/phase). This captures the canonical shifts (e.g., $EtCO_2$↓, SpO_2↓, pulse↑) but smooths within-cycle extremes. As such, inference about brief nadirs is therefore conservative. We infer respiratory alkalosis/hypocapnia from $EtCO_2$ trends; however, arterial and venous gases, as well as pH, were not measured, so mechanistic claims about alkalosis remain provisional. Our observed SpO_2 drop is small on average (~1–2% phase means) and consistent with breath–retention–induced desaturation; however, nadirs can be transiently lower at the end of holds. We excluded

cardiopulmonary risk and used abort criteria, but generalisation to clinical populations should be cautious and would benefit from continuous, cycle-locked pulse oximetry and arterial gases.

Convenience sample (N=17) with modest group sizes (L2=10; naïve=7), a slight age difference, and one group (L2) contributing the cold-immersion data only. Power is adequate for detecting large effects after cluster correction, but small to moderate effects may be missed, and some between-group contrasts are underpowered.

EDA is sensitive to non-neural factors (skin temperature, hydration, subtle movement). We minimised these by keeping room conditions stable and analysing the phasic component with standard event-detection thresholds; nonetheless, residual confounds cannot be fully excluded. Considering that phasic EDA (SCRs) is generated by sympathetic activation of eccrine sweat glands and circulating epinephrine is a hormonal output of the adrenal medulla, we did not interpret SCRs as direct proxies for epinephrine. Indeed, if both can rise during sympathetic arousal, they're different effectors with different time courses and determinants. Future studies should aim to measure both simultaneously, with sufficient temporal resolution, to model their coupling.

Even though our within-phase skin-temperature changes (ΔT) were close to the iButton uncertainty post-calibration, and our results remained within-phase, ΔT were near sensor uncertainty, temperature remains a mechanistically essential factor for future studies. Indeed, as reported in Tibetan g-Tummo reports, there are training-dependent increases in body temperature, consistent with strong sympathetic arousal components. We need to be able to explain why WHBM does not reproduce any part of that thermoregulatory phenotype. Moreover, measuring temperatures provides a peripheral effector readout to understand the mechanism that may link LC-NE arousal bursts, whether they are translated or not, to cutaneous vasoconstriction and redistribution versus metabolic heat production—distinctions that are crucial for interpreting EEG changes under hypocapnia/alkalosis and for affective adaptation to cold exposure.

Although our present results characterise the neural and physiological signatures of the standard WHBM round, many real-world claims and training practices centre on the power-breathing variant, which features larger tidal volumes and rates, longer low-lung-volume retentions, a forceful recovery inhalation, and end-squeeze (often mouth-ventilated). Future study should complement our findings with this variant, considering it should amplify the CO_2 and pH–O_2 perturbation (e.g., deeper hypocapnia/alkalosis, transient desaturation), increase sympathetic drive, and induce larger intrathoracic and CSF pressure swings that may provide more specific spectral and connectivity effects with sharper separations of respiratory-phase entrainment from blood-gas–driven changes improving the validity of our findings by matching how WHBM is commonly practised. Such a study may equally provide an opportunity to understand better how increased CO_2 leads to non-ordinary states of consciousness, considering that extreme physiological challenges, such as increased CO_2 levels, can trigger heightened perception and learning by upregulating serotonin signalling (Havenith et al., 2025) and possibly increase endogenous N, N-Dimethyltryptamine (DMT) (Chavez, 2021).

Because WHBM deliberately perturbs CO_2/pH and shifts the autonomic balance, hyperventilation, in contrast to resonance respiration, decreases Heart Rate Variability (HRV) (Goheen et al., 2023). Future research should design a longitudinal study to track baseline HRV, the possible within-session HRV drop during WHBM, and recovery in post-WHBM Rest across weeks to test training-related vagal tone to isolate WHBM-specific hypocapnic effects from generic breathing benefits, strengthening causal interpretation, and adding clinically relevant endpoints (e.g., vagal tone, stress recovery), further bridging neural findings to translational impact.

We may hypothetically inquire whether the robust mid- and high-gamma FC we observe in experts suggests that repeated practice may constitute an endogenous entrainment regimen for fast-

timescale cortical communication and could help in prodromal and early Alzheimer's disease (AD), notably marked by gamma-band dysregulation. Indeed, experts showed structured and frequency-specific connectivity patterns, including heightened gamma-band synchrony and fronto-parietal integration, which are associated with adaptive neural reorganization and efficient network communication which could enhanced FC. Future studies should test this possibility while simultaneously testing a plasticity-permissive NE/ACh milieu and the potential for enhancing CSF-mediated waste clearance, as hypothesised by Chavez and Zappaterra (2023), thereby offering a plausible route to neuroprotection and neuroplasticity in vulnerable populations.

Finally, although we collected Hallucinogen Rating Scale (HRS) data to probe the popular claim that WHBM produces DMT-like phenomenology—especially in the somaesthesia and perception domains—we did not analyse HRS in this report because of the already broad scope of the present paper spanning scalp power, source modelling, connectivity and physiology. Adding the analysis would have introduced multi-domain psychometrics to our dataset, which would have materially expanded the scope and the multiple-comparison burden of the paper.

Conclusion:

Breath-control practices are not monolithic. Slow breathing pranayama typically reduces respiratory frequency, improves vagal tone, and reduces CO_2 sensitivity; consequently, many benefits are physiologically derived from parasympathetic engagement (Melnychuk et al., 2018). WHM, by contrast, is an arousal-based practice.

Our data show textbook WHM physiology: a large hypocapnic shift ($EtCO_2$ reduction), moderate tachycardia (increased HR), moderate desaturation ($SpO_2\downarrow$), and no net change in mean

respiratory rate because rapid power breaths alternate with holds. The $EtCO_2$–HR and SpO_2–HR relationships are mechanistically coherent for a sympathetically biased, gas-swing protocol.

Neurally, WHM induces a physiologically aroused yet internally directed cortical state. Experts have shown dominant gamma power, and occipital alpha suppression, beta activity in the precuneus, and theta-band functional connectivity centred on somatosensory–salience–DMN hubs, as well as gamma-band coupling between the posterior DMN (precuneus/PCC) and frontal control regions (ACC/lateral PFC). Novices exhibit frontopolar-weighted gamma and posterior sensory–mnemonic coupling with little theta-FC. These expert–novice differences indicate a practice-dependent organisation of interoceptive control. Functionally, immersion elicited widespread increases in functional connectivity—dominated by posterior–frontal links integrating occipital/somatosensory with ACC/insular control nodes—indicative of heightened interoceptive–exteroceptive integration under thermal stress.

Taken together, the patterns align with (Braendholt et al., 2023): respiration drives the brain via multiple conduits—(i) a peripheral/nasal mechanosensory route that entrains limbic–insular circuits and phase-modulates faster bands, (ii) brainstem–LC–thalamic gain control that reshapes global spectral power, and (iii) top-down volitional scaffolding that strengthens respiration–neural coherence.

Conceptually, WHBM leverages sympathetic activation and hierarchical respiratory–brain coupling to heighten cortical precision while maintaining internal focus transiently. This mechanistic framing motivates longitudinal tests within a power-breathing context, including training-related plasticity (e.g., LC/NE-permissive windows) and translational endpoints that link gas dynamics more precisely to network-level control.

Appendix 1

EEG Results

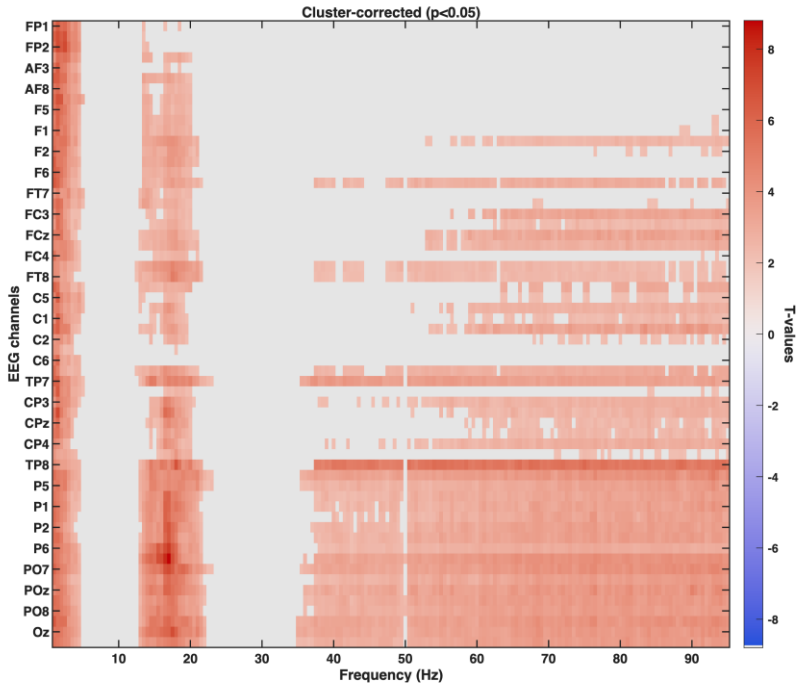

Figure S1

Whole group

Cluster 1: 1 to 5 Hz. Peak effect: CP1 at 1.5 Hz (t = 7.1)

Cluster 2: 12.5 to 23 Hz. Peak effect: P8 at 17 Hz (t = 8.8)

Cluster 3: 35 to 95 Hz. Peak effect: TP8 at 75 Hz (t = 5.9)

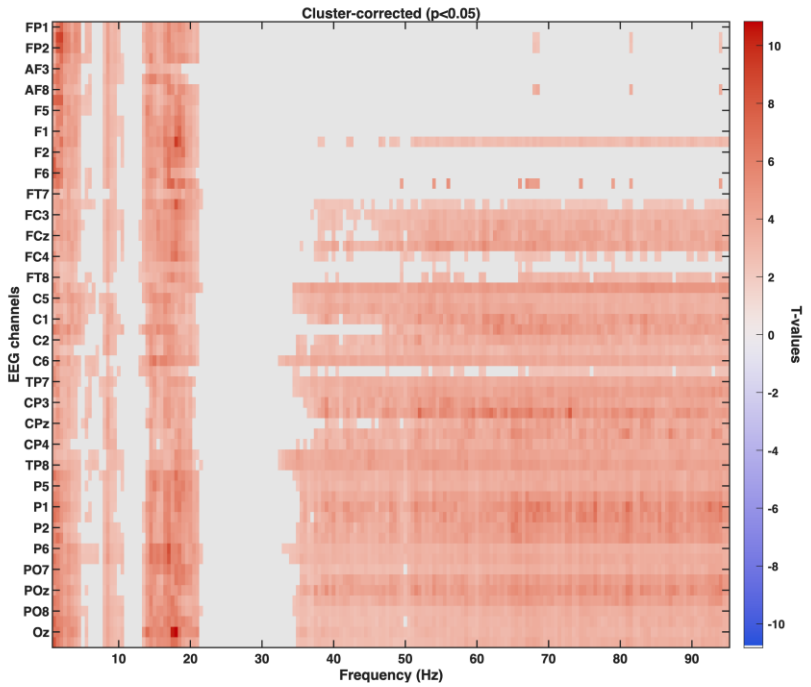

Figure S2

Experts (N = 10)

Cluster 1: 1 to 7 Hz. Peak effect: FPz at 2 Hz (t = 9.2)

Cluster 2: 7.5 to 10.5 Hz. Peak effect: P8 at 8.5 Hz (t = 4.6)

Cluster 3: 13 to 21.5 Hz. Peak effect: Oz at 18 Hz (t = 10.8)

Cluster 4: 32.5 to 95 Hz. Peak effect: CP1 at 73 Hz (t = 7.9)

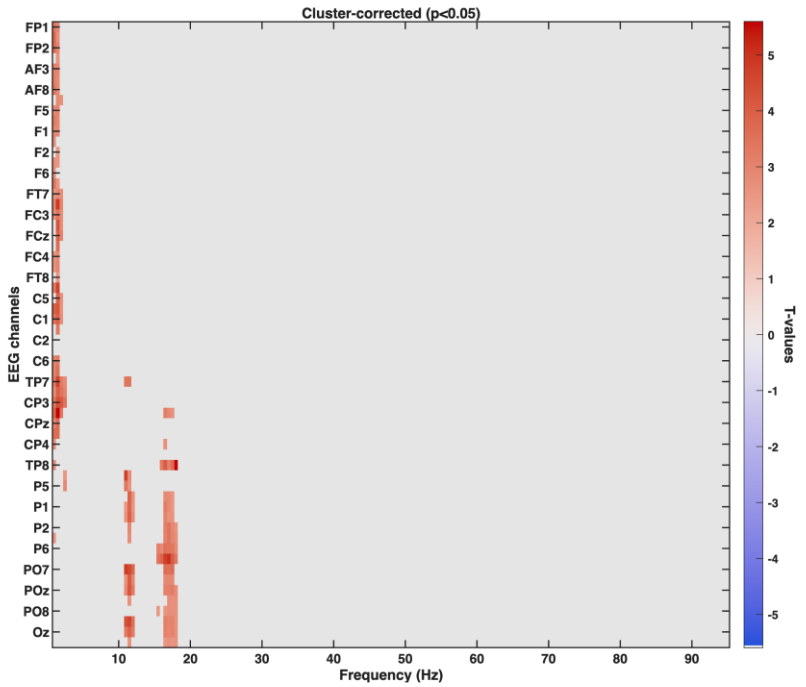

Figure S3

Novices (N = 7)

Cluster 1: 1 to 2.5 Hz. Peak effect: CP1 at 1.5 Hz (t = 5.6)

Cluster 2: 11 to 12 Hz. Peak effect: PO7 at 11 Hz (t = 4.9)

Cluster 3: 15.5 to 18 Hz. Peak effect: TP8 at 18 Hz (t = 5.6)

Source Spectral Analysis

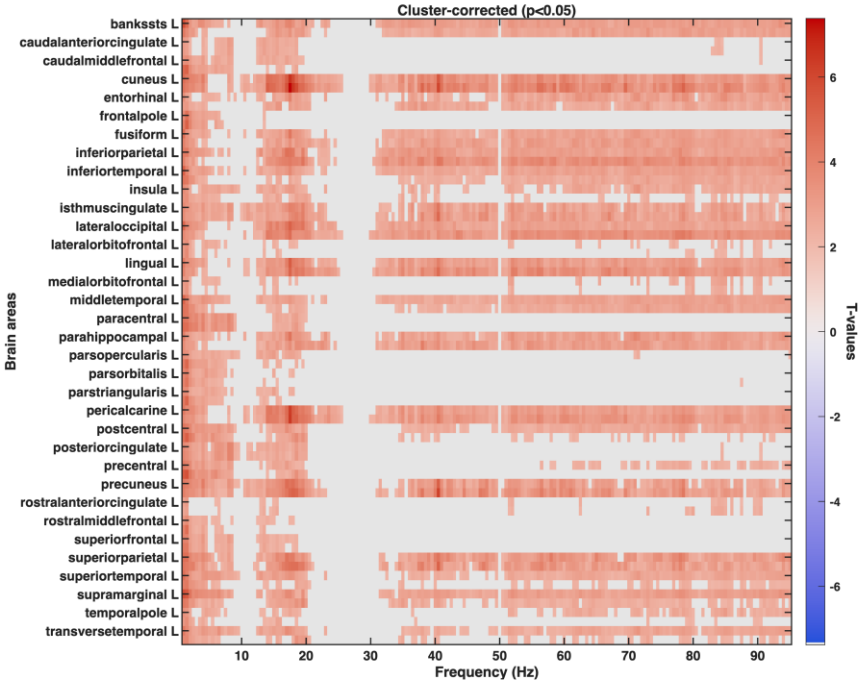

Figure S4

WHBM vs Rest

Whole group (N = 17

Cluster 1: 1 to 9.5 Hz. Peak effect: L at 1 Hz (t = 5.9)

Cluster 2: 10 to 25.5 Hz. Peak effect: cuneus R at 17.5 Hz (t = 7.4)

Cluster 3: 30 to 49.5 Hz. Peak effect: precuneus R at 40.5 Hz (t = 6.2)

Cluster 4: 50.5 to 95 Hz. Peak effect: cuneus R at 78.5 Hz (t = 5.1)

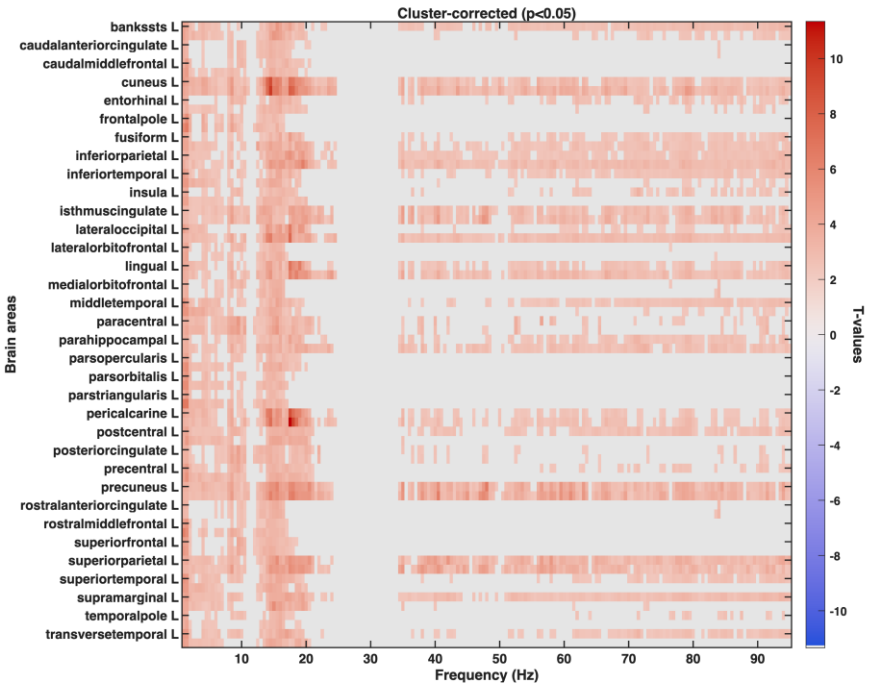

Figure S5

Experts (N = 10)

Cluster 1: 1 to 11 Hz. Peak effect: pars triangularis R at 1 Hz (t = 6.7)

Cluster 2: 12 to 24.5 Hz. Peak effect: pericalcarine R at 17.5 Hz (t = 11.3)

Cluster 3: 34.5 to 95 Hz. Peak effect: precuneus L at 48 Hz (t = 6.6)

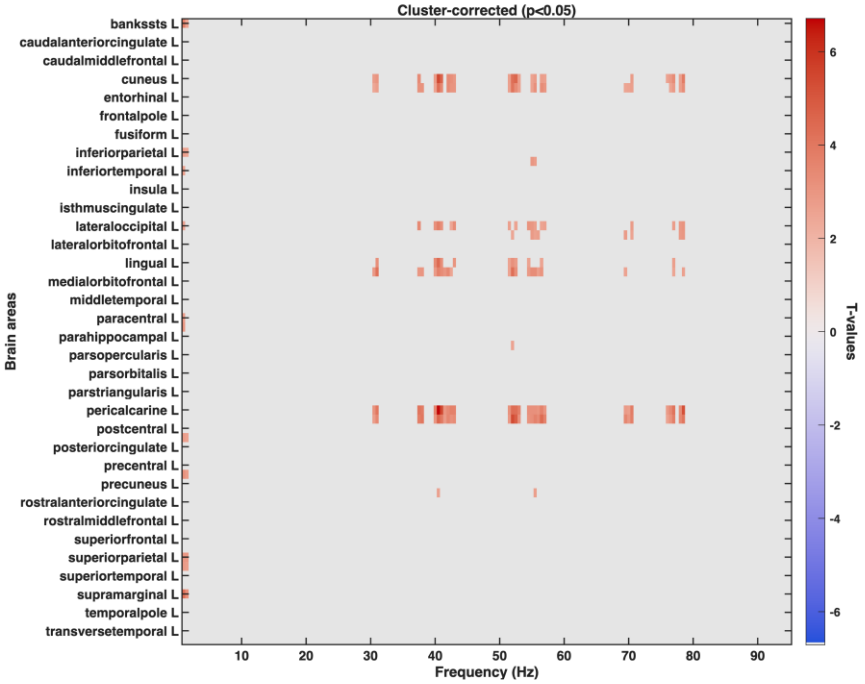

Figure S6

Novices (N = 7)

Cluster 1: 1 to 1.5 Hz. Peak effect: supramarginal L at 1 Hz (t = 4.3)

Cluster 2: 30.5 to 31 Hz. Peak effect: lingual R at 31 Hz (t = 4.2)

Cluster 3: 37.5 to 43 Hz. Peak effect: pericalcarine L at 40.5 Hz (t = 6.7)

Cluster 5: 51.5 to 57 Hz. Peak effect: pericalcarine R at 52 Hz (t = 5.4)

Cluster 7: 69.5 to 70.5 Hz. Peak effect: pericalcarine L at 70.5 Hz (t = 3.8)

Cluster 9: 76 to 78.5 Hz. Peak effect: pericalcarine L at 78.5 Hz (t = 5.2)

Source Spectral Analysis

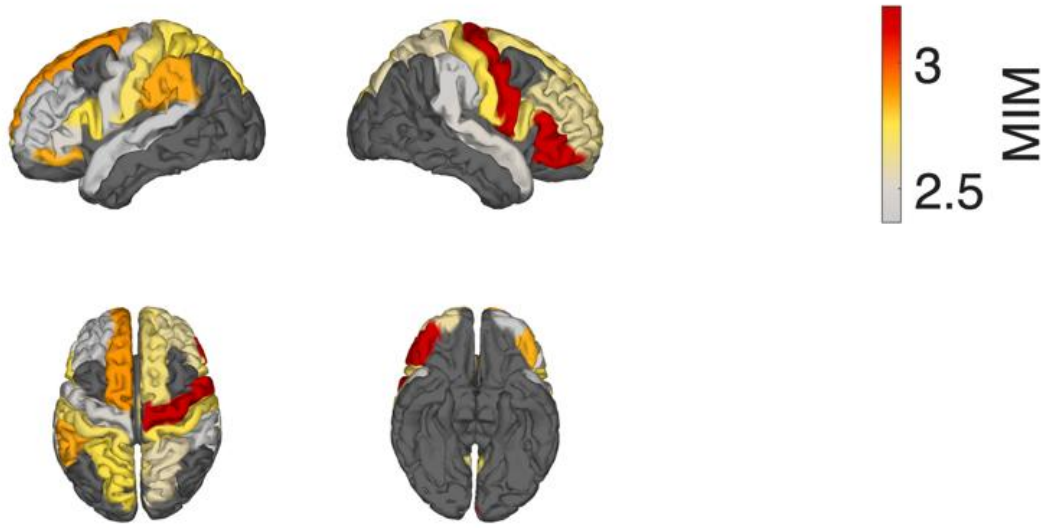

Figure S7

Whole Group Delta

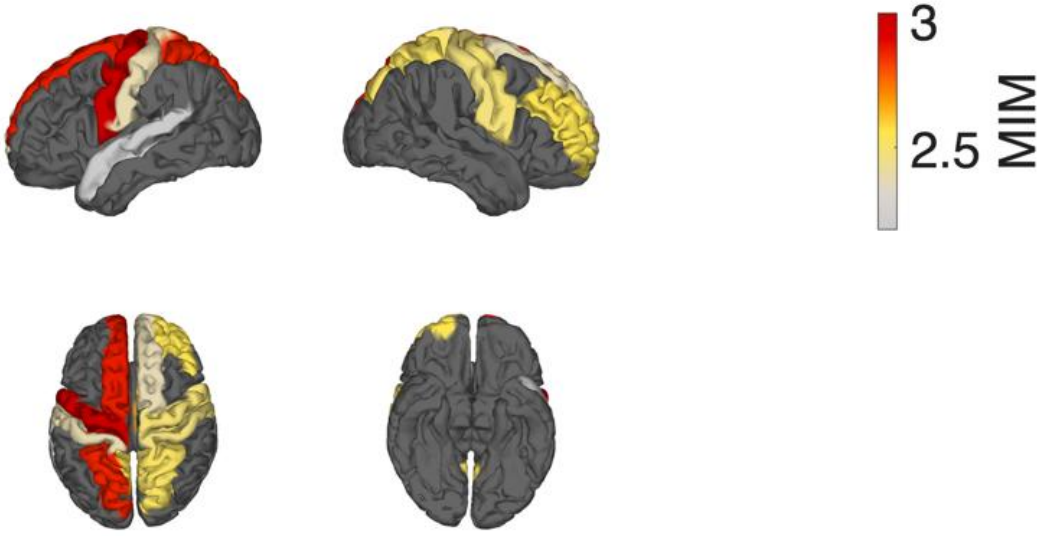

Figure S8

Whole Group Theta

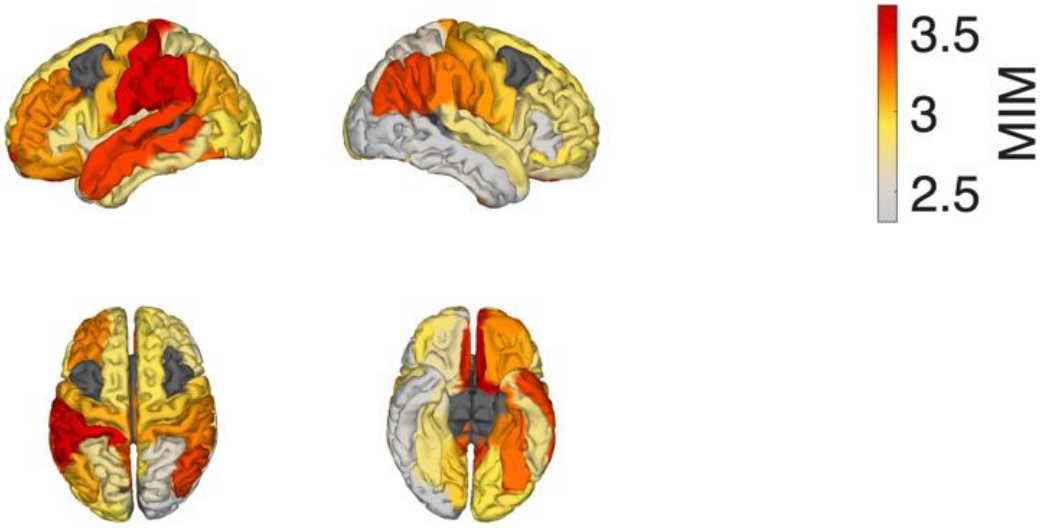

Figure S9

Whole Group Mid-Gamma (55-70 Hz)

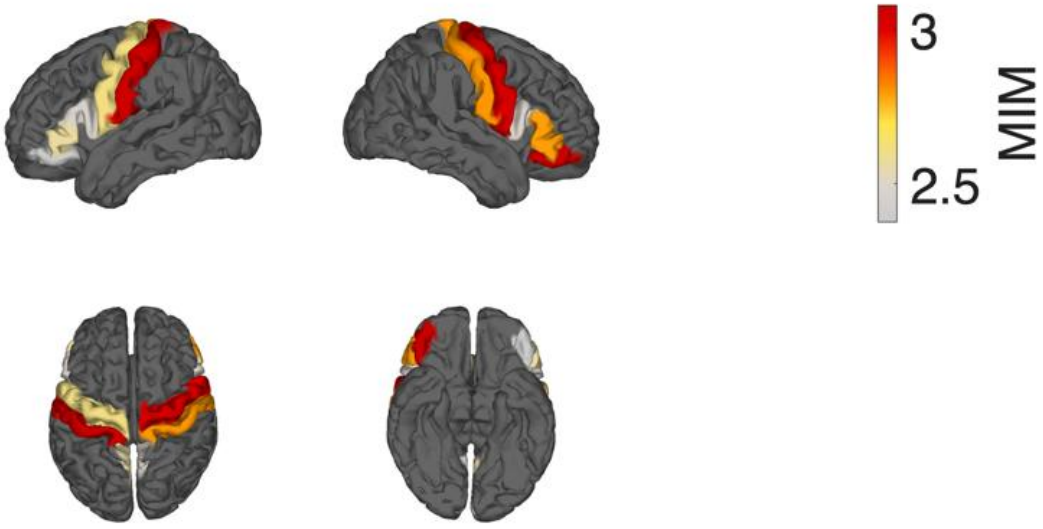

Figure S10

Expert Delta

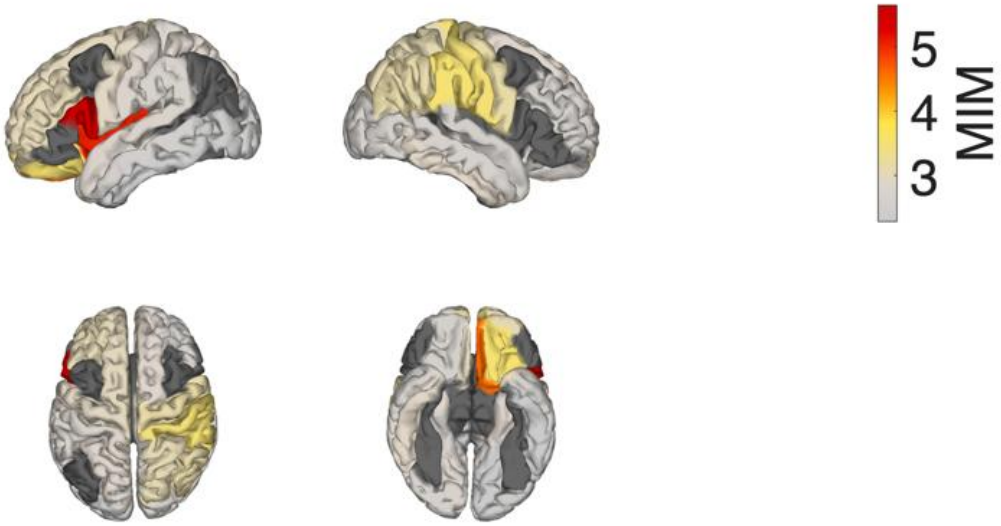

Figure S11

Expert High Gamma (70-95 Hz)

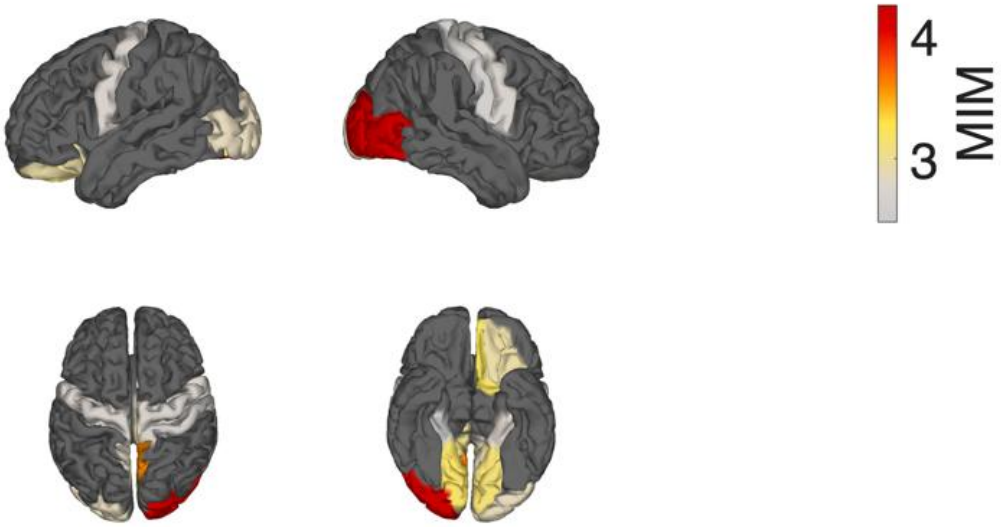

Figure S12

Novice Alpha (8-13 Hz)

Figure S13

Novice Beta (13-30 Hz)

Acknowledgements

We wish to express our deepest gratitude to Dr Ekaterina Igorevna Batissou for her rigorous and insightful revision of the capnographic data, which strengthened the methodological clarity of this work. Our thanks also go to Ena Soft, whose assistance during the physiological recordings and compilation of the data were indispensable to this study.

We equally extend a warm and heartfelt appreciation to Leandre Omeir from the *Wim Hof Method Centre France* for his invaluable help in coordinating participant recruitment and for the warm welcoming provided by the entire Centre France team. Their generosity, enthusiasm, and belief in the scientific exploration of the Wim Hof Method created an environment that inspired both researchers and participants alike.

Finally, we warmly acknowledge our esteemed colleague John Chavez from DMT Quest Foundation for its financial support in covering part of the research expenses. The funder contributed to the manuscript revision but had no role in study design and analysis.

REFERENCES

Ablin, P., Cardoso, J. F., & Gramfort, A. (2018). Faster Independent Component Analysis by Preconditioning With Hessian Approximations. *IEEE Transactions on Signal Processing*, *66*(15), 4040-4049. https://doi.org/10.1109/TSP.2018.2844203

Acharya, J. N., & Acharya, V. J. (2021). Hyperventilation-induced EEG slowing with altered awareness: Non-epileptic, epileptic or both? *Clin Neurophysiol Pract*, *6*, 189-190. https://doi.org/10.1016/j.cnp.2021.05.001

Alahmadi, A. A. S. (2021). Investigating the sub-regions of the superior parietal cortex using functional magnetic resonance imaging connectivity. *Insights Imaging*, *12*(1), 47. https://doi.org/10.1186/s13244-021-00993-9

Almahayni, O., & Hammond, L. (2024). Does the Wim Hof Method have a beneficial impact on physiological and psychological outcomes in healthy and non-healthy participants? A systematic review. *PLoS One*, *19*(3), e0286933. https://doi.org/10.1371/journal.pone.0286933

Aminoff, E. M., Kveraga, K., & Bar, M. (2013). The role of the parahippocampal cortex in cognition. *Trends Cogn Sci*, *17*(8), 379-390. https://doi.org/10.1016/j.tics.2013.06.009

Angioletti, L., & Balconi, M. (2022). Delta-Alpha EEG pattern reflects the interoceptive focus effect on interpersonal motor synchronization. *Front Neuroergon*, *3*, 1012810. https://doi.org/10.3389/fnrgo.2022.1012810

Aston-Jones, G., & Cohen, J. D. (2005). An integrative theory of locus coeruleus-norepinephrine function: adaptive gain and optimal performance. *Annu Rev Neurosci*, *28*, 403-450. https://doi.org/10.1146/annurev.neuro.28.061604.135709

Baird, B., Smallwood, J., Gorgolewski, K. J., & Margulies, D. S. (2013). Medial and lateral networks in anterior prefrontal cortex support metacognitive ability for memory and perception. *J Neurosci*, *33*(42), 16657-16665. https://doi.org/10.1523/JNEUROSCI.0786-13.2013

Barcomb, K., Olah, S. S., Kennedy, M. J., & Ford, C. P. (2022). Properties and modulation of excitatory inputs to the locus coeruleus. *The Journal of Physiology*, *600*(22), 4897-4916. https://doi.org/https://doi.org/10.1113/JP283605

Barone, J., & Rossiter, H. E. (2021). Understanding the Role of Sensorimotor Beta Oscillations. *Front Syst Neurosci*, *15*, 655886. https://doi.org/10.3389/fnsys.2021.655886

Bastos, A. M., Litvak, V., Moran, R., Bosman, C. A., Fries, P., & Friston, K. J. (2015). A DCM study of spectral asymmetries in feedforward and feedback connections between visual areas V1 and V4 in the monkey. *Neuroimage*, *108*, 460-475. https://doi.org/10.1016/j.neuroimage.2014.12.081

Bastos, A. M., Vezoli, J., Bosman, C. A., Schoffelen, J. M., Oostenveld, R., Dowdall, J. R., De Weerd, P., Kennedy, H., & Fries, P. (2015). Visual areas exert feedforward and feedback influences through distinct frequency channels. *Neuron*, *85*(2), 390-401. https://doi.org/10.1016/j.neuron.2014.12.018

Benson, H., Lehmann, J. W., Malhotra, M. S., Goldman, R. F., Hopkins, J., & Epstein, M. D. (1982). Body temperature changes during the practice of g Tum-mo yoga. *Nature*, *295*(5846), 234-236. https://doi.org/10.1038/295234a0

Blades, R., Mendes, W. B., Don, B. P., Mayer, S. E., Dileo, R., O'Bryan, J., Fromer, E., Guan, J. Y., Cheng, S. S., Mason, A. E., Prather, A. A., & Epel, E. S. (2024). A randomized controlled clinical trial of a Wim Hof Method intervention in women with high depressive symptoms. *Compr Psychoneuroendocrinol*, *20*, 100272. https://doi.org/10.1016/j.cpnec.2024.100272

Braboszcz, C., Cahn, B. R., Levy, J., Fernandez, M., & Delorme, A. (2017). Increased Gamma Brainwave Amplitude Compared to Control in Three Different Meditation Traditions. *PLoS One*, *12*(1), e0170647. https://doi.org/10.1371/journal.pone.0170647

Braendholt, M., Kluger, D. S., Varga, S., Heck, D. H., Gross, J., & Allen, M. G. (2023). Breathing in waves: Understanding respiratory-brain coupling as a gradient of predictive oscillations. *Neurosci Biobehav Rev*, *152*, 105262. https://doi.org/10.1016/j.neubiorev.2023.105262

Buijze, G. A., De Jong, H. M. Y., Kox, M., van de Sande, M. G., Van Schaardenburg, D., Van Vugt, R. M., Popa, C. D., Pickkers, P., & Baeten, D. L. P. (2019). An add-on training program involving breathing exercises, cold exposure, and meditation attenuates inflammation and disease activity in axial spondyloarthritis - A proof of concept trial. *PLoS One*, *14*(12), e0225749. https://doi.org/10.1371/journal.pone.0225749

Burgess, P. W., Dumontheil, I., & Gilbert, S. J. (2007). The gateway hypothesis of rostral prefrontal cortex (area 10) function. *Trends Cogn Sci*, *11*(7), 290-298. https://doi.org/10.1016/j.tics.2007.05.004

Busek, P., & Kemlink, D. (2005). The influence of the respiratory cycle on the EEG. *Physiol Res*, *54*(3), 327-333. https://www.ncbi.nlm.nih.gov/pubmed/15588159

Cahn, B. R., Delorme, A., & Polich, J. (2010). Occipital gamma activation during Vipassana meditation. *Cogn Process*, *11*(1), 39-56. https://doi.org/10.1007/s10339-009-0352-1

Cavanagh, J. F., & Frank, M. J. (2014). Frontal theta as a mechanism for cognitive control. *Trends Cogn Sci*, *18*(8), 414-421. https://doi.org/10.1016/j.tics.2014.04.012

Cavanna, A. E., & Trimble, M. R. (2006). The precuneus: a review of its functional anatomy and behavioural correlates. *Brain*, *129*(Pt 3), 564-583. https://doi.org/10.1093/brain/awl004

Chang, C. Y., Hsu, S. H., Pion-Tonachini, L., & Jung, T. P. (2018). Evaluation of Artifact Subspace Reconstruction for Automatic EEG Artifact Removal. *Annu Int Conf IEEE Eng Med Biol Soc*, *2018*, 1242-1245. https://doi.org/10.1109/EMBC.2018.8512547

Chavez, J. (2021). *DMT Quest Documentary* [Video]. https://youtu.be/My95s6ZryPg

Chavez, J. A., & Zappaterra, M. (2023). Can Wim Hof Method breathing induce conscious metabolic waste clearance of the brain? *Medical Hypotheses*, *177*, 111118. https://doi.org/https://doi.org/10.1016/j.mehy.2023.111118

Cheyne, D., & Ferrari, P. (2013). MEG studies of motor cortex gamma oscillations: evidence for a gamma "fingerprint" in the brain? *Front Hum Neurosci*, *7*, 575. https://doi.org/10.3389/fnhum.2013.00575

Citherlet, T., Crettaz von Roten, F., Kayser, B., & Guex, K. (2021). Acute Effects of the Wim Hof Breathing Method on Repeated Sprint Ability: A Pilot Study. *Front Sports Act Living*, *3*, 700757. https://doi.org/10.3389/fspor.2021.700757

Conway, B. R. (2018). The Organization and Operation of Inferior Temporal Cortex. *Annu Rev Vis Sci*, *4*, 381-402. https://doi.org/10.1146/annurev-vision-091517-034202

Craig, A. D. (2009). How do you feel--now? The anterior insula and human awareness. *Nat Rev Neurosci*, *10*(1), 59-70. https://doi.org/10.1038/nrn2555

Dijkstra, N., Bosch, S. E., & van Gerven, M. A. (2017). Vividness of Visual Imagery Depends on the Neural Overlap with Perception in Visual Areas. *J Neurosci*, *37*(5), 1367-1373. https://doi.org/10.1523/JNEUROSCI.3022-16.2016

Eisma, J., Rawls, E., Long, S., Mach, R., & Lamm, C. (2021). Frontal midline theta differentiates separate cognitive control strategies while still generalizing the need for cognitive control. *Sci Rep*, *11*(1), 14641. https://doi.org/10.1038/s41598-021-94162-z

Engel, A. K., & Fries, P. (2010). Beta-band oscillations--signalling the status quo? *Curr Opin Neurobiol*, *20*(2), 156-165. https://doi.org/10.1016/j.conb.2010.02.015

Fiebelkorn, I. C., & Kastner, S. (2019). A Rhythmic Theory of Attention. *Trends Cogn Sci*, *23*(2), 87-101. https://doi.org/10.1016/j.tics.2018.11.009

Fiebelkorn, I. C., Pinsk, M. A., & Kastner, S. (2018). A Dynamic Interplay within the Frontoparietal Network Underlies Rhythmic Spatial Attention. *Neuron*, *99*(4), 842-853 e848. https://doi.org/10.1016/j.neuron.2018.07.038

Fincham, G. W., Strauss, C., Montero-Marin, J., & Cavanagh, K. (2023). Effect of breathwork on stress and mental health: A meta-analysis of randomised-controlled trials. *Sci Rep*, *13*(1), 432. https://doi.org/10.1038/s41598-022-27247-y

Foxe, J. J., & Snyder, A. C. (2011). The Role of Alpha-Band Brain Oscillations as a Sensory Suppression Mechanism during Selective Attention. *Front Psychol*, *2*, 154. https://doi.org/10.3389/fpsyg.2011.00154

Friedman, N. P., & Robbins, T. W. (2022). The role of prefrontal cortex in cognitive control and executive function. *Neuropsychopharmacology*, *47*(1), 72-89. https://doi.org/10.1038/s41386-021-01132-0

Fries, P. (2015). Rhythms for Cognition: Communication through Coherence. *Neuron*, *88*(1), 220-235. https://doi.org/10.1016/j.neuron.2015.09.034

Gaetz, W., Liu, C., Zhu, H., Bloy, L., & Roberts, T. P. (2013). Evidence for a motor gamma-band network governing response interference. *Neuroimage*, *74*, 245-253. https://doi.org/10.1016/j.neuroimage.2013.02.013

Goheen, J., Anderson, J. A. E., Zhang, J., & Northoff, G. (2023). From Lung to Brain: Respiration Modulates Neural and Mental Activity. *Neurosci Bull*, *39*(10), 1577-1590. https://doi.org/10.1007/s12264-023-01070-5

Gregoriou, G. G., Gotts, S. J., Zhou, H., & Desimone, R. (2009). High-frequency, long-range coupling between prefrontal and visual cortex during attention. *Science*, *324*(5931), 1207-1210. https://doi.org/10.1126/science.1171402

Griffiths, B. J., Parish, G., Roux, F., Michelmann, S., van der Plas, M., Kolibius, L. D., Chelvarajah, R., Rollings, D. T., Sawlani, V., Hamer, H., Gollwitzer, S., Kreiselmeyer, G., Staresina, B., Wimber, M., & Hanslmayr, S. (2019). Directional coupling of slow and fast hippocampal gamma with neocortical alpha/beta oscillations in human episodic memory. *Proc Natl Acad Sci U S A*, *116*(43), 21834-21842. https://doi.org/10.1073/pnas.1914180116

Grill-Spector, K., & Weiner, K. S. (2014). The functional architecture of the ventral temporal cortex and its role in categorization. *Nat Rev Neurosci*, *15*(8), 536-548. https://doi.org/10.1038/nrn3747

Havenith, M. N., Leidenberger, M., Brasanac, J., Corvacho, M., Carmo Figueiredo, I., Schwarz, L., Uthaug, M., Rakusa, S., Bernardic, M., Vasquez-Mock, L., Perez Rosal, S., Carhart-Harris, R., Gold, S. M., Jungaberle, H., & Jungaberle, A. (2025). Decreased CO(2) saturation during circular breathwork supports emergence of altered states of consciousness. *Commun Psychol*, *3*(1), 59. https://doi.org/10.1038/s44271-025-00247-0

Heck, D. H., McAfee, S. S., Liu, Y., Babajani-Feremi, A., Rezaie, R., Freeman, W. J., Wheless, J. W., Papanicolaou, A. C., Ruszinko, M., Sokolov, Y., & Kozma, R. (2016). Breathing as a Fundamental Rhythm of Brain Function. *Front Neural Circuits*, *10*, 115. https://doi.org/10.3389/fncir.2016.00115

Herrero, J. L., Khuvis, S., Yeagle, E., Cerf, M., & Mehta, A. D. (2018). Breathing above the brain stem: volitional control and attentional modulation in humans. *J Neurophysiol*, *119*(1), 145-159. https://doi.org/10.1152/jn.00551.2017

Hipp, J. F., Engel, A. K., & Siegel, M. (2011). Oscillatory synchronization in large-scale cortical networks predicts perception. *Neuron*, *69*(2), 387-396. https://doi.org/10.1016/j.neuron.2010.12.027

Hof, W. (2019). *Guided Wim Hof Method Breathing* Youtube, Youtube. https://youtu.be/tybOi4hjZFQ

Hogeveen, J., Mullins, T. S., Romero, J. D., Eversole, E., Rogge-Obando, K., Mayer, A. R., & Costa, V. D. (2022). The neurocomputational bases of explore-exploit decision-making. *Neuron*, *110*(11), 1869-1879 e1865. https://doi.org/10.1016/j.neuron.2022.03.014

Keitel, A., Ince, R. A. A., Gross, J., & Kayser, C. (2017). Auditory cortical delta-entrainment interacts with oscillatory power in multiple fronto-parietal networks. *Neuroimage*, *147*, 32-42. https://doi.org/10.1016/j.neuroimage.2016.11.062

Kenville, R., Gross, D., Helbich, M., Ragert, P., & Maudrich, T. (2025). Exploring the relationship between somatosensory-evoked potentials, resting-state theta power, and acute balance performance. *Sci Rep*, *15*(1), 36123. https://doi.org/10.1038/s41598-025-23878-z

Kim, H., Luo, J., Chu, S., Cannard, C., Hoffmann, S., & Miyakoshi, M. (2023). ICA's bug: How ghost ICs emerge from effective rank deficiency caused by EEG electrode interpolation and incorrect re-referencing [Original Research]. *Frontiers in Signal Processing*, *Volume 3 - 2023*. https://doi.org/10.3389/frsip.2023.1064138

Kleckner, I. R., Zhang, J., Touroutoglou, A., Chanes, L., Xia, C., Simmons, W. K., Quigley, K. S., Dickerson, B. C., & Barrett, L. F. (2017). Evidence for a Large-Scale Brain System Supporting Allostasis and Interoception in Humans. *Nat Hum Behav*, *1*. https://doi.org/10.1038/s41562-017-0069

Kluger, D. S., & Gross, J. (2021). Respiration modulates oscillatory neural network activity at rest. *PLoS Biol*, *19*(11), e3001457. https://doi.org/10.1371/journal.pbio.3001457

Kong, J., Tu, P. C., Zyloney, C., & Su, T. P. (2010). Intrinsic functional connectivity of the periaqueductal gray, a resting fMRI study. *Behav Brain Res*, *211*(2), 215-219. https://doi.org/10.1016/j.bbr.2010.03.042

Kox, M., van Eijk, L. T., Zwaag, J., van den Wildenberg, J., Sweep, F. C., van der Hoeven, J. G., & Pickkers, P. (2014). Voluntary activation of the sympathetic nervous system and attenuation of the innate immune response in humans. *Proc Natl Acad Sci U S A*, *111*(20), 7379-7384. https://doi.org/10.1073/pnas.1322174111

Kozhevnikov, M., Elliott, J., Shephard, J., & Gramann, K. (2013). Neurocognitive and somatic components of temperature increases during g-tummo meditation: legend and reality. *PLoS One*, *8*(3), e58244. https://doi.org/10.1371/journal.pone.0058244

Laborde, S., Allen, M. S., Borges, U., Dosseville, F., Hosang, T. J., Iskra, M., Mosley, E., Salvotti, C., Spolverato, L., Zammit, N., & Javelle, F. (2022). Effects of voluntary slow breathing on heart rate and heart rate variability: A systematic review and a meta-analysis. *Neurosci Biobehav Rev*, *138*, 104711. https://doi.org/10.1016/j.neubiorev.2022.104711

Leech, R., & Sharp, D. J. (2014). The role of the posterior cingulate cortex in cognition and disease. *Brain*, *137*(Pt 1), 12-32. https://doi.org/10.1093/brain/awt162

Li, Z., Zhang, L., Zeng, Y., Zhao, Q., & Hu, L. (2023). Gamma-band oscillations of pain and nociception: A systematic review and meta-analysis of human and rodent studies. *Neurosci Biobehav Rev*, *146*, 105062. https://doi.org/10.1016/j.neubiorev.2023.105062

Liu, C. C., Chien, J. H., Chang, Y. W., Kim, J. H., Anderson, W. S., & Lenz, F. A. (2015). Functional role of induced gamma oscillatory responses in processing noxious and innocuous sensory events in humans. *Neuroscience*, *310*, 389-400. https://doi.org/10.1016/j.neuroscience.2015.09.047

Lucan, J. N., Foxe, J. J., Gomez-Ramirez, M., Sathian, K., & Molholm, S. (2010). Tactile shape discrimination recruits human lateral occipital complex during early perceptual processing. *Hum Brain Mapp*, *31*(11), 1813-1821. https://doi.org/10.1002/hbm.20983

Lundqvist, M., Herman, P., Warden, M. R., Brincat, S. L., & Miller, E. K. (2018). Gamma and beta bursts during working memory readout suggest roles in its volitional control. *Nat Commun*, *9*(1), 394. https://doi.org/10.1038/s41467-017-02791-8

Makeig, S., Bell, A. J., Jung, T.-P., & Sejnowski, T. J. (1995). *Independent component analysis of electroencephalographic data* Proceedings of the 9th International Conference on Neural Information Processing Systems, Denver, Colorado.

Makeig, S., Debener, S., Onton, J., & Delorme, A. (2004). Mining event-related brain dynamics. *Trends in Cognitive Sciences*, *8*(5), 204-210. https://doi.org/10.1016/j.tics.2004.03.008

Makeig, S., Debener, S., Onton, J., & Delorme, A. (2004). Mining event-related brain dynamics. *Trends Cogn Sci*, *8*(5), 204-210. https://doi.org/10.1016/j.tics.2004.03.008

Mather, M., Clewett, D., Sakaki, M., & Harley, C. W. (2016). Norepinephrine ignites local hotspots of neuronal excitation: How arousal amplifies selectivity in perception and memory. *Behavioral and Brain Sciences*, *39*, e200, Article e200. https://doi.org/10.1017/S0140525X15000667

McGinley, M. J., Vinck, M., Reimer, J., Batista-Brito, R., Zagha, E., Cadwell, C. R., Tolias, A. S., Cardin, J. A., & McCormick, D. A. (2015). Waking State: Rapid Variations Modulate Neural and Behavioral Responses. *Neuron*, *87*(6), 1143-1161. https://doi.org/10.1016/j.neuron.2015.09.012

Melnychuk, M. C., Dockree, P. M., O'Connell, R. G., Murphy, P. R., Balsters, J. H., & Robertson, I. H. (2018). Coupling of respiration and attention via the locus coeruleus: Effects of meditation and pranayama. *Psychophysiology*, *55*(9), e13091. https://doi.org/10.1111/psyp.13091

Menon, V. (2023). 20 years of the default mode network: A review and synthesis. *Neuron*, *111*(16), 2469-2487. https://doi.org/10.1016/j.neuron.2023.04.023

Menon, V. (2025). Insular cortex: A hub for saliency, cognitive control, and interoceptive awareness. In J. H. Grafman (Ed.), *Encyclopedia of the Human Brain (Second Edition)* (pp. 159-183). Elsevier. https://doi.org/https://doi.org/10.1016/B978-0-12-820480-1.00093-0

Michalareas, G., Vezoli, J., van Pelt, S., Schoffelen, J.-M., Kennedy, H., & Fries, P. (2016). Alpha-Beta and Gamma Rhythms Subserve Feedback and Feedforward Influences among Human Visual Cortical Areas. *Neuron*, *89*(2), 384-397. https://doi.org/10.1016/j.neuron.2015.12.018

Muzik, O., Reilly, K. T., & Diwadkar, V. A. (2018). "Brain over body"-A study on the willful regulation of autonomic function during cold exposure. *Neuroimage*, *172*, 632-641. https://doi.org/10.1016/j.neuroimage.2018.01.067

Orlov, T., Makin, T. R., & Zohary, E. (2010). Topographic representation of the human body in the occipitotemporal cortex. *Neuron*, *68*(3), 586-600. https://doi.org/10.1016/j.neuron.2010.09.032

Pagnotta, M. F., Riddle, J., & D'Esposito, M. (2024). Multiplexed Levels of Cognitive Control through Delta and Theta Neural Oscillations. *J Cogn Neurosci*, *36*(5), 916-935. https://doi.org/10.1162/jocn_a_02124

Palejwala, A. H., O'Connor, K. P., Milton, C. K., Anderson, C., Pelargos, P., Briggs, R. G., Conner, A. K., O'Donoghue, D. L., Glenn, C. A., & Sughrue, M. E. (2020). Anatomy and white matter connections of the fusiform gyrus. *Sci Rep*, *10*(1), 13489. https://doi.org/10.1038/s41598-020-70410-6

Passarelli, L., Gamberini, M., & Fattori, P. (2021). The superior parietal lobule of primates: a sensory-motor hub for interaction with the environment. *J Integr Neurosci*, *20*(1), 157-171. https://doi.org/10.31083/j.jin.2021.01.334

Pellegrini, F., Delorme, A., Nikulin, V., & Haufe, S. (2023). Identifying good practices for detecting inter-regional linear functional connectivity from EEG. *Neuroimage*, *277*, 120218. https://doi.org/10.1016/j.neuroimage.2023.120218

Perrin, F., Pernier, J., Bertrand, O., & Echallier, J. F. (1989). Spherical splines for scalp potential and current density mapping. *Electroencephalogr Clin Neurophysiol*, *72*(2), 184-187. https://doi.org/10.1016/0013-4694(89)90180-6

Petraskova Touskova, T., Bob, P., Bares, Z., Vanickova, Z., Nyvlt, D., & Raboch, J. (2022). A novel Wim Hof psychophysiological training program to reduce stress responses during an Antarctic expedition. *J Int Med Res*, *50*(4), 3000605221089883. https://doi.org/10.1177/03000605221089883

Pion-Tonachini, L., Kreutz-Delgado, K., & Makeig, S. (2019). ICLabel: An automated electroencephalographic independent component classifier, dataset, and website. *Neuroimage*, *198*, 181-197. https://doi.org/10.1016/j.neuroimage.2019.05.026

Reimer, J., McGinley, M. J., Liu, Y., Rodenkirch, C., Wang, Q., McCormick, D. A., & Tolias, A. S. (2016). Pupil fluctuations track rapid changes in adrenergic and cholinergic activity in cortex. *Nat Commun*, *7*, 13289. https://doi.org/10.1038/ncomms13289

Rho, G., Callara, A. L., Bernardi, G., Scilingo, E. P., & Greco, A. (2023). EEG cortical activity and connectivity correlates of early sympathetic response during cold pressor test. *Sci Rep*, *13*(1), 1338. https://doi.org/10.1038/s41598-023-27480-z

Rimmele, J. M., Poeppel, D., & Ghitza, O. (2021). Acoustically Driven Cortical delta Oscillations Underpin Prosodic Chunking. *eNeuro*, *8*(4). https://doi.org/10.1523/ENEURO.0562-20.2021

Rolls, E. T. (2019). The orbitofrontal cortex and emotion in health and disease, including depression. *Neuropsychologia*, *128*, 14-43. https://doi.org/10.1016/j.neuropsychologia.2017.09.021

Rothé, M., Quilodran, R., Sallet, J., & Procyk, E. (2011). Coordination of high gamma activity in anterior cingulate and lateral prefrontal cortical areas during adaptation. *J Neurosci*, *31*(31), 11110-11117. https://doi.org/10.1523/JNEUROSCI.1016-11.2011

Sadaghiani, S., Scheeringa, R., Lehongre, K., Morillon, B., Giraud, A. L., D'Esposito, M., & Kleinschmidt, A. (2012). alpha-band phase synchrony is related to activity in the fronto-parietal adaptive control network. *J Neurosci*, *32*(41), 14305-14310. https://doi.org/10.1523/JNEUROSCI.1358-12.2012

Samuels, E. R., & Szabadi, E. (2008). Functional neuroanatomy of the noradrenergic locus coeruleus: its roles in the regulation of arousal and autonomic function part I: principles of functional organisation. *Curr Neuropharmacol*, *6*(3), 235-253. https://doi.org/10.2174/157015908785777229

Siegel, M., Donner, T. H., & Engel, A. K. (2012). Spectral fingerprints of large-scale neuronal interactions. *Nat Rev Neurosci*, *13*(2), 121-134. https://doi.org/10.1038/nrn3137

Simon, T., Kirk, J., Dolezalova, N., Guyot, M., Panzolini, C., Bondue, A., Lavergne, J., Hugues, S., Hypolite, N., Saeb-Parsy, K., Perkins, J., Macia, E., Sridhar, A., Vervoordeldonk, M. J., Glaichenhaus, N., Donega, M., & Blancou, P. (2023). The cholinergic anti-inflammatory pathway inhibits inflammation without lymphocyte relay. *Front Neurosci*, *17*, 1125492. https://doi.org/10.3389/fnins.2023.1125492

Son, S., Kwon, O. Y., Jung, S., Kim, Y. S., Kim, S. K., Kang, H., Park, K. J., Choi, N. C., & Lim, B. H. (2012). Relationship between Hyperventilation-Induced Electroencephalographic Changes and PCO2 Level. *J Epilepsy Res*, *2*(1), 5-9. https://doi.org/10.14581/jer.12002

Spitzer, B., & Haegens, S. (2017). Beyond the Status Quo: A Role for Beta Oscillations in Endogenous Content (Re)Activation. *eNeuro*, *4*(4). https://doi.org/10.1523/ENEURO.0170-17.2017

Utevsky, A. V., Smith, D. V., & Huettel, S. A. (2014). Precuneus is a functional core of the default-mode network. *J Neurosci*, *34*(3), 932-940. https://doi.org/10.1523/JNEUROSCI.4227-13.2014

van Middendorp, H., Kox, M., Pickkers, P., & Evers, A. W. (2016). The role of outcome expectancies for a training program consisting of meditation, breathing exercises, and cold exposure on the response to endotoxin administration: a proof-of-principle study. *Clin Rheumatol*, *35*(4), 1081-1085. https://doi.org/10.1007/s10067-015-3009-8

Vittrant, B., Ayoub, H., & Brunswick, P. (2024). From Sudoscan to bedside: theory, modalities, and application of electrochemical skin conductance in medical diagnostics. *Front Neuroanat*, *18*, 1454095. https://doi.org/10.3389/fnana.2024.1454095

Volle, E., Gonen-Yaacovi, G., Costello Ade, L., Gilbert, S. J., & Burgess, P. W. (2011). The role of rostral prefrontal cortex in prospective memory: a voxel-based lesion study. *Neuropsychologia*, *49*(8), 2185-2198. https://doi.org/10.1016/j.neuropsychologia.2011.02.045

Wang, C., Rajagovindan, R., Han, S. M., & Ding, M. (2016). Top-Down Control of Visual Alpha Oscillations: Sources of Control Signals and Their Mechanisms of Action. *Front Hum Neurosci*, *10*, 15. https://doi.org/10.3389/fnhum.2016.00015

Xu, J., Wang, J., Fan, L., Li, H., Zhang, W., Hu, Q., & Jiang, T. (2015). Tractography-based Parcellation of the Human Middle Temporal Gyrus. *Sci Rep*, *5*, 18883. https://doi.org/10.1038/srep18883

Yamaguchi, A., & Jitsuishi, T. (2024). Structural connectivity of the precuneus and its relation to resting-state networks. *Neurosci Res*, *209*, 9-17. https://doi.org/10.1016/j.neures.2023.12.004

Yang, K., Tong, L., Shu, J., Zhuang, N., Yan, B., & Zeng, Y. (2020). High Gamma Band EEG Closely Related to Emotion: Evidence From Functional Network. *Front Hum Neurosci*, *14*, 89. https://doi.org/10.3389/fnhum.2020.00089

Yankouskaya, A., Williamson, R., Stacey, C., Totman, J. J., & Massey, H. (2023). Short-Term Head-Out Whole-Body Cold-Water Immersion Facilitates Positive Affect and Increases Interaction between Large-Scale Brain Networks. *Biology (Basel)*, *12*(2). https://doi.org/10.3390/biology12020211

Zaehle, T., & Herrmann, C. S. (2011). Neural synchrony and white matter variations in the human brain--relation between evoked gamma frequency and corpus callosum morphology. *Int J Psychophysiol*, *79*(1), 49-54. https://doi.org/10.1016/j.ijpsycho.2010.06.029

Zelano, C., Jiang, H., Zhou, G., Arora, N., Schuele, S., Rosenow, J., & Gottfried, J. A. (2016). Nasal Respiration Entrains Human Limbic Oscillations and Modulates Cognitive Function. *J Neurosci*, *36*(49), 12448-12467. https://doi.org/10.1523/JNEUROSCI.2586-16.2016

Zion Golumbic, E. M., Ding, N., Bickel, S., Lakatos, P., Schevon, C. A., McKhann, G. M., Goodman, R. R., Emerson, R., Mehta, A. D., Simon, J. Z., Poeppel, D., & Schroeder, C. E. (2013). Mechanisms underlying selective neuronal tracking of attended speech at a "cocktail party". *Neuron*, *77*(5), 980-991. https://doi.org/10.1016/j.neuron.2012.12.037

Zis, P., Liampas, A., Artemiadis, A., Tsalamandris, G., Neophytou, P., Unwin, Z., Kimiskidis, V. K., Hadjigeorgiou, G. M., Varrassi, G., Zhao, Y., & Sarrigiannis, P. G. (2022). EEG Recordings as Biomarkers of Pain Perception: Where Do We Stand and Where to Go? *Pain Ther*, *11*(2), 369-380. https://doi.org/10.1007/s40122-022-00372-2

Zwaag, J., Naaktgeboren, R., van Herwaarden, A. E., Pickkers, P., & Kox, M. (2022). The Effects of Cold Exposure Training and a Breathing Exercise on the Inflammatory Response in Humans: A Pilot Study. *Psychosom Med*, *84*(4), 457-467. https://doi.org/10.1097/PSY.0000000000001065

Zwaag, J., Ter Horst, R., Blazenovic, I., Stoessel, D., Ratter, J., Worseck, J. M., Schauer, N., Stienstra, R., Netea, M. G., Jahn, D., Pickkers, P., & Kox, M. (2020). Involvement of Lactate and Pyruvate in the Anti-Inflammatory Effects Exerted by Voluntary Activation of the Sympathetic Nervous System. *Metabolites*, *10*(4). https://doi.org/10.3390/metabo10040148